Supporting information for:

Self-assembled $M_{12}L_{12}$ nanospheres as a reaction vessel to facilitate dinuclear Cu(I) catalyzed cyclization reactions

Sergio Gonell, Xavier Caumes, Nicole Orth, Ivana Ivanović-Burmazović and Joost. N. H. Reek*

General methods **2**

1. Synthesis and characterization of the compounds **3**

2. Encapsulation studies **6**

2.1 2D ^{1}H-DOSY spectra 6

2.2 CSI-HRMS 8

3. Catalytic experiments 30

3.1 Nanoconcentraor effect 31

3.2 Control experiments 32

3.3 Higher TON experiment 33

3.4 Kinetic analysis and detection of intermediates 34

4. Spectra **45**

4.1 ^{1}H, ^{31}P and ^{13}C NMR spectra of **XantphosCu(I)** 45

4.2^{1}H, ^{31}P and ^{13}C NMR spectra of **SXantphos** 46

4.3 ^{1}H, ^{31}P and ^{13}C NMR spectra of **SXantphosCu(I)** 48

4.4 ^{1}H, ^{31}P and ^{13}C NMR spectra of **XantphosPt** 49

5. References **51**

General Methods

All operations were carried out by using standard Schlenk techniques under argon atmosphere unless otherwise stated. Solvents were distilled prior utilization by conventional methods and degassed by bubbling Ar at least during 30 min. NMR spectra were measured on a Bruker AMX 400, DRX 500 and DRX 300 spectrometer. ^{1}H NMR spectral data were referenced to solvent residual signal (5.32 for CD_2Cl_2, 1.94 ppm for CD_3CN). ^{13}C NMR chemical shifts are reported relative to deuterated solvents [53.8 for CD_2Cl_2, 118.26 for CD_3CN]. 2D ^{1}H-DOSY were performed on a DRX 500 spectrometer with temperature and gradient calibration prior to the measurements, and the temperature was controlled at 298 K during the measurements.

Mass spectra were collected on an AccuToF LC, JMS-T100LP Mass spectrometer (JEOL, Japan) (for ESI) and AccuToF GC v 4g, JMST100GCV Mass spectrometer (JEOL, Japan) (for FD). Elemental analysis was performed by Microanalytisches Laboratorium Kolbe (Mulheim an der Ruhr, Germany). CSI-HRMS measurements for figure S3-S40 were recorded on a UHR-ToF Bruker Daltonik (Bremen, Germany) maXis, an ESI-quadrupole time-of-flight (qToF) mass spectrometer capable of resolution of at least 60.000 FWHM, which was coupled to a Bruker cryospray unit. Detection was in positive ion mode and the source voltage was 4 kV. The flow rates were 280 μL/hour. The drying gas (N_2) was held at –35 °C and the spray gas was held at –40 °C. The machine was calibrated prior to every experiment via direct infusion of the Agilent ESI-ToF low concentration tuning mixture, which provided an *m/z* range of singly charged peaks up to 2700 Da in both ion modes. CSI-HRMS measurement for figure S47 was recorded on a UHR-ToF Bruker Daltonik (Bremen, Germany) impact-II, an ESI-quadrupole time-of-flight (qToF) mass spectrometer capable of resolution of at least 40.000 FWHM, which was coupled to a Bruker cryospray unit. Detection was in positive ion mode and the source voltage was between 3.5 and 5 kV. The flow rates were 180 μL/hour. The drying gas (N2) was held at –35 °C and the spray gas was held at –40 °C. The machine was calibrated prior to every experiment via direct infusion of the TFA-Na solution, which provided an *m/z* range of singly charged peaks up to 3500 Da in both ion modes. All reagents were purchased from commercial suppliers and used without further purification. Compounds **HSXantphos**,[1] the spheres,[2] BuGu(OTf)[2] were synthesized according to reported procedures.

1. Synthesis and characterization of the compounds

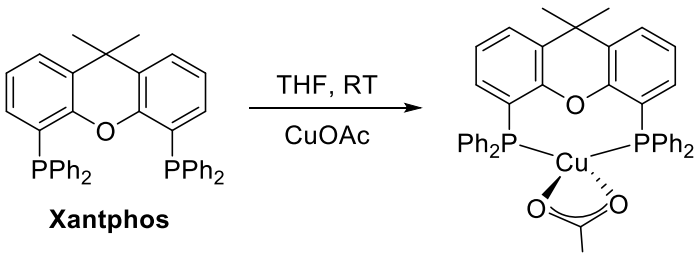

Xantphos **XantphosCu(I)**

XantphosCu(I): inside the globebox **Xantphos** (300 mg, 0.5 mmol) and CuOAc (63.8 mg, 0.5 mmol) were introduced in a Schlenk tube. Outside the globebox 20 mL of THF were added. The mixture was stirred at room temperature for 4 h. The solvent was removed on a rotatory evaporator. The crude was dissolved in dichloromethane and filtered to remove insoluble brown solids. Addition of pentane allowed precipitation of the desired product as a white solid, which was collected by filtration and washed with pentane. Yield: 342 mg, 97 %. ^{1}H NMR (400 MHz, CD_2Cl_2): δ 7.55 (dd, *J* = 7.8, 1.3 Hz, 2H, C*H*), 7.46 – 7.18 (m, 20H, C*H*), 7.11 (t, *J* = 7.7 Hz, 2H, C*H*), 6.61 (m, 2H, C*H*), 1.91 (bs, 3H, O_2CCH_3), 1.64 (s, 6H, $C(CH_3)_2$). ^{31}P{^{1}H} NMR (162 MHz, CD_2Cl_2): δ -17.42. ^{13}C{^{1}H} NMR (75 MHz, CD_2Cl_2): δ 179.1 (O_2CCH_3), 155.5 (*C*O), 134.1 (C_q), 132.6 (C_q), 131.8 (*C*H), 130.1 (*C*H), 128.9 (*C*H), 127.0 (*C*H), 124.8 (*C*H), 120.6 (C_q), 36.2 (CCH_3), 28.2 (CCH_3), 23.4 (O_2CCH_3). HRMS (ESI): 641.1236 $[M-OAc]^+$ (calculated 641.1224). Anal. Calcd for $CuP_2O_3C_{41}H_{35}$ (700.14): C, 70.23; H, 5.03. Found: C, 69.99; H, 5.49.

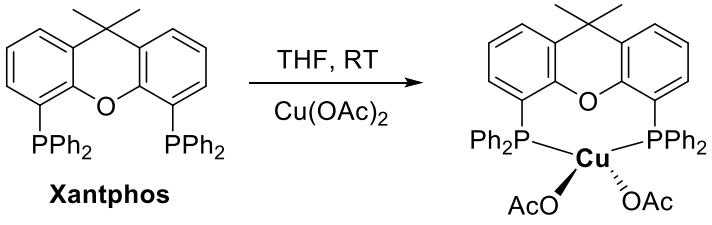

Xantphos **XantphosCu(II)**

XantphosCu(II): **Xantphos** (100 mg, 0.17 mmol) and $Cu(OAc)_2$ (30.9 mg, 0.17 mmol) were dissolved in 10 mL of THF. The blue mixture was stirred at room temperature for 1 h. The solvent was removed on a rotatory evaporator. The crude was dissolved in dichloromethane and filtered. Addition of pentane allowed precipitation of the desired product as a blue solid, which was collected by filtration and washed with pentane. Yield: 65 mg, 51 %. HRMS (FD): 700.1381 $[M-OAc]^+$ (calculated 700.1357). Anal. Calcd for $CuP_2O_5C_{43}H_{38}$ (759.15): C, 67.93; H, 5.04. Found: C, 67.62; H, 4.75.

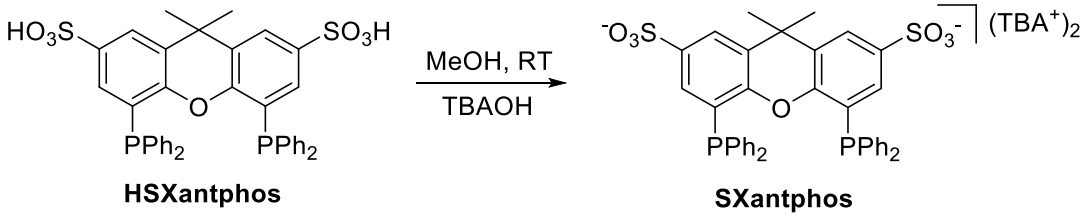

HSXantphos **SXantphos**

SXantphos: **HSXantphos** (400 mg, 0.54 mmol) was dissolved in 2 mL of MeOH. To this solution 1.08 mL of tetrabutylammonium hydroxide (TBAOH) in MeOH (1 M) were added dropwise. The mixture was stirred at room temperature 5 min. The solvent was removed under vacuum. The residue was dissolved in 10 mL of CH_2Cl_2 and under aerobic conditions washed with water (3x5 mL). The organic phase was filtered through a thin pad a neutral alumina and the solvent was removed under vacuum, yielding **SXantphos** as white solid. Yield: 392.4 mg, 59 %. ^{1}H NMR (400 MHz, CD_3CN): δ 7.85 (d, $^{4}J_{H\text{-}H}$ = 1.9 Hz, 2H, CH_{Xant}), 7.34 (m, 12H, CH_{Ph}), 7.15 (m, 8H, CH_{Ph}), 6.91 (m, 2H, CH_{Xant}), 3.08 (m, 16H, Bu_4N CH_2), 1.63 (s, 6H, C(CH_3)$_2$), 1.59 (m, 16H, Bu_4N CH_2), 1.35 (m, 16H, Bu_4N CH_2), 0.96 (t, $^{3}J_{H\text{-}H}$ = 7.3 Hz, 24H, Bu_4N CH_3). ^{31}P{^{1}H} NMR (162 MHz, CD_3CN): δ -17.78. ^{13}C{^{1}H} NMR (75 MHz, CD_3CN): δ 153.1 (t, J = 3.8 Hz, *C*O), 145.6 (C_q), 138.0 (t, J = 2.5 Hz, C_q), 134.8 (t, J = 4.2 Hz, *C*H), 130.5 (C_q), 130.2 (*C*H), 129.7 (*C*H), 129.5 (*C*H), 125.8 (t, J = 4.1 Hz), 125.3 (*C*H), 59.3 (Bu_4N *C*H_2), 35.6 (*C*CH_3), 31.8 (C*C*H_3), 24.3 (Bu_4N *C*H_2), 20.3 (Bu_4N *C*H_2), 13.8 (Bu_4N *C*H_3). HRMS (ESI): 368.0489 [M−2TBA]$^-$ (calculated 368.0454), 978.3772 [M−TBA]$^-$ (calculated 978.3756). Anal. Calcd for $P_2S_2O_7N_2C_{71}H_{102}(H_2O)_2$ (1256.68): C, 67.80; H, 8.50; N, 2.23. Found: C, 67.85; H, 8.38; N, 2.05.

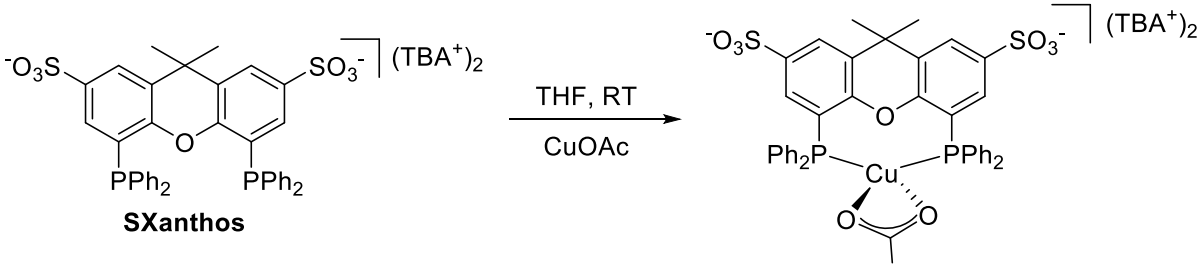

SXanthos **SXantphosCu(I)**

SXantphosCu(I): inside the globebox **SXantphos** (100 mg, 0.082 mmol) and CuOAc (10.35 mg, 0.082 mmol) were introduced in a Schlenk tube. Outside the globebox 30 mL of THF were added. The reaction was stirred at room temperature for 4 h. Under aerobic conditions, the mixture was filtrated. The solvent was removed under vacuum. The crude was dissolved in the minimum amount of dichloromethane and precipitated with ether. The mixture was stored at 5 ºC for 1 hour. Then, the white solid was collected by filtration and washed with diethyl ether.

Yield: 57.6 mg, 52 %. ^{1}H NMR (400 MHz, CD_3CN): δ 7.98 (d, $^{4}J_{H\text{-}H}$ = 1.9 Hz, 2H, CH_{Xant}), 7.37 (m, 20H, CH_{Ph}), 7.02 (m, 2H, CH_{Xant}), 3.08 (m, 16H, Bu_4N CH_2), 1.64 (s, 6H, C(CH_3)$_2$), 1.59 (m, 16H, Bu_4N CH_2), 1.35 (m, 16H, Bu_4N CH_2), 0.97 (t, $^{3}J_{H\text{-}H}$, 24H, Bu_4N CH_3). The signal corresponding to the protons of the acetate ligand were not observed, probably because its broadening and the overlap with the residual signal of CD_3CN. ^{31}P{^{1}H} NMR (162 MHz, CD_3CN): δ -16.3. ^{13}C{^{1}H} NMR (75 MHz, CD_3CN): δ 155.7 (*C*O), 146.6 (C_q), 134.8 (*C*H), 134.1 (C_q), 133.3 (C_q), 130.9 (*C*H), 129.8 (*C*H), 129.6 (*C*H), 125.3 (*C*H), 121.0 (C_q), 59.3 (Bu_4N *C*H_2), 37.0 (C*C*H_3), 28.2 (C*C*H_3), 24.3 (Bu_4N *C*H_2), 20.3 (Bu_4N *C*H_2), 13.8 (Bu_4N *C*H_3). The signals corresponding to the carbonyl and the methyl groups of the acetate ligand were not observed. This situation is in agreement with previous Cu based complexes reported in the literature containing an acetate ligand.[3] HRMS (ESI): 799.0177 [M−2TBA−OAc]$^{-}$ (calculated 799.0204). 737.1003 [2M−2OAc+Na]$^{-}$ (calculated 737.0941). Anal. Calcd for $CuP_2S_2O_9N_2C_{73}H_{105}(H_2O)_2$ (1378.62): C, 63.52; H, 7.92; N, 2.03. Found: C, 63.40; H, 7.42; N, 2.02.

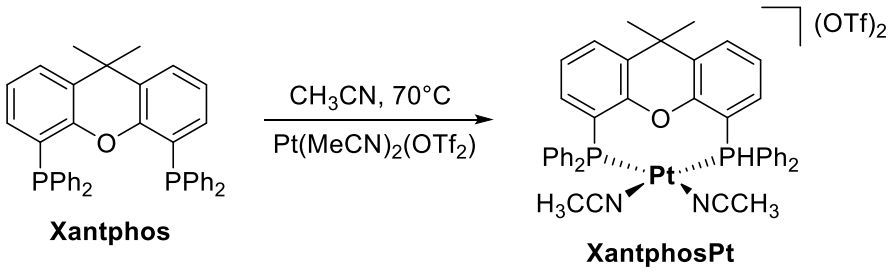

Xantphos **XantphosPt**

XantphosPt: **Xantphos** (50 mg, 0.084 mmol) and $Pt(MeCN)_4(OTf)_2$ (54.6 mg, 0.084 mmol) were dissolved in 10 mL of MeCN and the mixture was stirred at 70°C overnight. At room temperature the solvent was removed under vacuum till almost dryness. Addition of diethyl ether allowed precipitation the desired product as a white solid, which was collected by filtration and washed with diethyl ether. Yield: 85.4 mg, 87 %. ^{1}H NMR (400 MHz, CD_3CN): δ 7.98 (d, $^{3}J_{H\text{-}H}$ = 7.7 Hz, 2H, C*H*), 7.42 (m, 16H, C*H*), 7.27 (m, 8H, C*H*), 1.90 (s, 6H, C(CH_3)$_2$). ^{31}P{^{1}H} NMR (162 MHz, CD_3CN): δ 7.7 ($^{1}J_{P\text{-}Pt}$ = 3793.6 Hz). ^{13}C{^{1}H} NMR (75 MHz, CD_3CN): δ 156.5 (*C*O), 137.8 (C_q), 135.3 (*C*H), 134.3 (C_q), 133.7 (*C*H), 131.4 (*C*H), 130.6 (*C*H), 130.3 (*C*H), 127.9 (*C*H), 124.8 (C_q), 38.4 (C*C*H_3), 26.7 (C*C*H_3). HRMS (FD): 872.1783 [M−2OTf+OH]$^{+}$ (calculated 872.2138). Anal. Calcd for $PtP_2N_2O_7S_2F_6C_{45}H_{38}$ (1153.11): C, 46.84; H, 3.32; N, 2.43. Found: C, 46.27; H, 3.81; N, 1.98.

2. Encapsulation studies

2.1 2D ^{1}H-DOSY spectra

All tests were performed in CD_3CN at 298 K. 10/24 mM (0.42 mM) sphere solutions were used, and the required amounts of **SXantphosCu** (in stock solutions) was added. The spheres have very large size and accordingly, very small diffusion coefficient (*D*). On the contrary, **SXantphosCu** is much smaller and has significantly bigger diffusion coefficient. So in the DOSY measurements, if the band of the (bound) guest signals was in the same line with that of the sphere, this means the guest and the sphere have the same *D* and it was considered as the case strong binding.

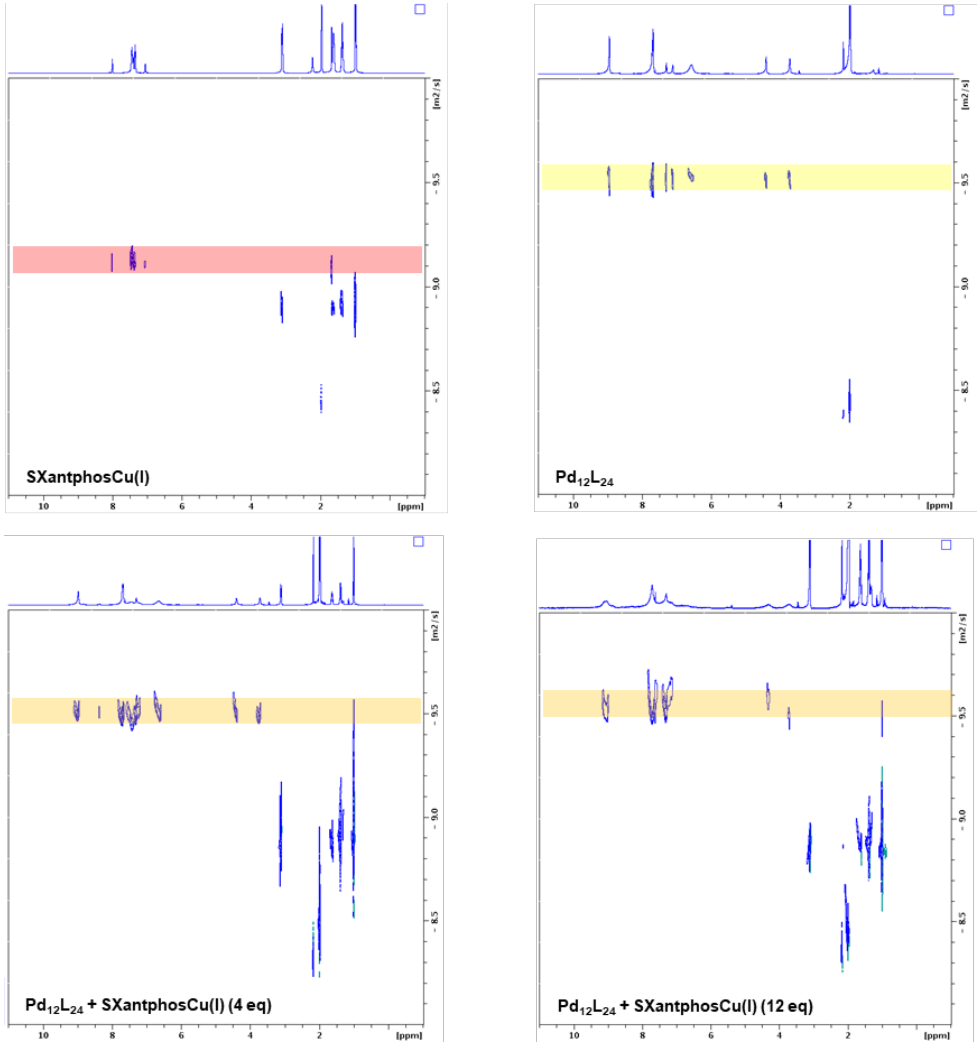

Figure S1. 2D ^{1}H-DOSY (298 K, CD_3CN) of the free **SXantphosCu(I)** (top left), $Pd_{12}L_{24}$ without any guest (top right), $Pd_{12}L_{24}$ + 4 equivalents of **SXantphosCu(I)** (bottom left) and $Pd_{12}L_{24}$ + 12 equivalents of **SXantphosCu(I)** (bottom right).

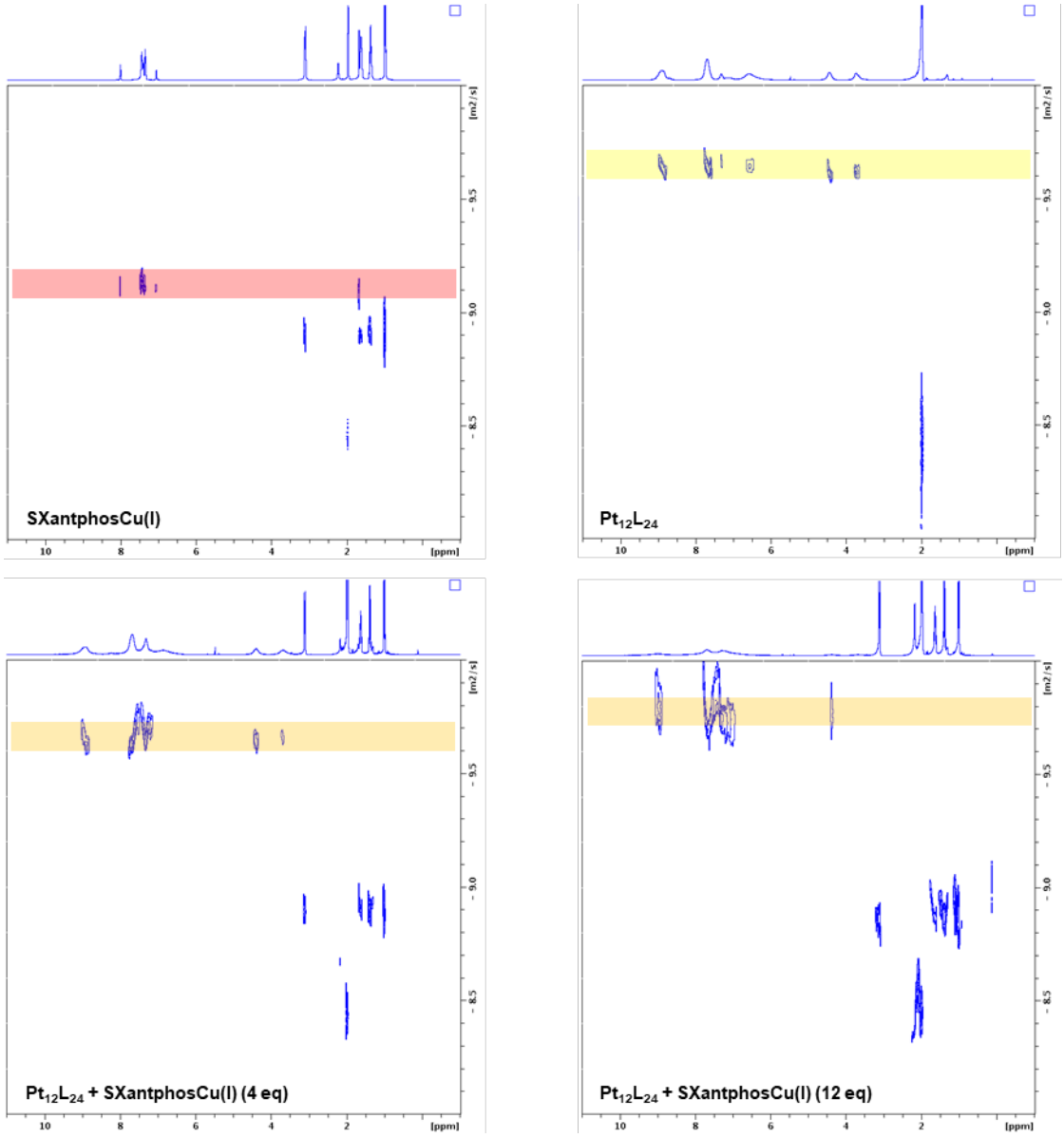

Figure S2. 2D ^{1}H-DOSY (298 K, CD_3CN) of the free **SXantphosCu(I)** (top left), $Pt_{12}L_{24}$ without any guest (top right), $Pt_{12}L_{24}$ + 4 equivalents of **SXantphosCu(I)** (bottom left) and $Pt_{12}L_{24}$ + 12 equivalents of **SXantphosCu(I)** (bottom right).

2.2 CSI-HRMS

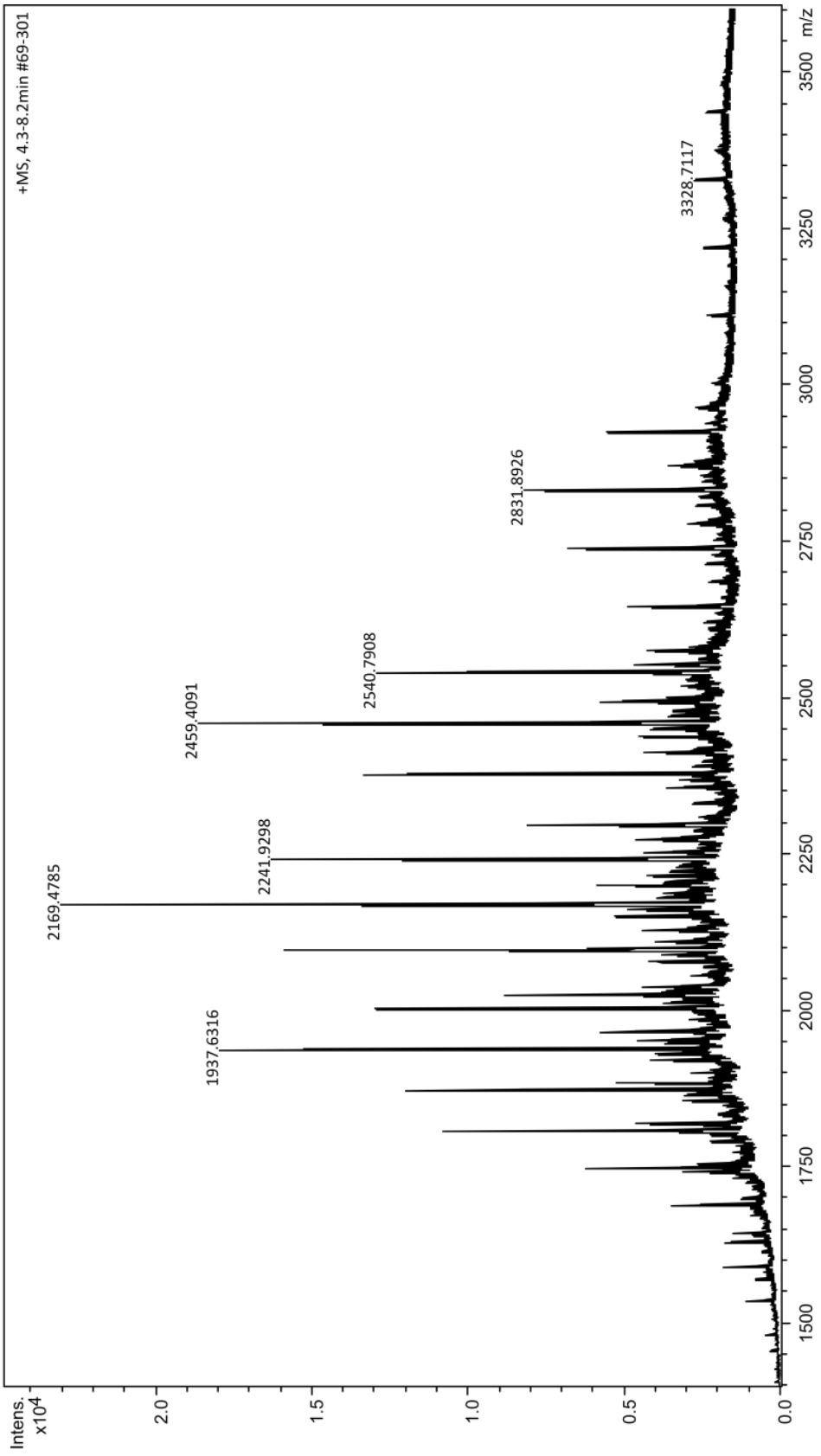

Figure S3. UHR CSI-TOF mass spectrum (full spectrum) of the sphere $(Pd_{12}L_{24})(OTf)_{48}$ with 4 eq. of **SXanpthosCu(I)** added, with a spray temperature of –40 ºC and dry gas temperature of –35 ºC

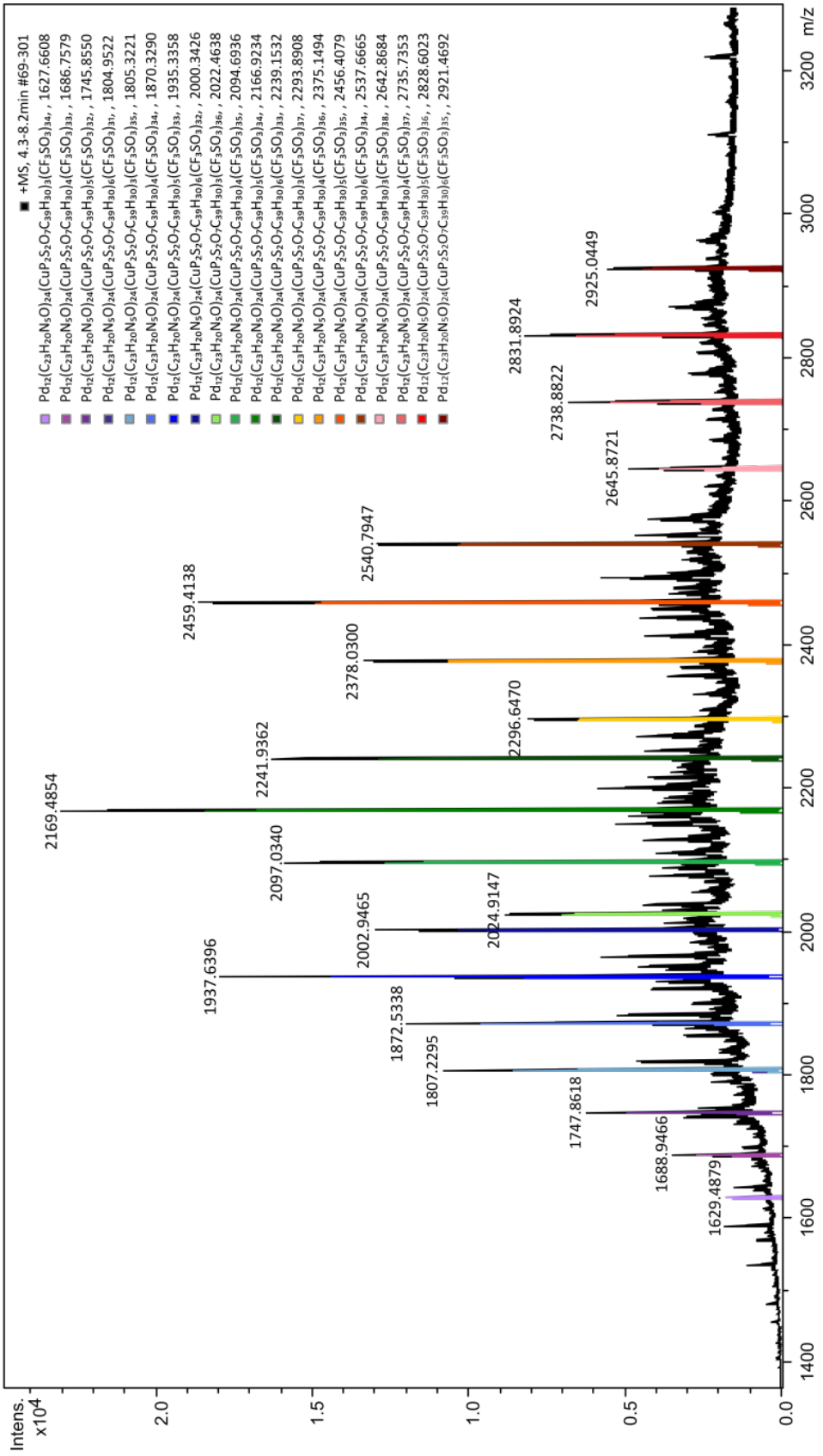

Figure S4. UHR CSI-TOF mass spectrum (full spectrum) of the sphere $(Pd_{12}L_{24})(OTf)_{48}$ with 4 eq. of **SXanpthosCu(I)** added, along with simulated isotopic patterns (in color) overlaid

Table S1. Different charged species observed in the CSI-TOF mass spectrum of the sphere $(Pd_{12}L_{24})(OTf)_{48}$ ($Pd_{12}(C_{23}H_{20}N_5O)_{24}(CF_3SO_3)_{48}$) with 4 eq. of **SXanpthosCu(I)** ($CuP_2S_2O_7C_{39}H_{30}$) added and the corresponding found and calculated [m/z]. Note that in all cases the mass corresponding to the **SXanpthosCu(I)** does not involve the TBA counter-cation and the acetate co-ligand as they are not encapsulated within the sphere

Species	Charge	Found [m/z]	Calculated [m/z]
$Pd_{12}(C_{23}H_{20}N_5O)_{24}(CuP_2S_2O_7C_{39}H_{30})_3(CF_3SO_3)_{34}$	11+	1629.4785	1629.4813
$Pd_{12}(C_{23}H_{20}N_5O)_{24}(CuP_2S_2O_7C_{39}H_{30})_4(CF_3SO_3)_{33}$	11+	1688.6670	1688.6694
$Pd_{12}(C_{23}H_{20}N_5O)_{24}(CuP_2S_2O_7C_{39}H_{30})_5(CF_3SO_3)_{32}$	11+	1747.8530	1747.8575
$Pd_{12}(C_{23}H_{20}N_5O)_{24}(CuP_2S_2O_7C_{39}H_{30})_6(CF_3SO_3)_{31}$	11+	1807.2210	1807.2274
$Pd_{12}(C_{23}H_{20}N_5O)_{24}(CuP_2S_2O_7C_{39}H_{30})_3(CF_3SO_3)_{35}$	10+	1807.2210	1807.2247
$Pd_{12}(C_{23}H_{20}N_5O)_{24}(CuP_2S_2O_7C_{39}H_{30})_4(CF_3SO_3)_{34}$	10+	1872.5256	1872.5316
$Pd_{12}(C_{23}H_{20}N_5O)_{24}(CuP_2S_2O_7C_{39}H_{30})_5(CF_3SO_3)_{33}$	10+	1937.6316	1937.6385
$Pd_{12}(C_{23}H_{20}N_5O)_{24}(CuP_2S_2O_7C_{39}H_{30})_6(CF_3SO_3)_{32}$	10+	2002.6382	2002.6454
$Pd_{12}(C_{23}H_{20}N_5O)_{24}(CuP_2S_2O_7C_{39}H_{30})_3(CF_3SO_3)_{36}$	9+	2024.6845	2024.6888
$Pd_{12}(C_{23}H_{20}N_5O)_{24}(CuP_2S_2O_7C_{39}H_{30})_4(CF_3SO_3)_{35}$	9+	2097.1374	2097.1409
$Pd_{12}(C_{23}H_{20}N_5O)_{24}(CuP_2S_2O_7C_{39}H_{30})_5(CF_3SO_3)_{34}$	9+	2169.4785	2169.4819
$Pd_{12}(C_{23}H_{20}N_5O)_{24}(CuP_2S_2O_7C_{39}H_{30})_6(CF_3SO_3)_{33}$	9+	2241.8198	2241.8229
$Pd_{12}(C_{23}H_{20}N_5O)_{24}(CuP_2S_2O_7C_{39}H_{30})_3(CF_3SO_3)_{37}$	8+	2296.3917	2296.3939
$Pd_{12}(C_{23}H_{20}N_5O)_{24}(CuP_2S_2O_7C_{39}H_{30})_4(CF_3SO_3)_{36}$	8+	2377.9002	2377.9026
$Pd_{12}(C_{23}H_{20}N_5O)_{24}(CuP_2S_2O_7C_{39}H_{30})_5(CF_3SO_3)_{35}$	8+	2459.2830	2459.2862
$Pd_{12}(C_{23}H_{20}N_5O)_{24}(CuP_2S_2O_7C_{39}H_{30})_6(CF_3SO_3)_{34}$	8+	2540.6667	2540.6699
$Pd_{12}(C_{23}H_{20}N_5O)_{24}(CuP_2S_2O_7C_{39}H_{30})_3(CF_3SO_3)_{38}$	7+	2645.8695	2645.8720
$Pd_{12}(C_{23}H_{20}N_5O)_{24}(CuP_2S_2O_7C_{39}H_{30})_4(CF_3SO_3)_{37}$	7+	2738.8809	2738.8819
$Pd_{12}(C_{23}H_{20}N_5O)_{24}(CuP_2S_2O_7C_{39}H_{30})_5(CF_3SO_3)_{36}$	7+	2831.8926	2831.8918
$Pd_{12}(C_{23}H_{20}N_5O)_{24}(CuP_2S_2O_7C_{39}H_{30})_6(CF_3SO_3)_{35}$	7+	2924.9031	2924.9016

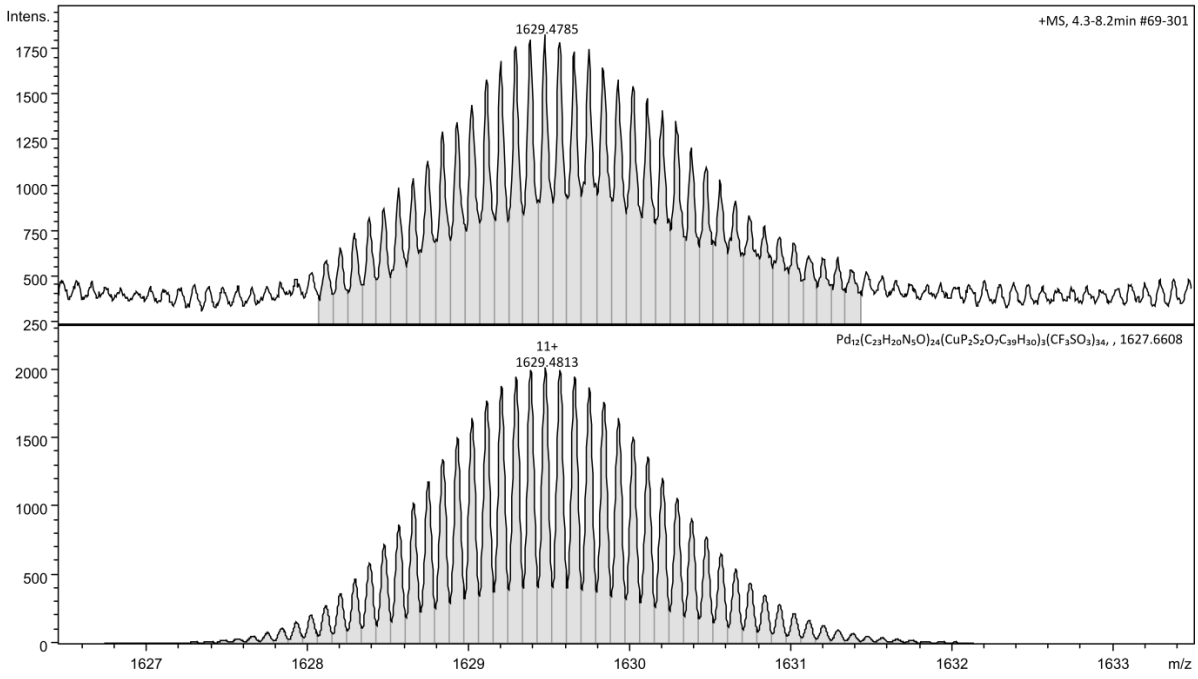

Figure S5. Expanded spectrum for the charged species $[Pd_{12}L_{24}(\mathbf{SXanpthosCu(I)})_3(OTf)_{34}]^{11+}$ observed (above) in the UHR CSI-TOF mass spectrum and simulated isotopic distribution (below)

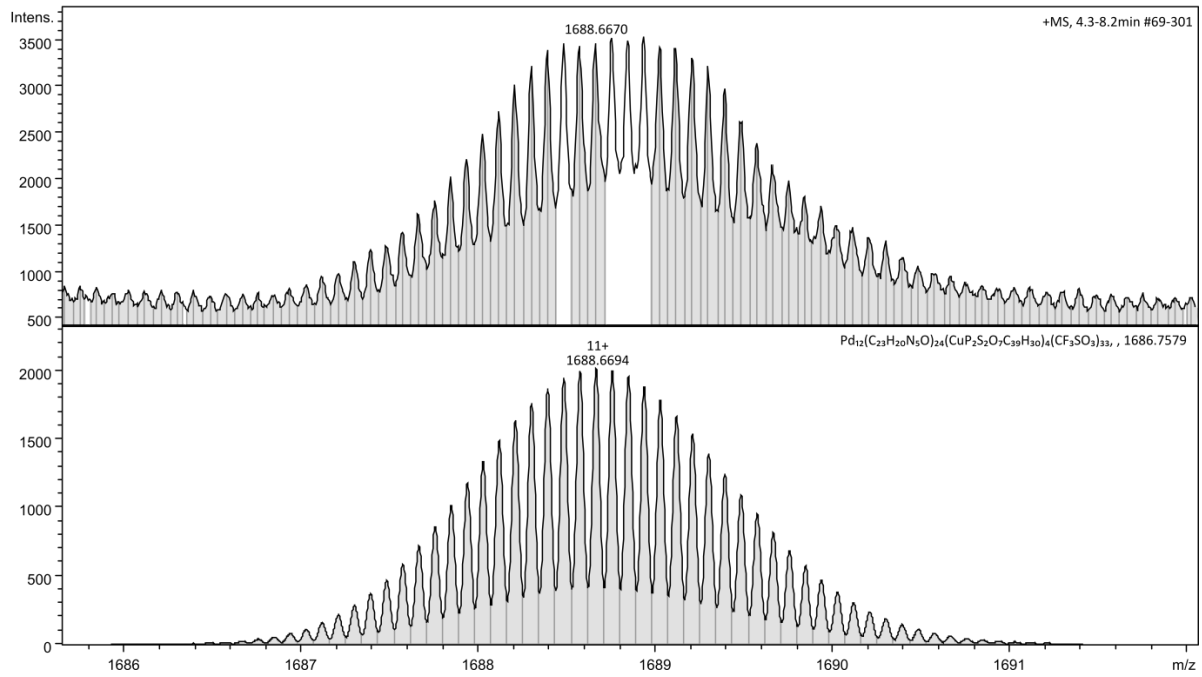

Figure S6. Expanded spectrum for the charged species $[Pd_{12}L_{24}(\mathbf{SXanpthosCu(I)})_4(OTf)_{33}]^{11+}$ observed (above) in the UHR CSI-TOF mass spectrum and simulated isotopic distribution (below)

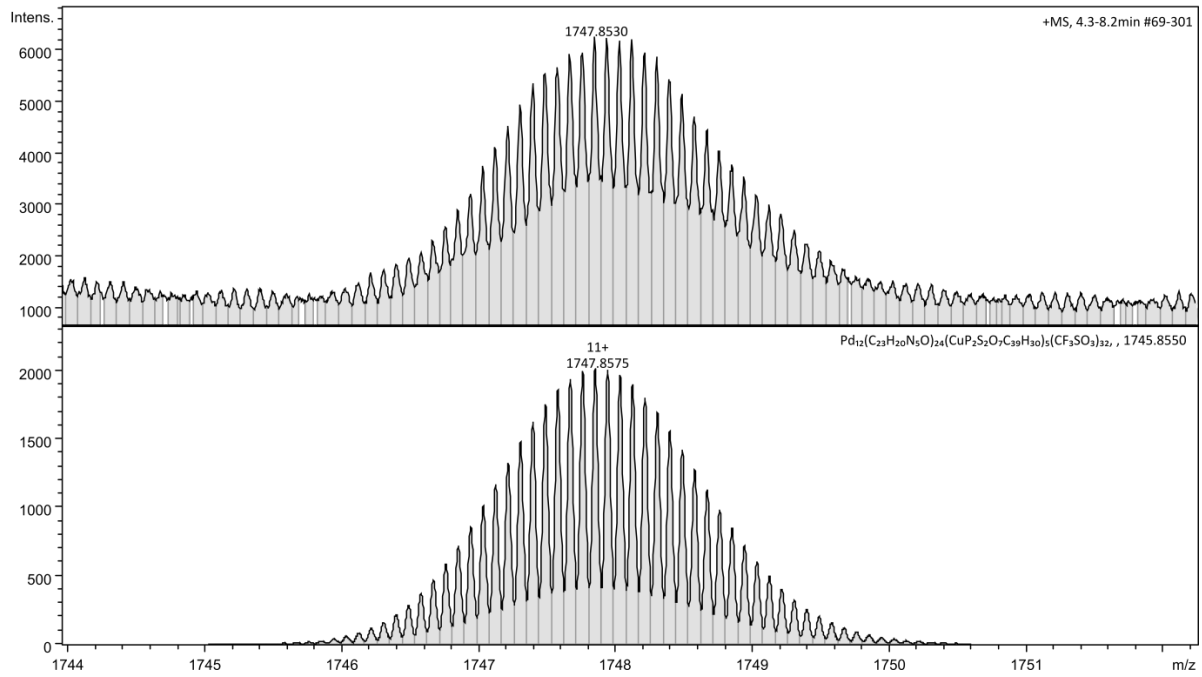

Figure S7. Expanded spectrum for the charged species $[Pd_{12}L_{24}(\mathbf{SXanpthosCu(I)})_5(OTf)_{32}]^{11+}$ observed (above) in the UHR CSI-TOF mass spectrum and simulated isotopic distribution (below)

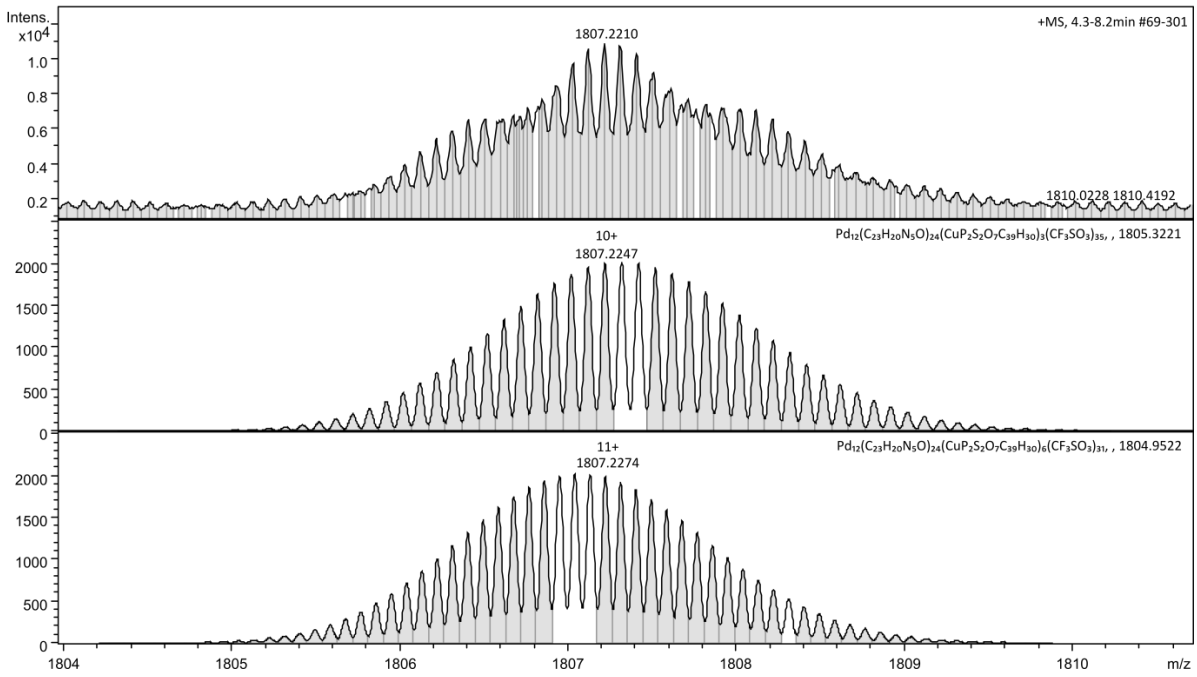

Figure S8. Expanded spectrum for the charged species $[Pd_{12}L_{24}(\mathbf{SXanpthosCu(I)})_3(OTf)_{35}]^{10+}$+ $[Pd_{12}L_{24}(\mathbf{SXanpthosCu})_6(OTf)_{31}]^{11+}$ observed (above) in the UHR CSI-TOF mass spectrum and simulated isotopic distribution (below)

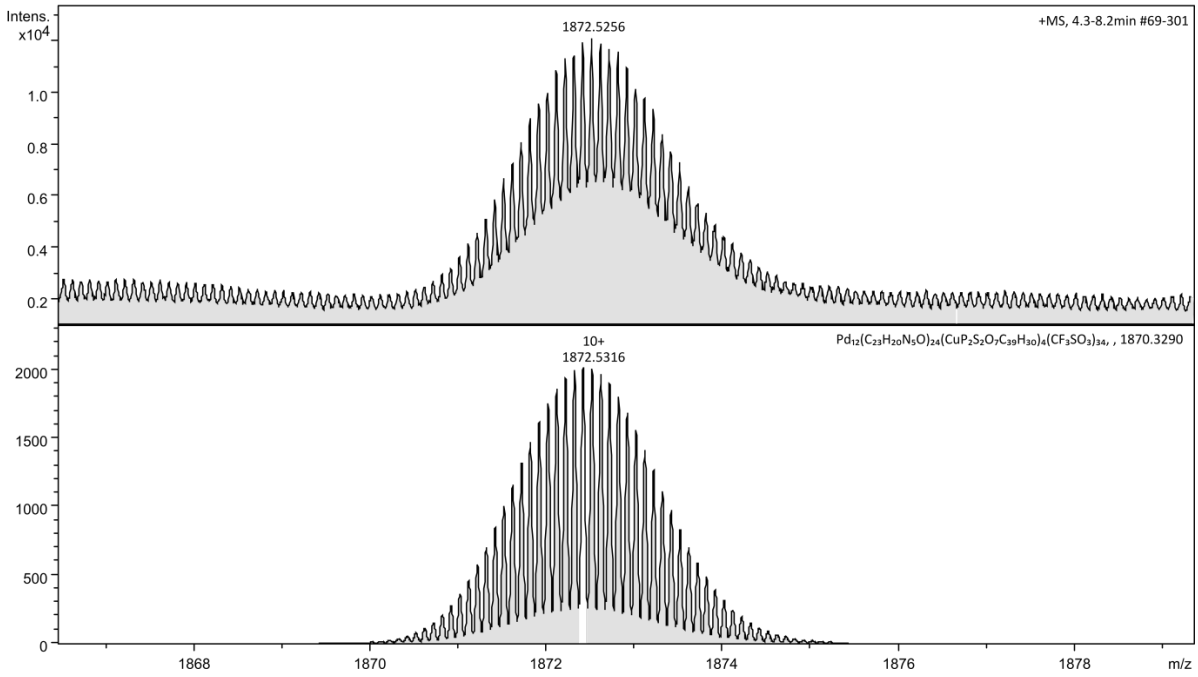

Figure S9. Expanded spectrum for the charged species $[Pd_{12}L_{24}(\mathbf{SXanpthosCu(I)})_4(OTf)_{34}]^{10+}$ observed (above) in the UHR CSI-TOF mass spectrum and simulated isotopic distribution (below)

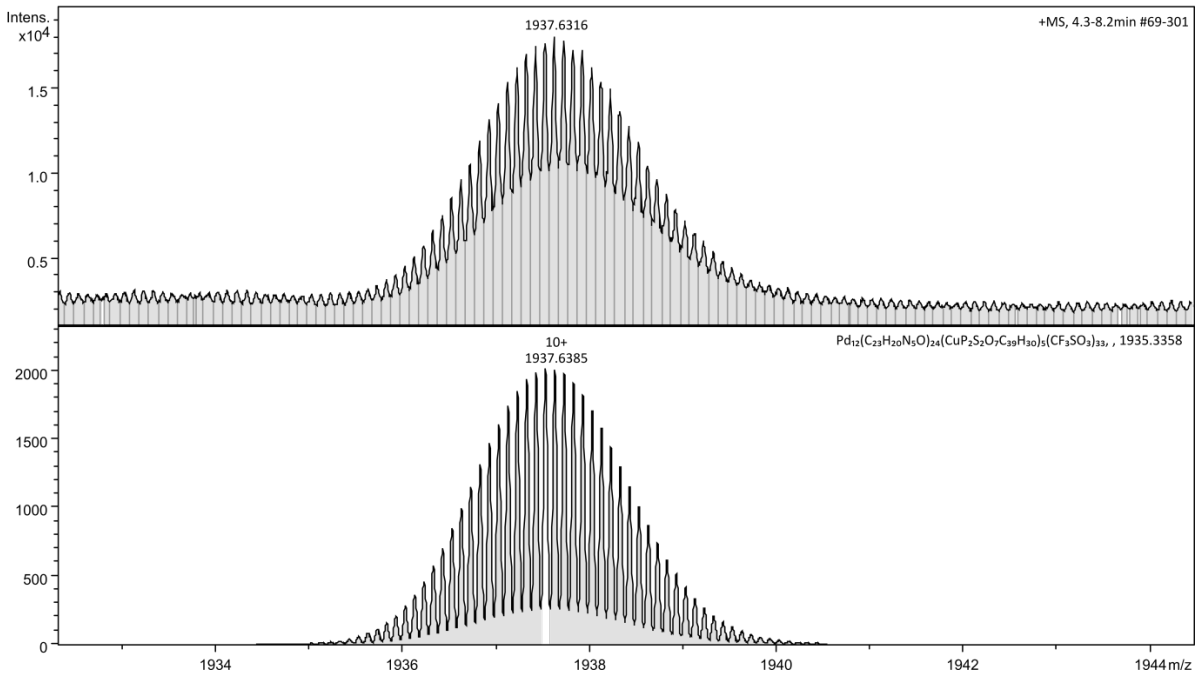

Figure S10. Expanded spectrum for the charged species $[Pd_{12}L_{24}(\mathbf{SXanpthosCu(I)})_5(OTf)_{33}]^{10+}$ observed (above) in the UHR CSI-TOF mass spectrum and simulated isotopic distribution (below)

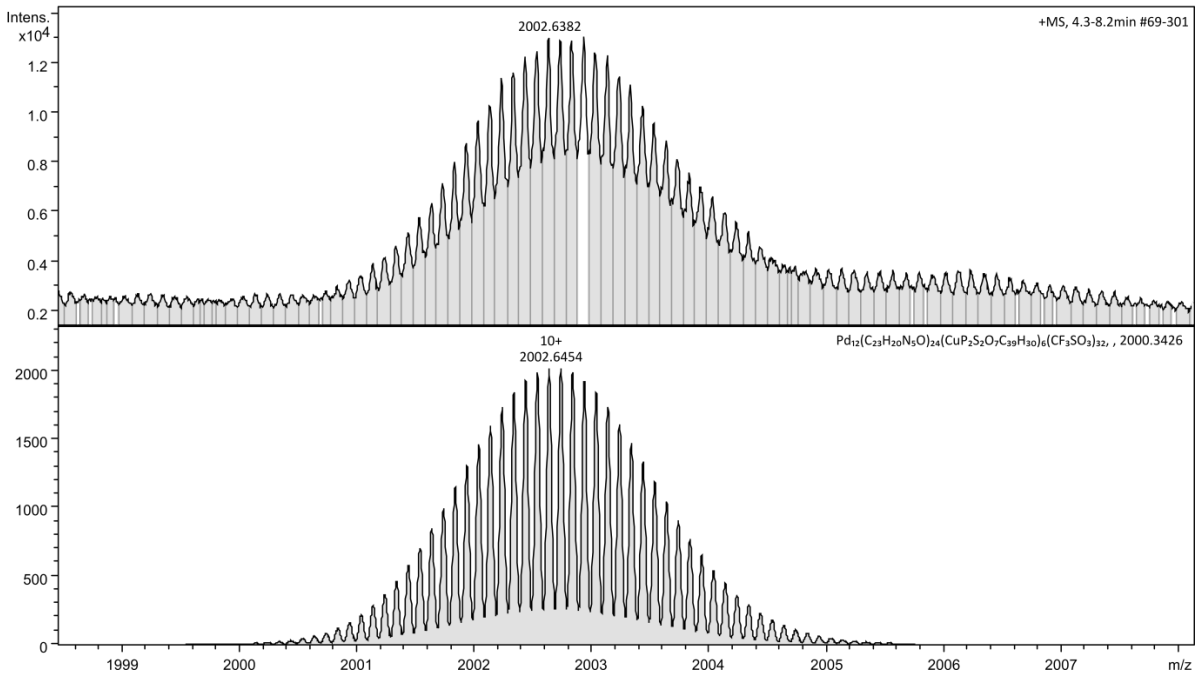

Figure S11. Expanded spectrum for the charged species $[Pd_{12}L_{24}(\mathbf{SXanpthosCu(I)})_6(OTf)_{32}]^{10+}$ observed (above) in the UHR CSI-TOF mass spectrum and simulated isotopic distribution (below)

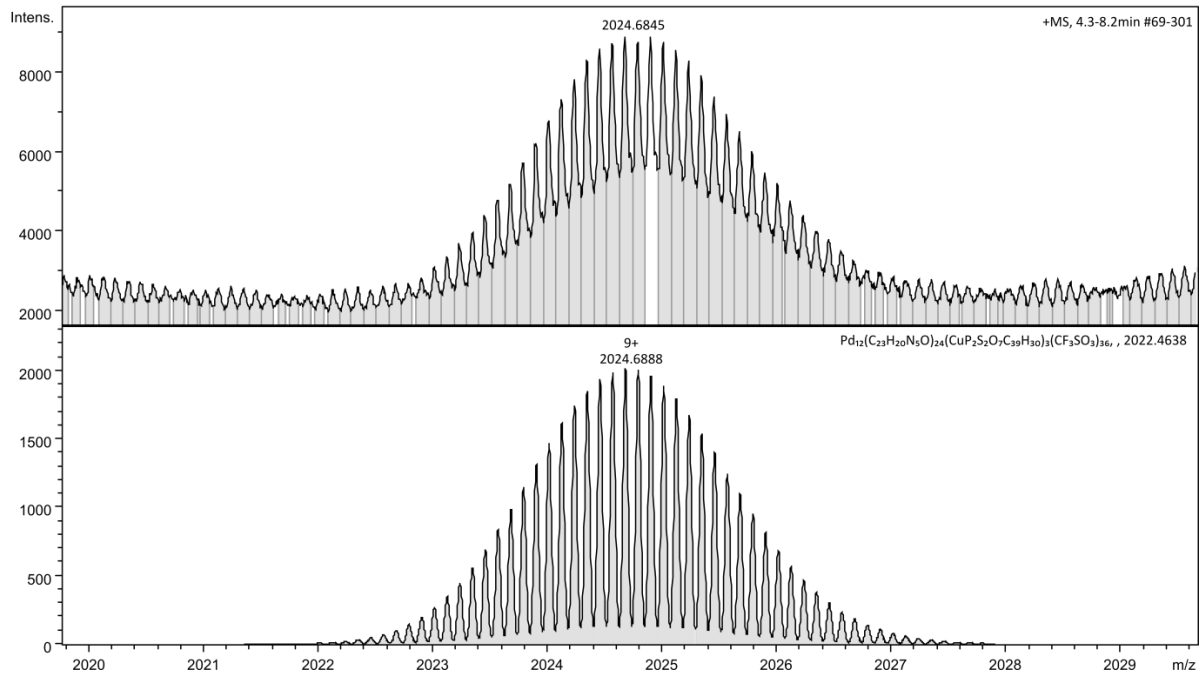

Figure S12. Expanded spectrum for the charged species $[Pd_{12}L_{24}(\mathbf{SXanpthosCu(I)})_3(OTf)_{36}]^{9+}$ observed (above) in the UHR CSI-TOF mass spectrum and simulated isotopic distribution (below)

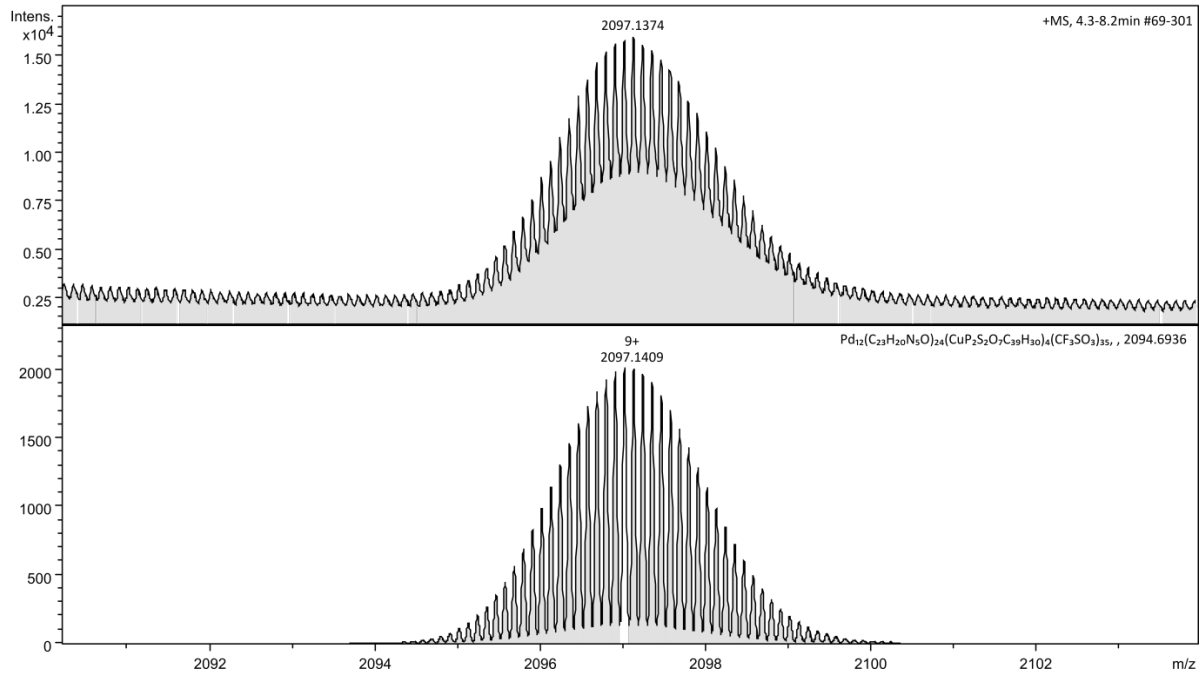

Figure S13. Expanded spectrum for the charged species $[Pd_{12}L_{24}(\mathbf{SXanpthosCu(I)})_4(OTf)_{35}]^{9+}$ observed (above) in the UHR CSI-TOF mass spectrum and simulated isotopic distribution (below)

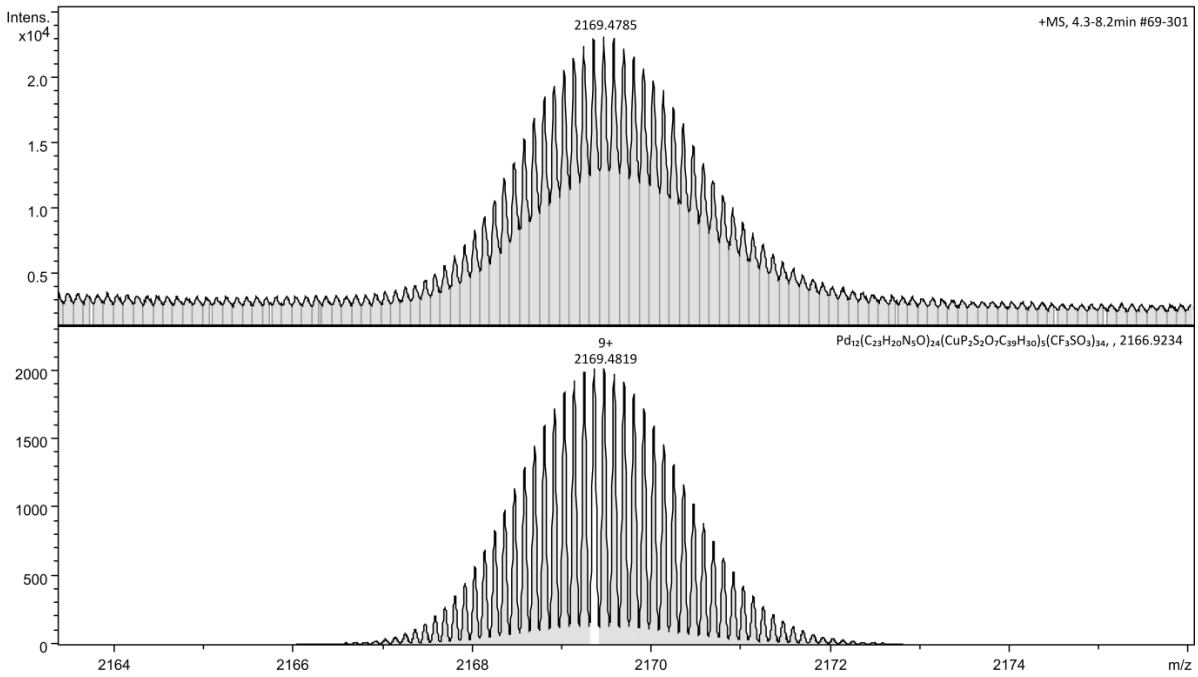

Figure S14. Expanded spectrum for the charged species $[Pd_{12}L_{24}(\mathbf{SXanpthosCu(I)})_5(OTf)_{34}]^{9+}$ observed (above) in the UHR CSI-TOF mass spectrum and simulated isotopic distribution (below).

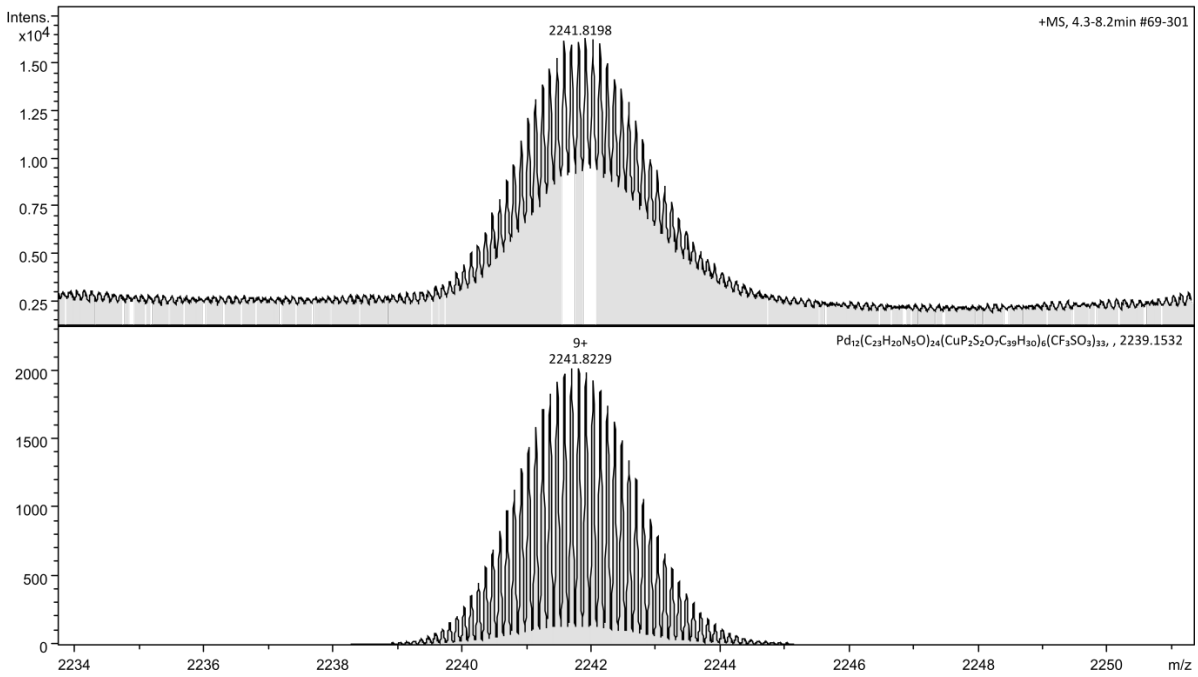

Figure S15. Expanded spectrum for the charged species $[Pd_{12}L_{24}(\mathbf{SXanpthosCu(I)})_6(OTf)_{33}]^{9+}$ observed (above) in the UHR CSI-TOF mass spectrum and simulated isotopic distribution (below)

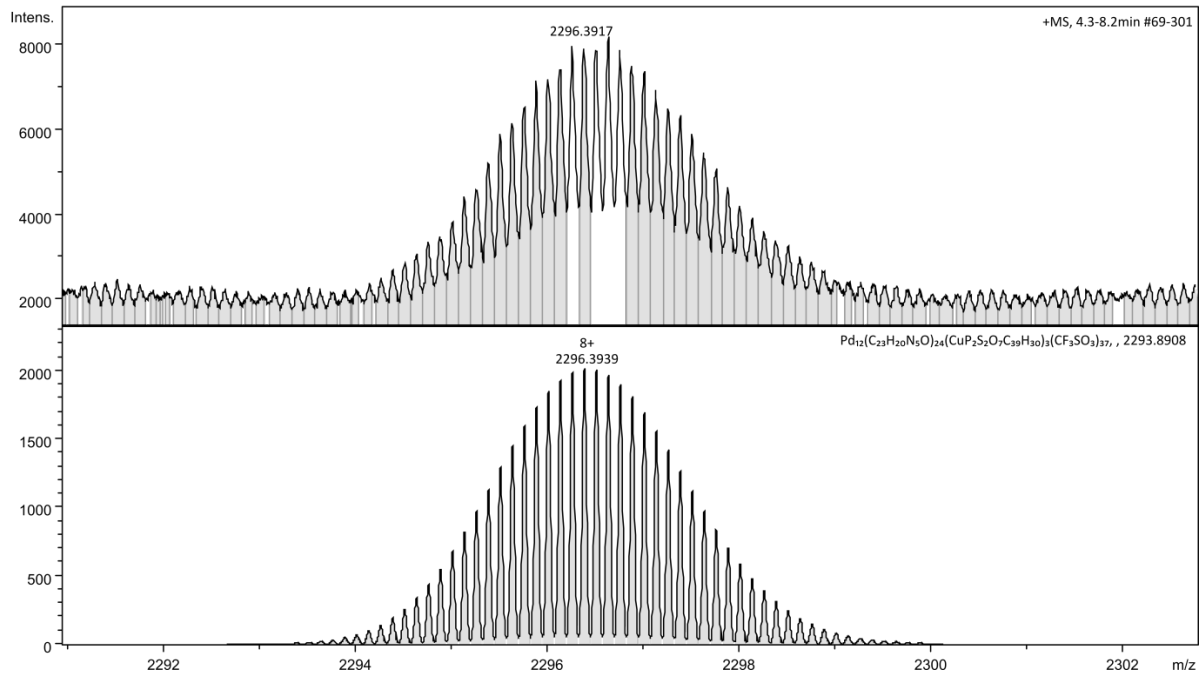

Figure S16. Expanded spectrum for the charged species $[Pd_{12}L_{24}(\mathbf{SXanpthosCu(I)})_3(OTf)_{37}]^{8+}$ observed (above) in the UHR CSI-TOF mass spectrum and simulated isotopic distribution (below)

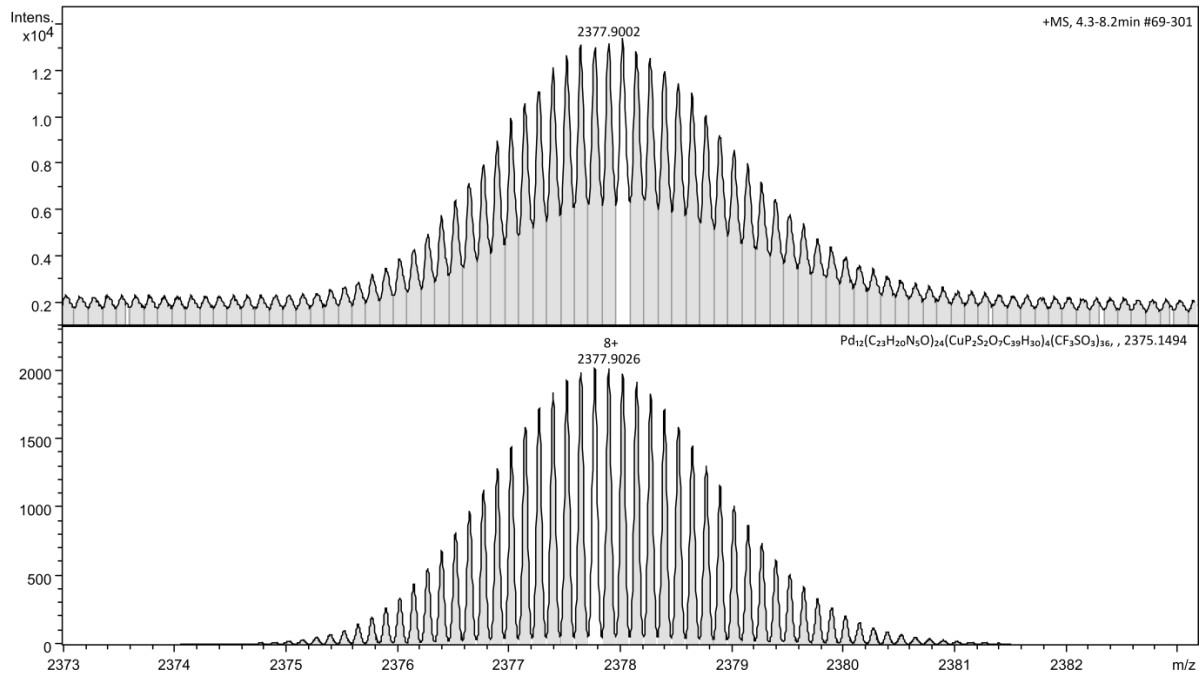

Figure S17. Expanded spectrum for the charged species $[Pd_{12}L_{24}(\mathbf{SXanpthosCu(I)})_4(OTf)_{36}]^{8+}$ observed (above) in the UHR CSI-TOF mass spectrum and simulated isotopic distribution (below)

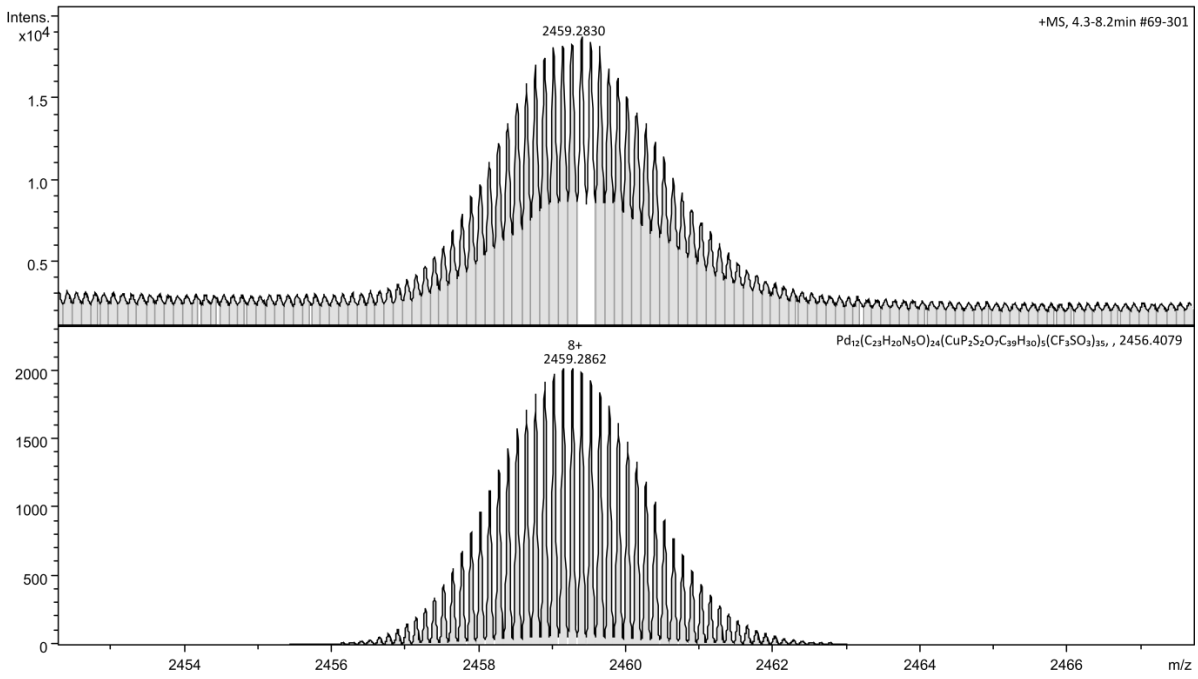

Figure S18. Expanded spectrum for the charged species $[Pd_{12}L_{24}(\mathbf{SXanpthosCu(I)})_5(OTf)_{35}]^{8+}$ observed (above) in the UHR CSI-TOF mass spectrum and simulated isotopic distribution (below)

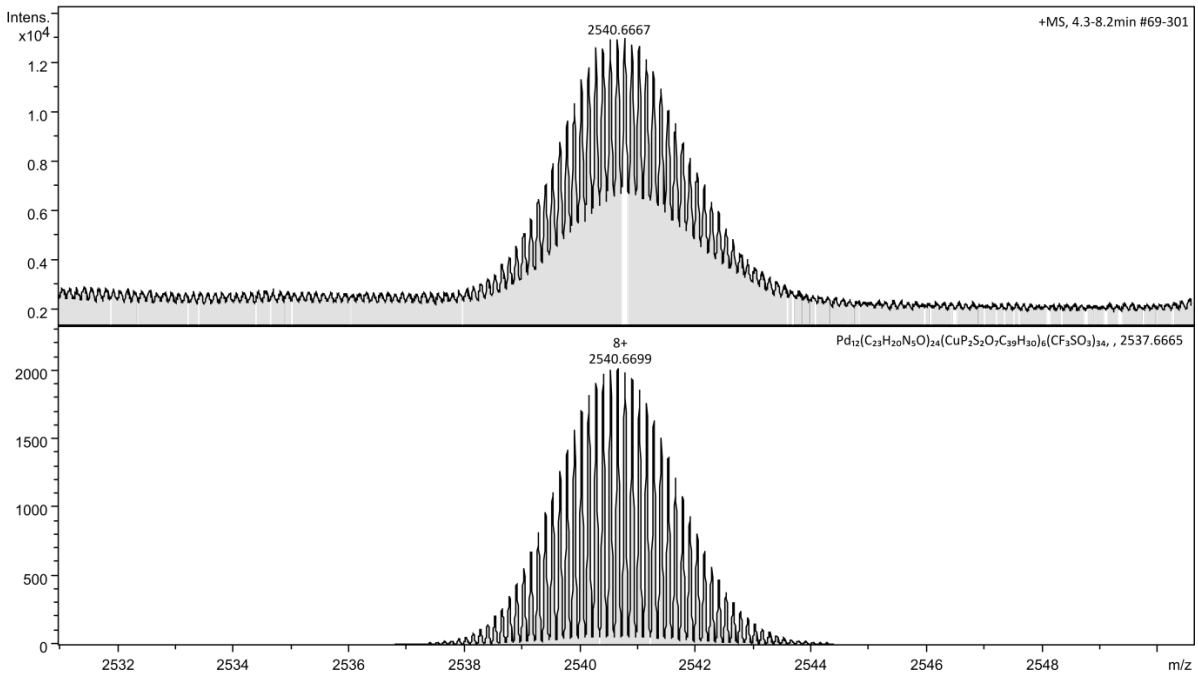

Figure S19. Expanded spectrum for the charged species $[Pd_{12}L_{24}(\mathbf{SXanpthosCu(I)})_6(OTf)_{34}]^{8+}$ observed (above) in the UHR CSI-TOF mass spectrum and simulated isotopic distribution (below)

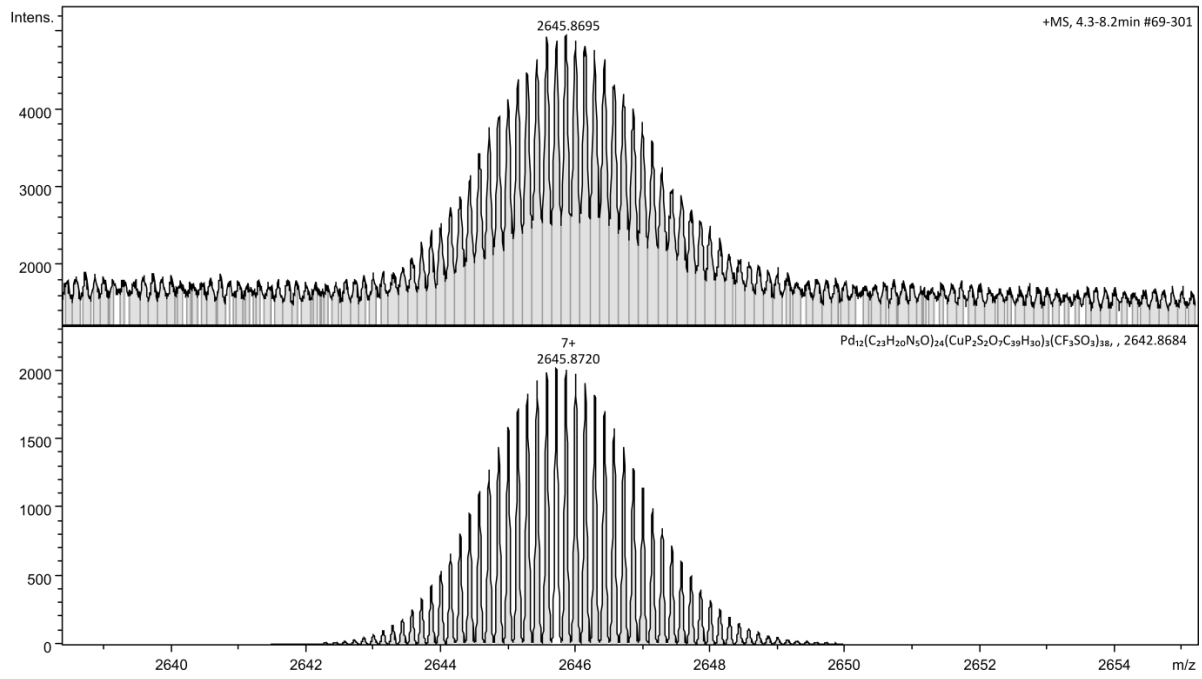

Figure S20. Expanded spectrum for the charged species $[Pd_{12}L_{24}(\mathbf{SXanpthosCu(I)})_3(OTf)_{38}]^{7+}$ observed (above) in the UHR CSI-TOF mass spectrum and simulated isotopic distribution (below)

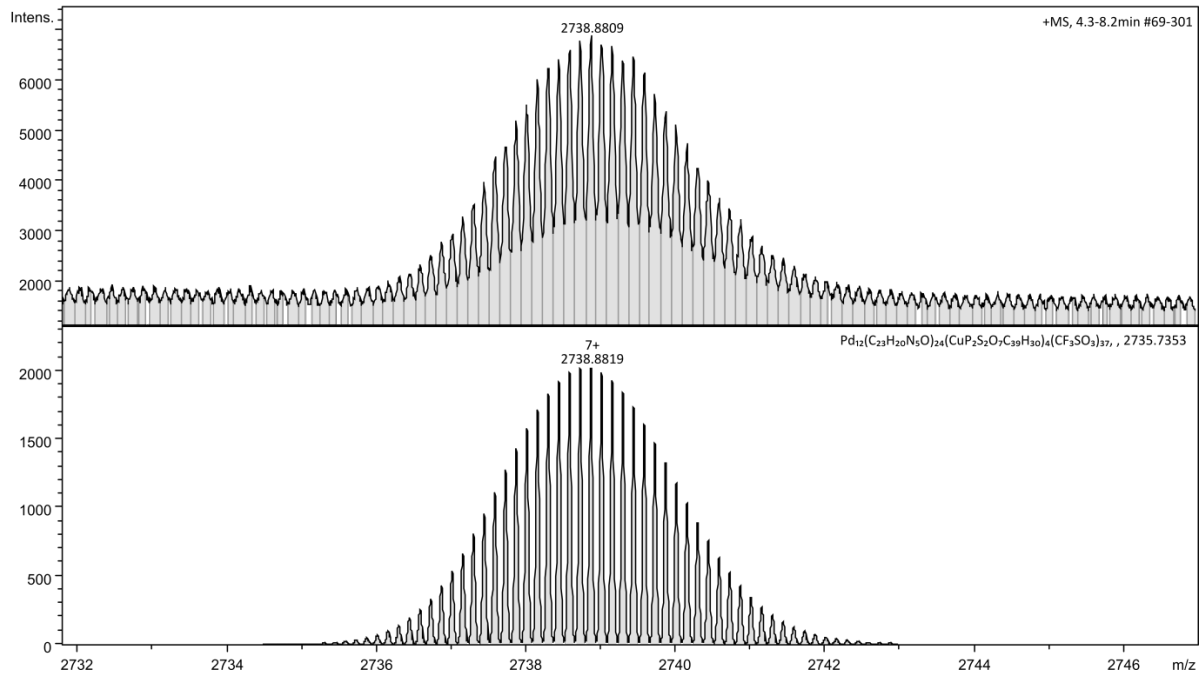

Figure S21. Expanded spectrum for the charged species $[Pd_{12}L_{24}(\mathbf{SXanpthosCu(I)})_4(OTf)_{37}]^{7+}$ observed (above) in the UHR CSI-TOF mass spectrum and simulated isotopic distribution (below)

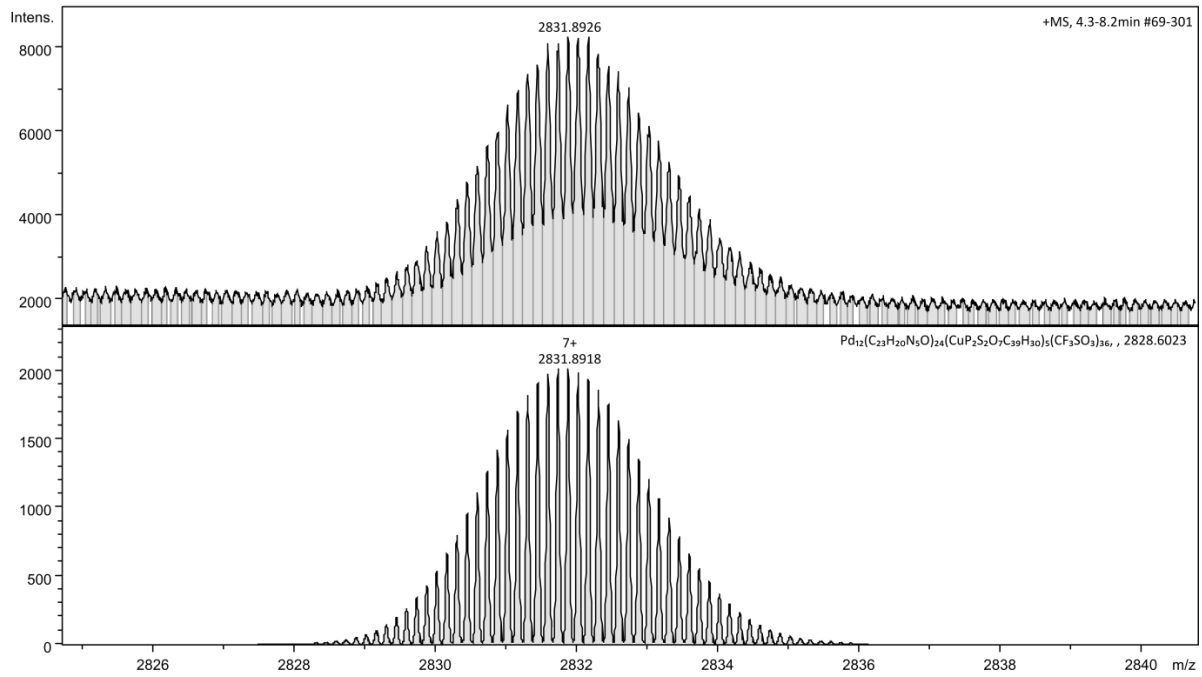

Figure S22. Expanded spectrum for the charged species $[Pd_{12}L_{24}(\mathbf{SXanpthosCu(I)})_5(OTf)_{36}]^{7+}$ observed (above) in the UHR CSI-TOF mass spectrum and simulated isotopic distribution (below)

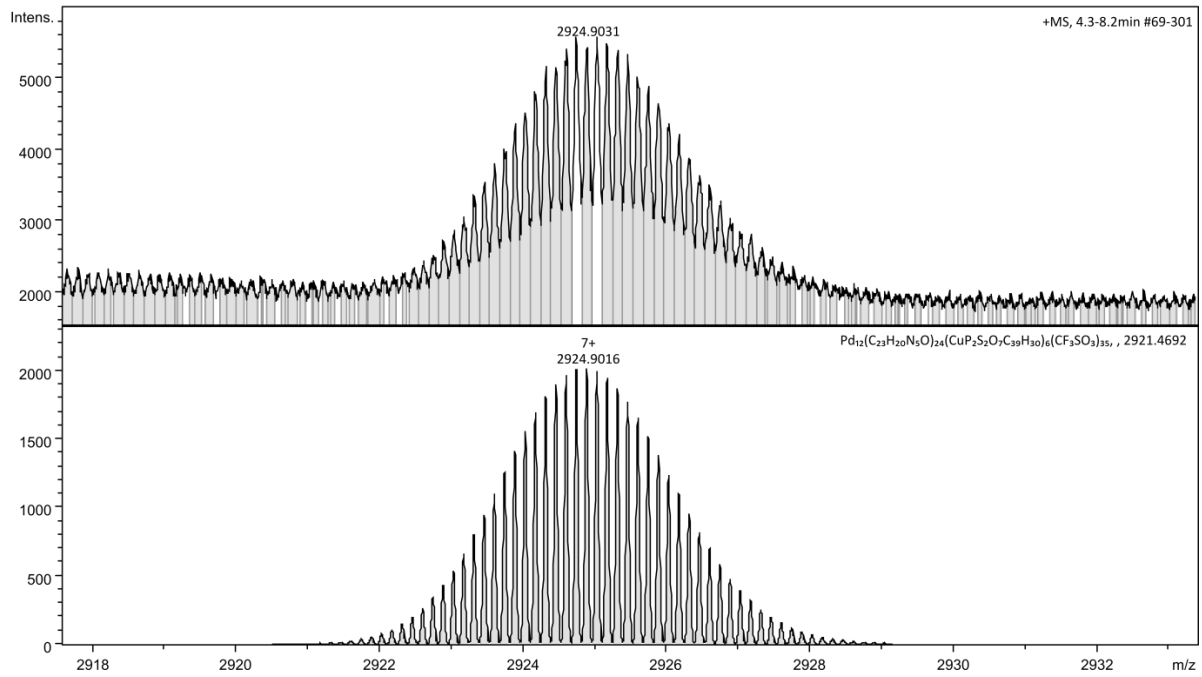

Figure S23. Expanded spectrum for the charged species $[Pd_{12}L_{24}(\mathbf{SXanpthosCu(I)})_6(OTf)_{35}]^{7+}$ observed (above) in the UHR CSI-TOF mass spectrum and simulated isotopic distribution (below)

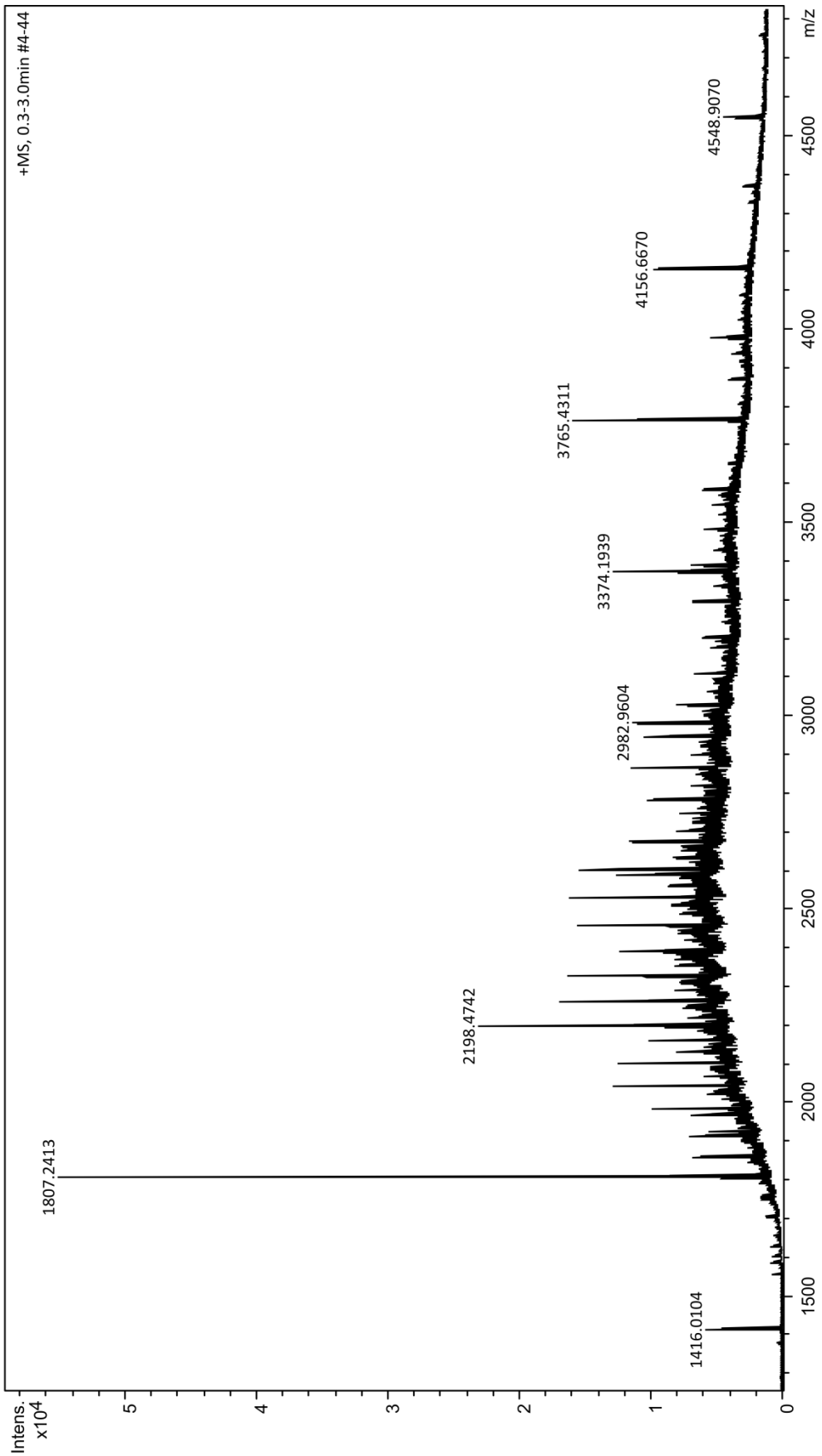

Figure S24. UHR CSI-TOF mass spectrum (full spectrum) of the sphere $(Pd_{12}L_{24})(OTf)_{48}$ with 12 eq. of **SXanpthosCu(I)** added, with a spray temperature of –40 ºC and dry gas temperature of –35 ºC

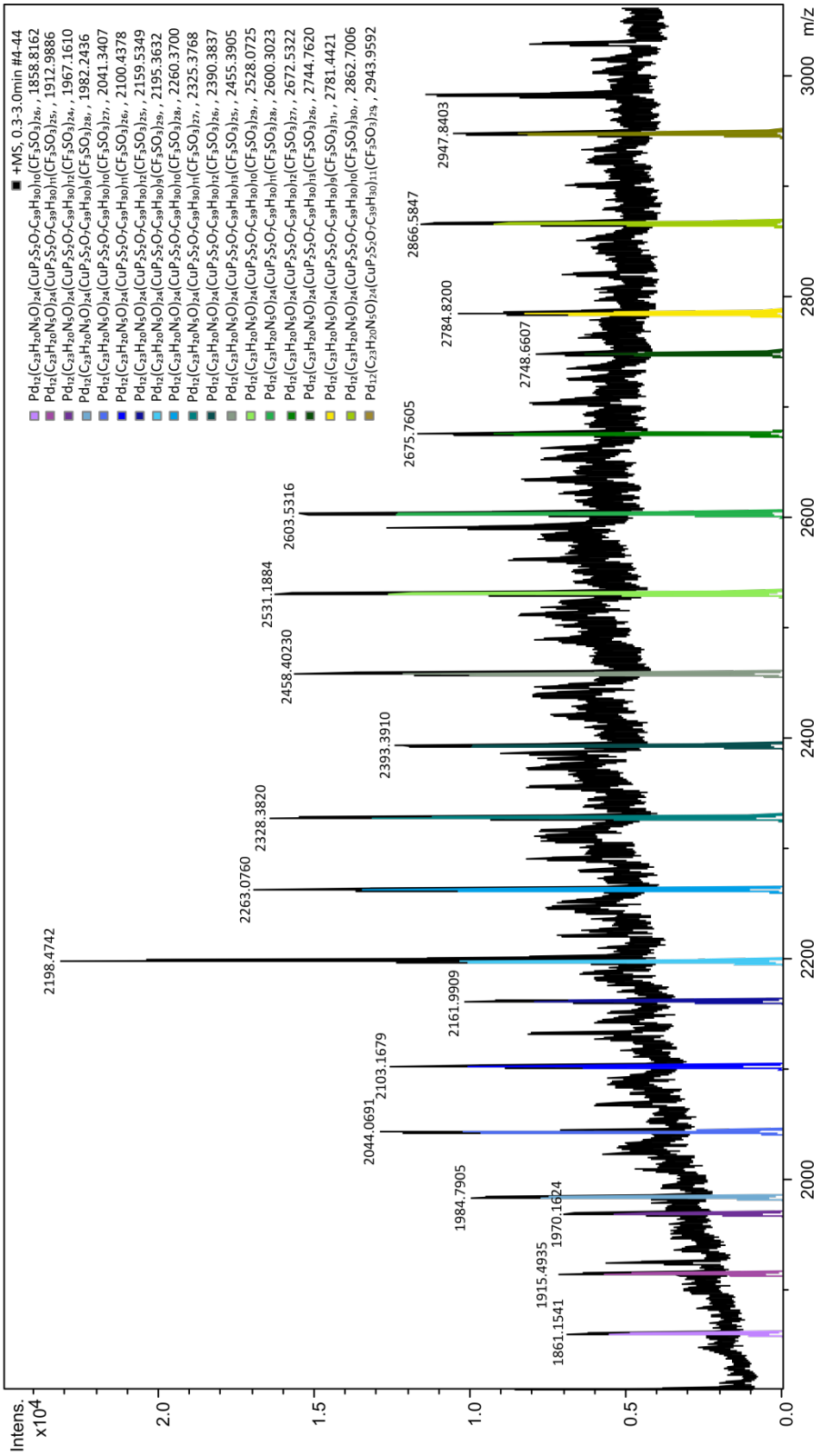

Figure S25. UHR CSI-TOF mass spectrum (full spectrum) of the sphere $(Pd_{12}L_{24})(OTf)_{48}$ with 12 eq. of **SXanpthosCu(I)** added, along with simulated isotopic patterns (in color) overlaid.

Table S2. Different charged species observed in the CSI-TOF mass spectrum of the sphere $(Pd_{12}L_{24})(OTf)_{48}$ ($Pd_{12}(C_{23}H_{20}N_5O)_{24}(CF_3SO_3)_{48}$) with 12 eq. of **SXanpthosCu(I)** ($CuP_2S_2O_7C_{39}H_{30}$) added and the corresponding found and calculated [m/z]. Note that in all cases the mass corresponding to the **SXanpthosCu(I)** does not involve the TBA counter-cation and the acetate co-ligand as they are not encapsulated within the sphere

Species	Charge	Found [m/z]	Calculated [m/z]
$Pd_{12}(C_{23}H_{20}N_5O)_{24}(CuP_2S_2O_7C_{39}H_{30})_{10}(CF_3SO_3)_{26}$	12+	1861.1541	1861.1521
$Pd_{12}(C_{23}H_{20}N_5O)_{24}(CuP_2S_2O_7C_{39}H_{30})_{11}(CF_3SO_3)_{25}$	12+	1915.4111	1915.4079
$Pd_{12}(C_{23}H_{20}N_5O)_{24}(CuP_2S_2O_7C_{39}H_{30})_{12}(CF_3SO_3)_{24}$	12+	1969.6702	1969.6636
$Pd_{12}(C_{23}H_{20}N_5O)_{24}(CuP_2S_2O_7C_{39}H_{30})_{9}(CF_3SO_3)_{28}$	11+	1984.6982	1984.7008
$Pd_{12}(C_{23}H_{20}N_5O)_{24}(CuP_2S_2O_7C_{39}H_{30})_{10}(CF_3SO_3)_{27}$	11+	2043.8869	2043.8889
$Pd_{12}(C_{23}H_{20}N_5O)_{24}(CuP_2S_2O_7C_{39}H_{30})_{11}(CF_3SO_3)_{26}$	11+	2103.0759	2103.0770
$Pd_{12}(C_{23}H_{20}N_5O)_{24}(CuP_2S_2O_7C_{39}H_{30})_{12}(CF_3SO_3)_{25}$	11+	2162.2677	2162.2651
$Pd_{12}(C_{23}H_{20}N_5O)_{24}(CuP_2S_2O_7C_{39}H_{30})_{9}(CF_3SO_3)_{29}$	10+	2198.1680	2198.1661
$Pd_{12}(C_{23}H_{20}N_5O)_{24}(CuP_2S_2O_7C_{39}H_{30})_{10}(CF_3SO_3)_{28}$	10+	2263.1746	2263.1730
$Pd_{12}(C_{23}H_{20}N_5O)_{24}(CuP_2S_2O_7C_{39}H_{30})_{11}(CF_3SO_3)_{27}$	10+	2328.2822	2328.2799
$Pd_{12}(C_{23}H_{20}N_5O)_{24}(CuP_2S_2O_7C_{39}H_{30})_{12}(CF_3SO_3)_{26}$	10+	2393.3910	2393.3868
$Pd_{12}(C_{23}H_{20}N_5O)_{24}(CuP_2S_2O_7C_{39}H_{30})_{13}(CF_3SO_3)_{25}$	10+	2458.4023	2458.4937
$Pd_{12}(C_{23}H_{20}N_5O)_{24}(CuP_2S_2O_7C_{39}H_{30})_{10}(CF_3SO_3)_{29}$	9+	2531.1884	2531.1870
$Pd_{12}(C_{23}H_{20}N_5O)_{24}(CuP_2S_2O_7C_{39}H_{30})_{11}(CF_3SO_3)_{28}$	9+	2603.5316	2603.5280
$Pd_{12}(C_{23}H_{20}N_5O)_{24}(CuP_2S_2O_7C_{39}H_{30})_{12}(CF_3SO_3)_{27}$	9+	2675.8725	2675.8690
$Pd_{12}(C_{23}H_{20}N_5O)_{24}(CuP_2S_2O_7C_{39}H_{30})_{13}(CF_3SO_3)_{26}$	9+	2748.2178	2748.2100
$Pd_{12}(C_{23}H_{20}N_5O)_{24}(CuP_2S_2O_7C_{39}H_{30})_{9}(CF_3SO_3)_{31}$	8+	2784.8200	2784.8208
$Pd_{12}(C_{23}H_{20}N_5O)_{24}(CuP_2S_2O_7C_{39}H_{30})_{10}(CF_3SO_3)_{30}$	8+	2866.2093	2866.2044
$Pd_{12}(C_{23}H_{20}N_5O)_{24}(CuP_2S_2O_7C_{39}H_{30})_{11}(CF_3SO_3)_{29}$	8+	2947.8403	2947.8381

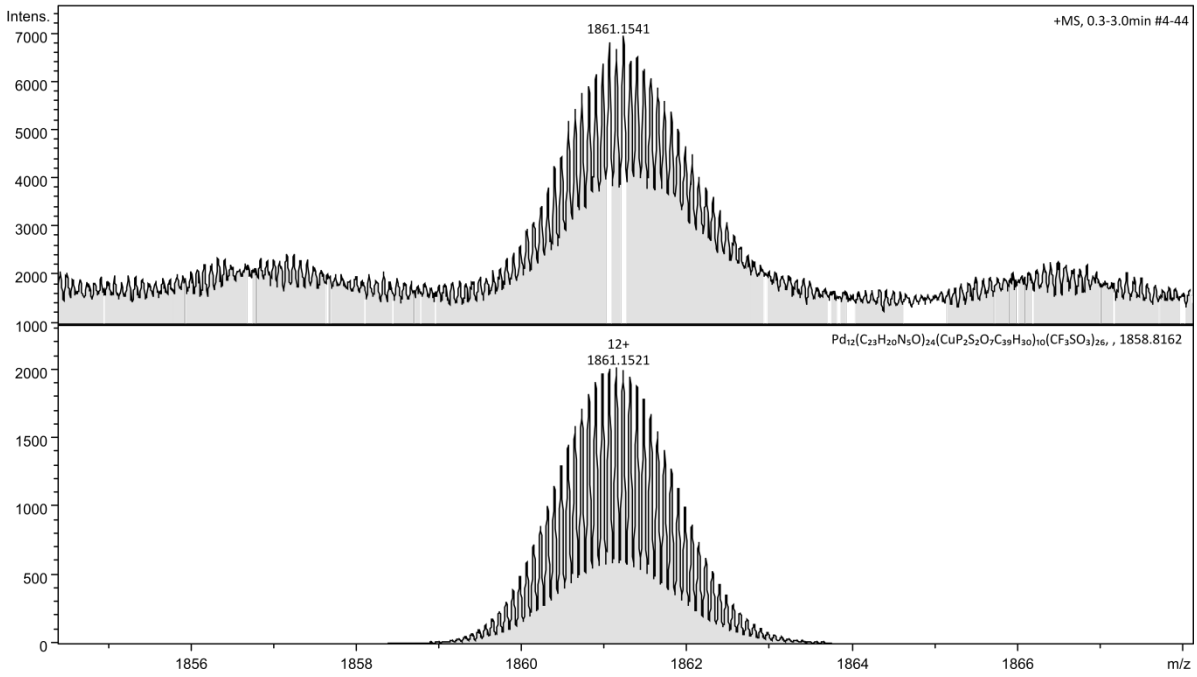

Figure S26. Expanded spectrum for the charged species $[Pd_{12}L_{24}(\mathbf{SXanpthosCu(I)})_{10}(OTf)_{26}]^{12+}$ observed (above) in the UHR CSI-TOF mass spectrum and simulated isotopic distribution (below)

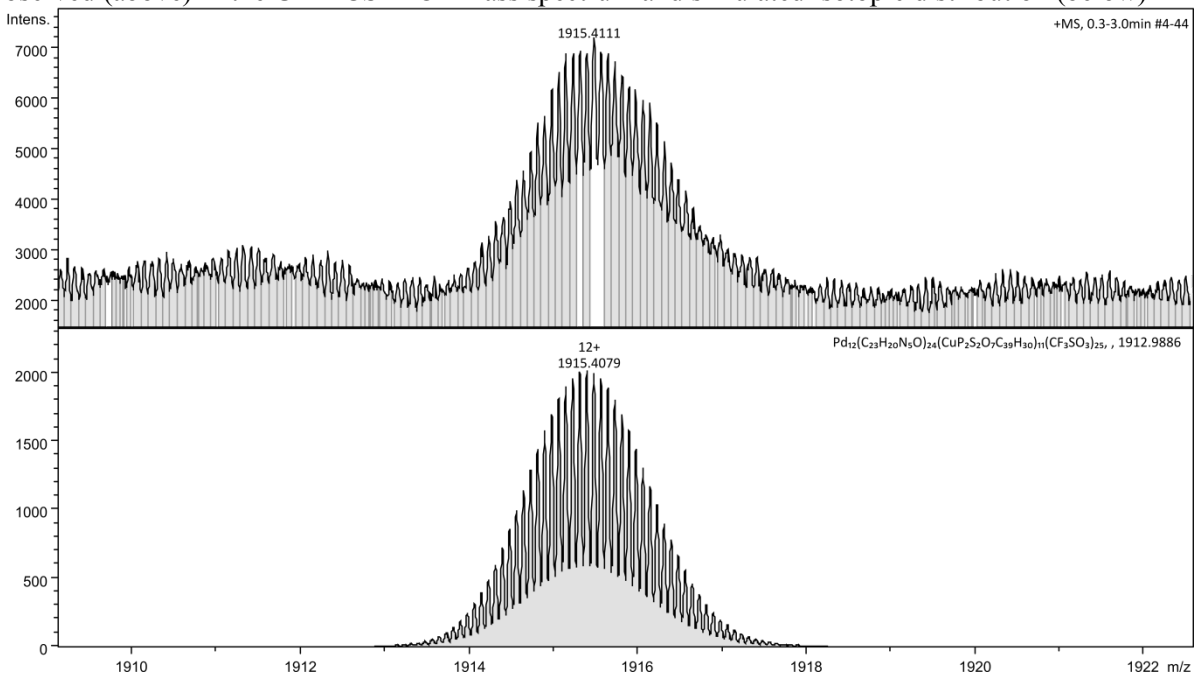

Figure S27. Expanded spectrum for the charged species $[Pd_{12}L_{24}(\mathbf{SXanpthosCu(I)})_{11}(OTf)_{25}]^{12+}$ observed (above) in the UHR CSI-TOF mass spectrum and simulated isotopic distribution (below)

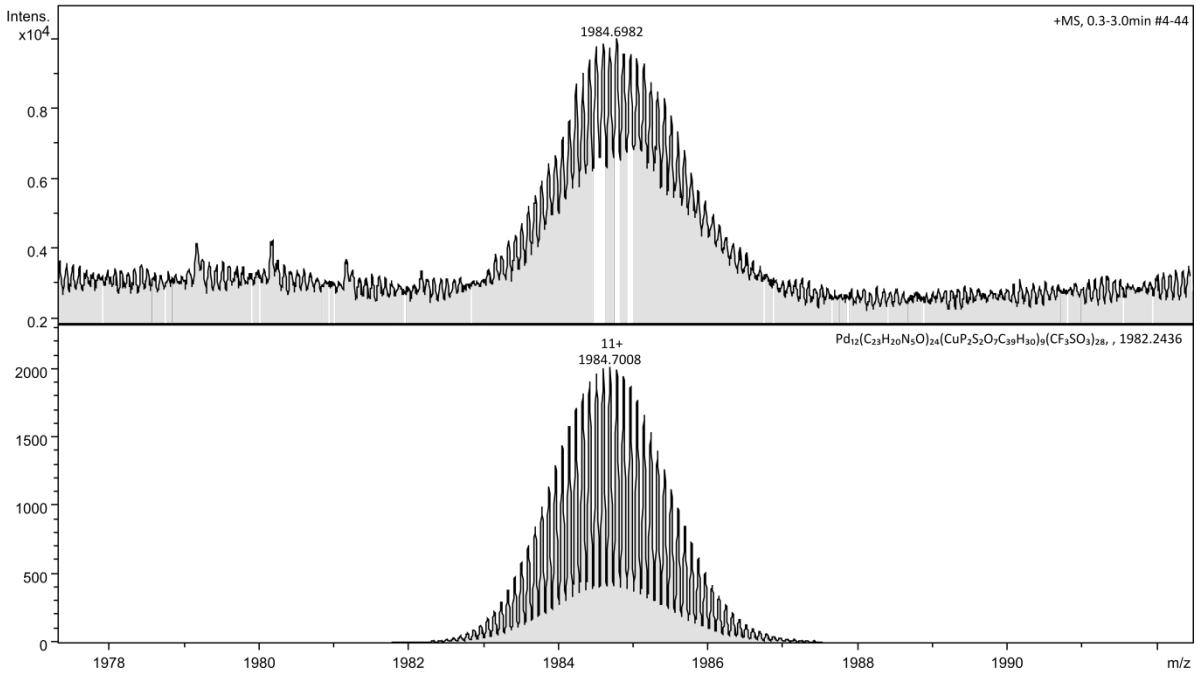

Figure S28. Expanded spectrum for the charged species $[Pd_{12}L_{24}(\mathbf{SXanpthosCu(I)})_9(OTf)_{28}]^{11+}$ observed (above) in the UHR CSI-TOF mass spectrum and simulated isotopic distribution (below)

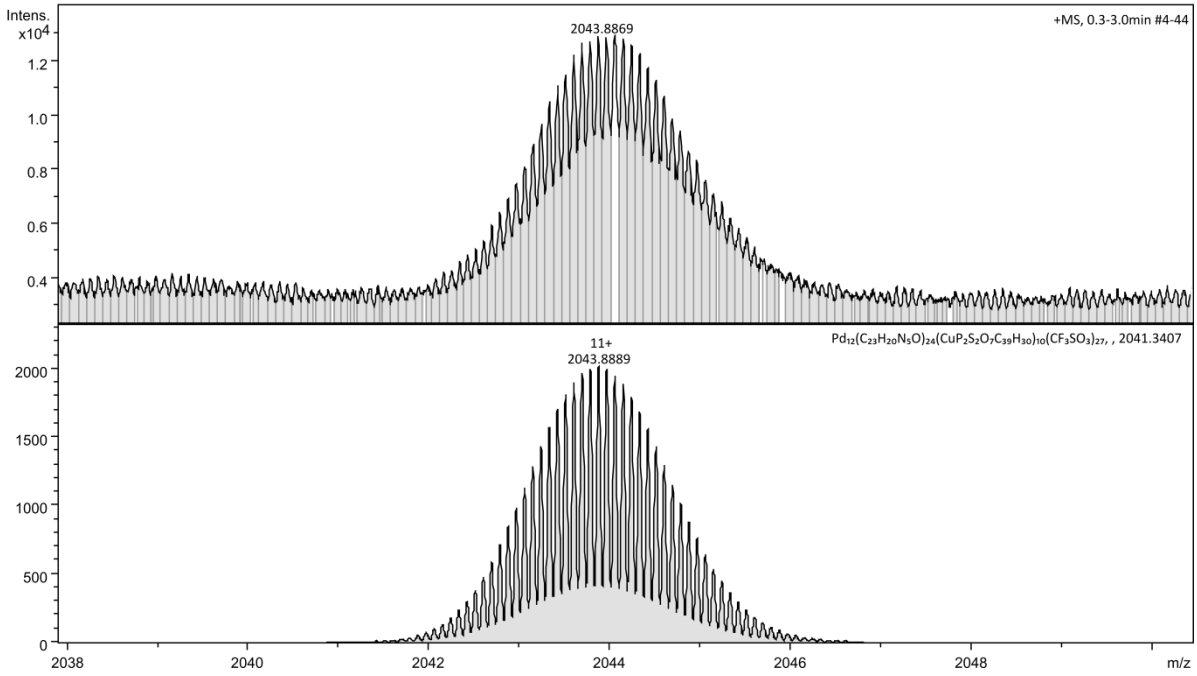

Figure S29. Expanded spectrum for the charged species $[Pd_{12}L_{24}(\mathbf{SXanpthosCu(I)})_{10}(OTf)_{27}]^{11+}$ observed (above) in the UHR CSI-TOF mass spectrum and simulated isotopic distribution (below)

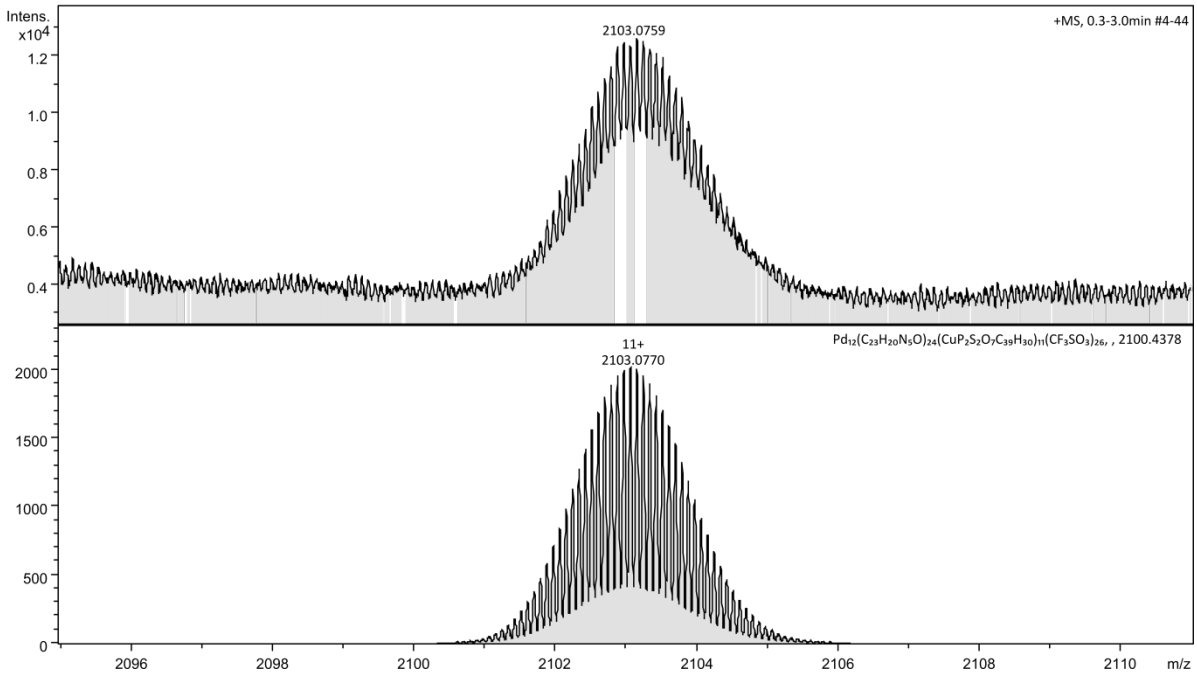

Figure S30. Expanded spectrum for the charged species $[Pd_{12}L_{24}(\mathbf{SXanpthosCu(I)})_{11}(OTf)_{26}]^{11+}$ observed (above) in the UHR CSI-TOF mass spectrum and simulated isotopic distribution (below)

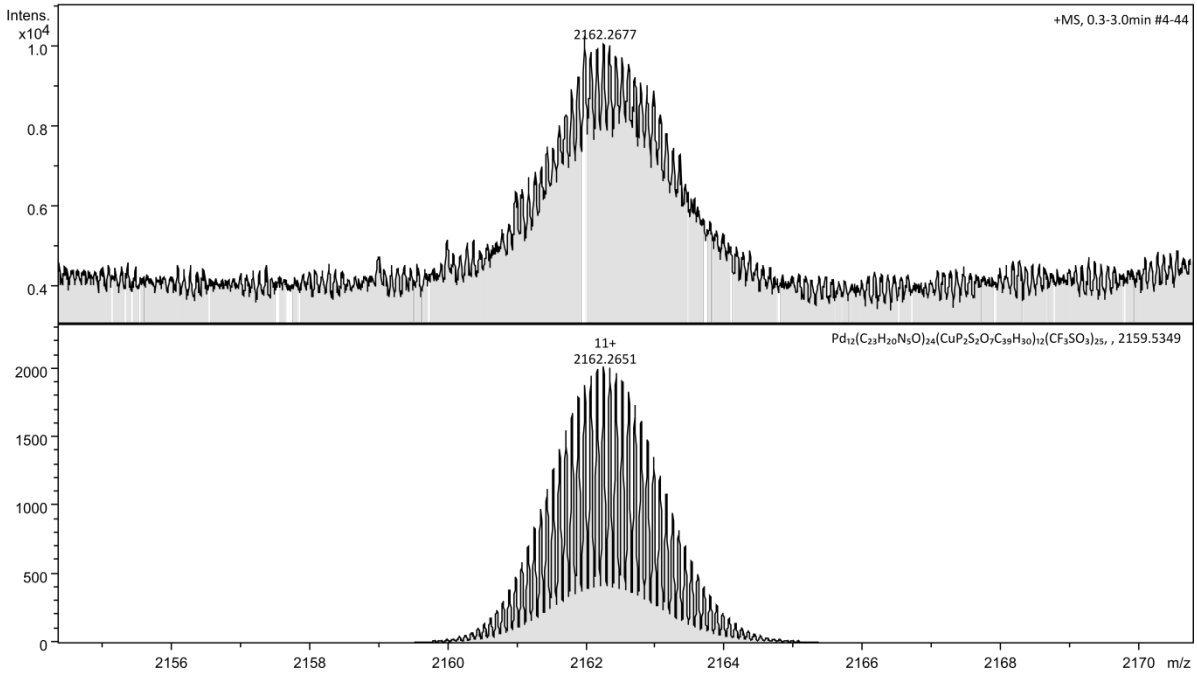

Figure S31. Expanded spectrum for the charged species $[Pd_{12}L_{24}(\mathbf{SXanpthosCu(I)})_{12}(OTf)_{25}]^{11+}$ observed (above) in the UHR CSI-TOF mass spectrum and simulated isotopic distribution (below)

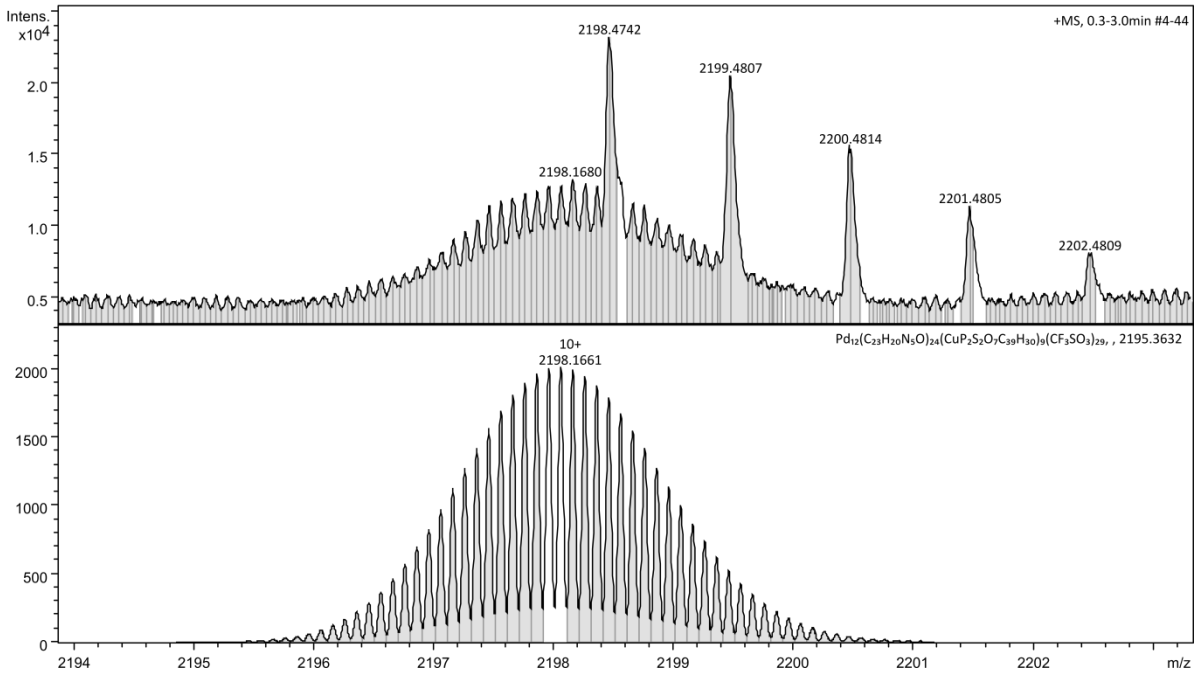

Figure S32. Expanded spectrum for the charged species $[Pd_{12}L_{24}(\mathbf{SXanpthosCu(I)})_9(OTf)_{29}]^{10+}$ observed (above) in the UHR CSI-TOF mass spectrum and simulated isotopic distribution (below)

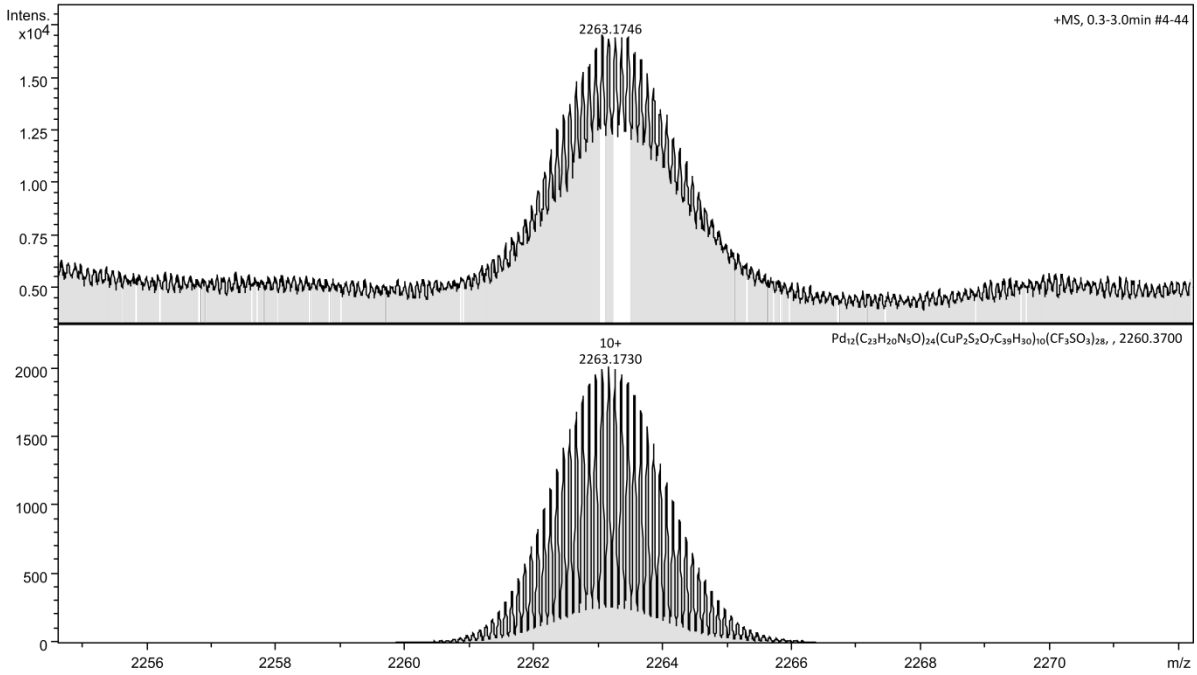

Figure S33. Expanded spectrum for the charged species $[Pd_{12}L_{24}(\mathbf{SXanpthosCu(I)})_{10}(OTf)_{28}]^{10+}$ observed (above) in the UHR CSI-TOF mass spectrum and simulated isotopic distribution (below)

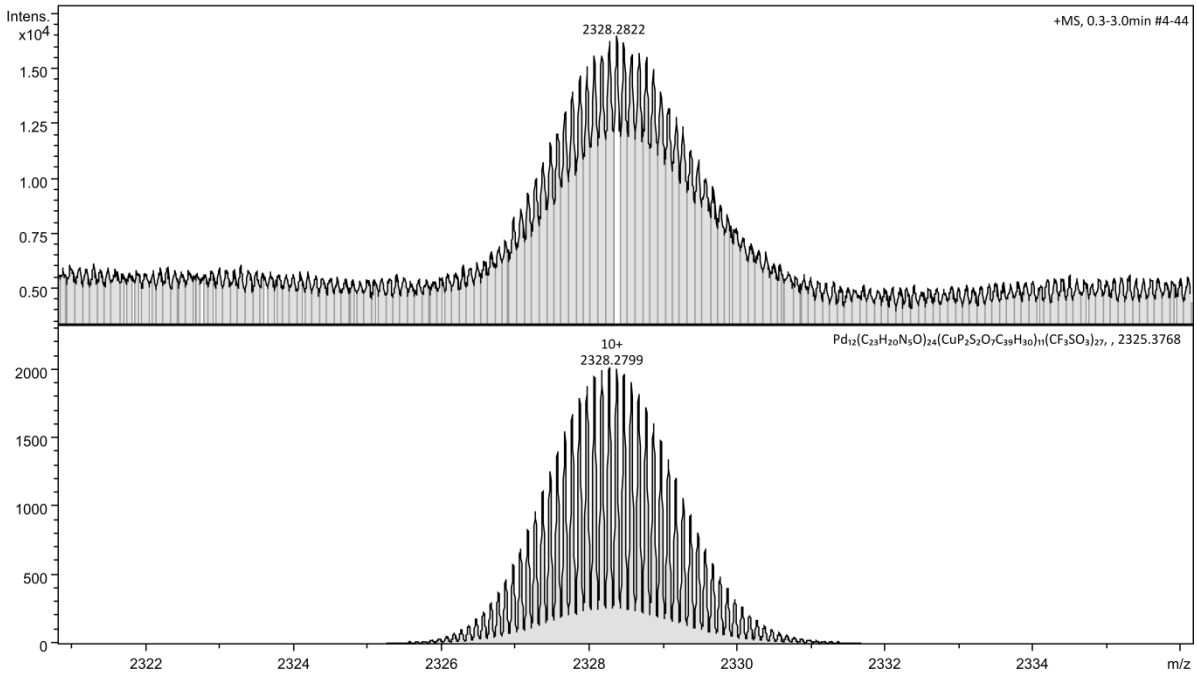

Figure S34. Expanded spectrum for the charged species $[Pd_{12}L_{24}(\mathbf{SXanpthosCu(I)})_{11}(OTf)_{27}]^{10+}$ observed (above) in the UHR CSI-TOF mass spectrum and simulated isotopic distribution (below)

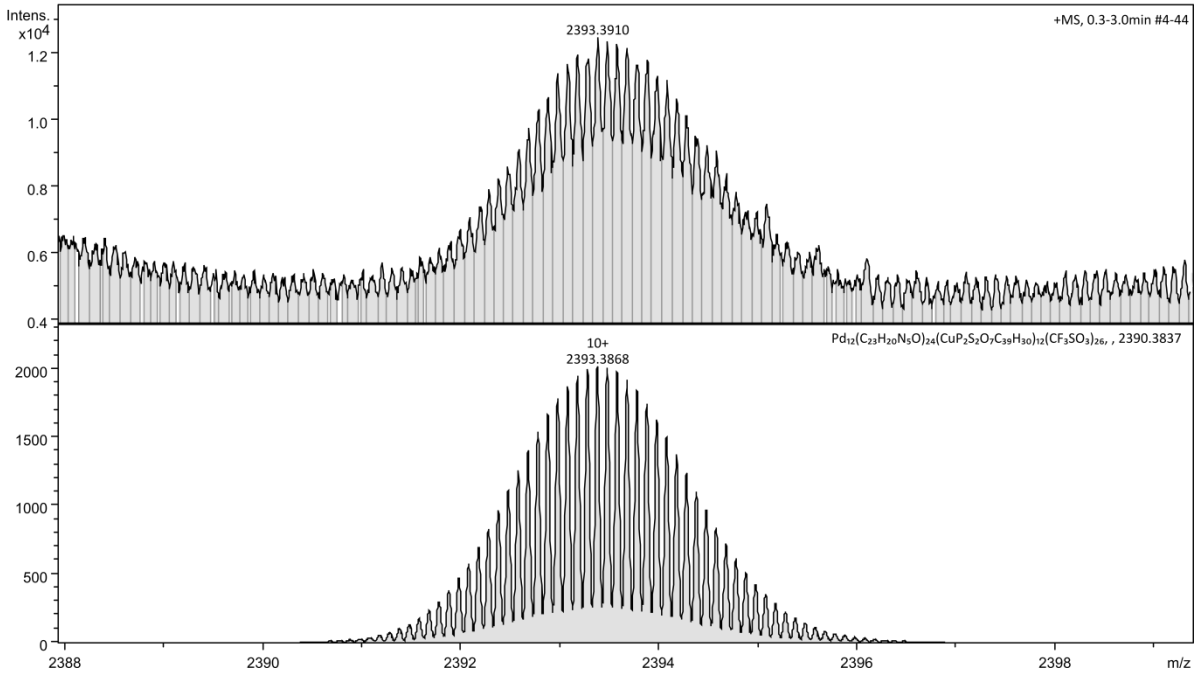

Figure S35. Expanded spectrum for the charged species $[Pd_{12}L_{24}(\mathbf{SXanpthosCu(I)})_{12}(OTf)_{26}]^{10+}$ observed (above) in the UHR CSI-TOF mass spectrum and simulated isotopic distribution (below)

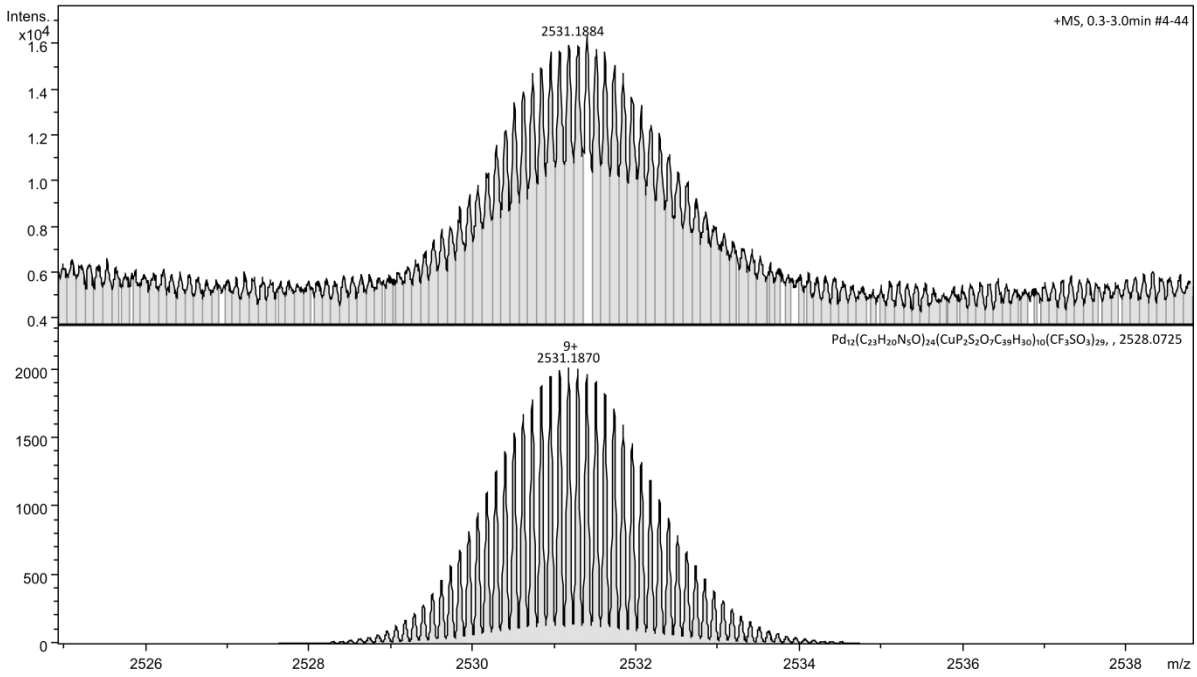

Figure S36. Expanded spectrum for the charged species $[Pd_{12}L_{24}(\mathbf{SXanpthosCu(I)})_{10}(OTf)_{29}]^{9+}$ observed (above) in the UHR CSI-TOF mass spectrum and simulated isotopic distribution (below)

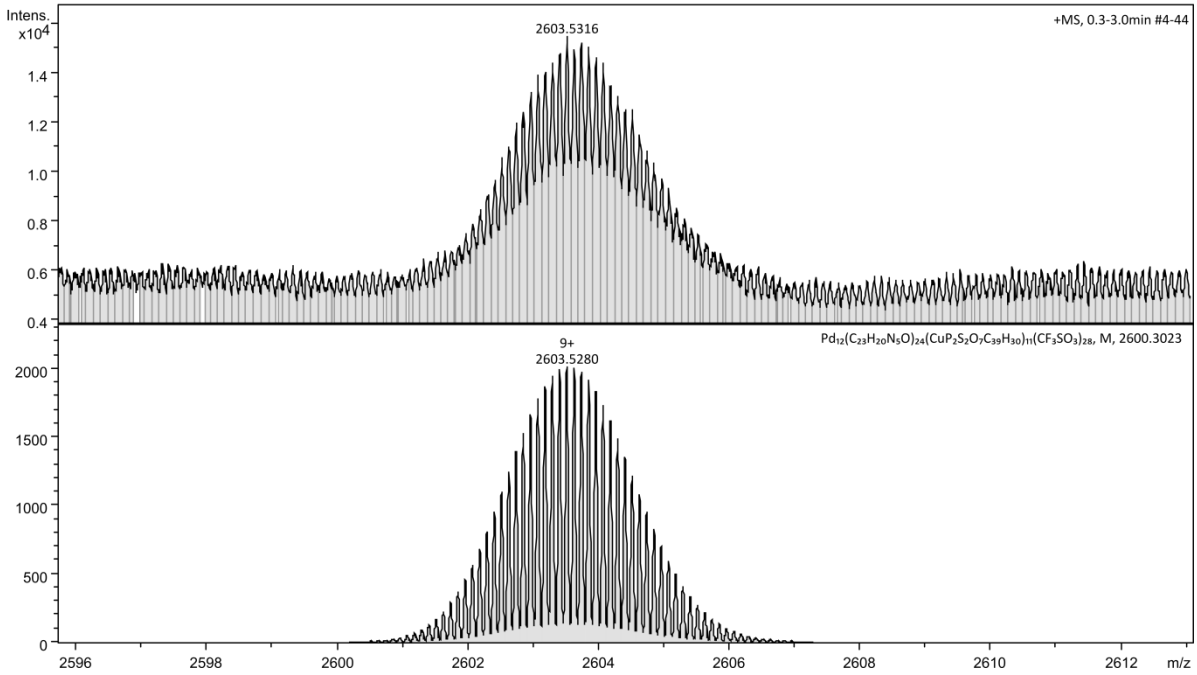

Figure S37. Expanded spectrum for the charged species $[Pd_{12}L_{24}(\mathbf{SXanpthosCu(I)})_{11}(OTf)_{28}]^{9+}$ observed (above) in the UHR CSI-TOF mass spectrum and simulated isotopic distribution (below)

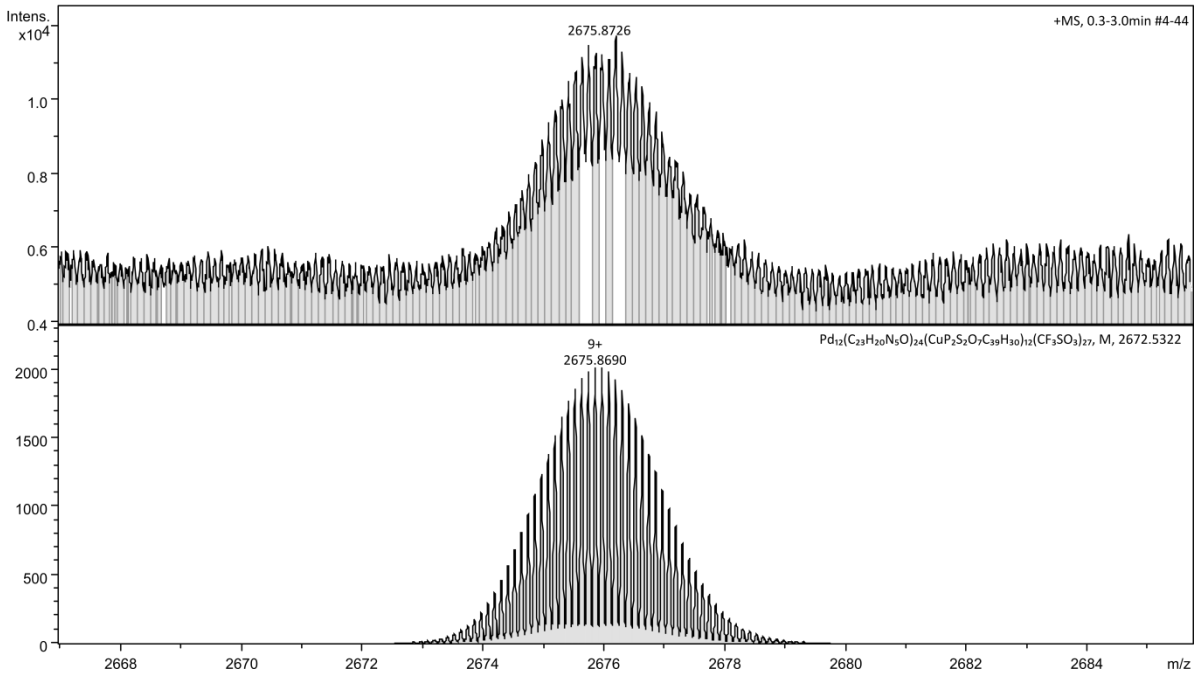

Figure S38. Expanded spectrum for the charged species $[Pd_{12}L_{24}(\mathbf{SXanpthosCu(I)})_{12}(OTf)_{27}]^{9+}$ observed (above) in the UHR CSI-TOF mass spectrum and simulated isotopic distribution (below)

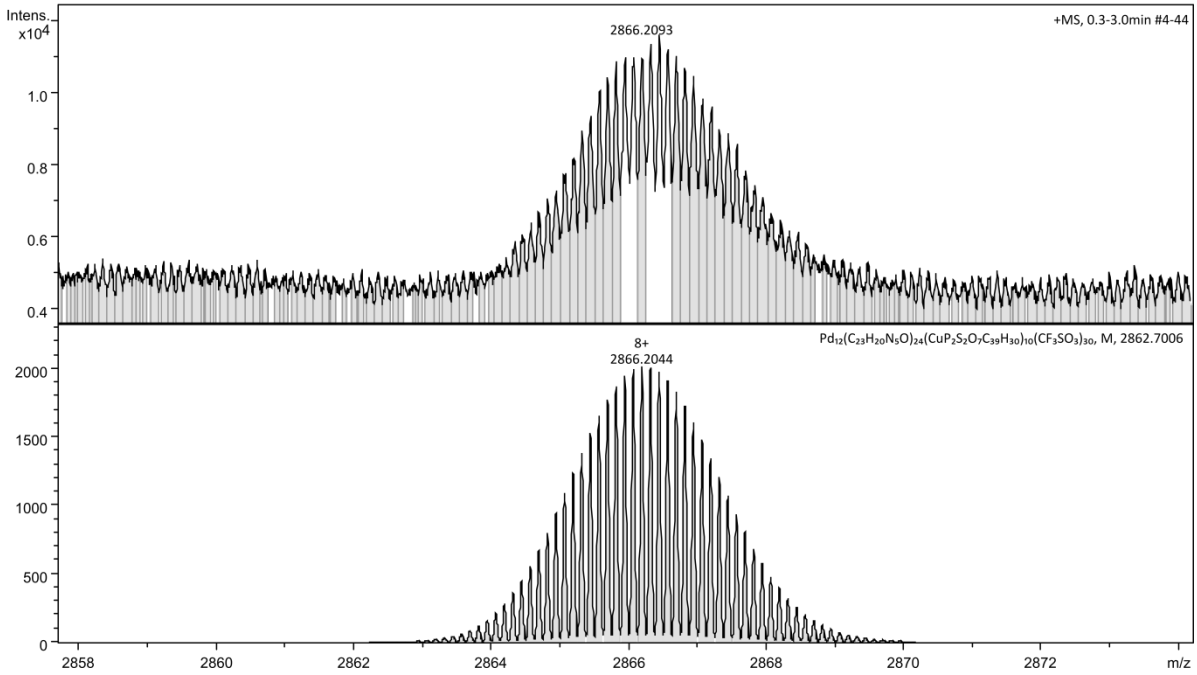

Figure S39. Expanded spectrum for the charged species $[Pd_{12}L_{24}(\mathbf{SXanpthosCu(I)})_{10}(OTf)_{30}]^{8+}$ observed (above) in the UHR CSI-TOF mass spectrum and simulated isotopic distribution (below)

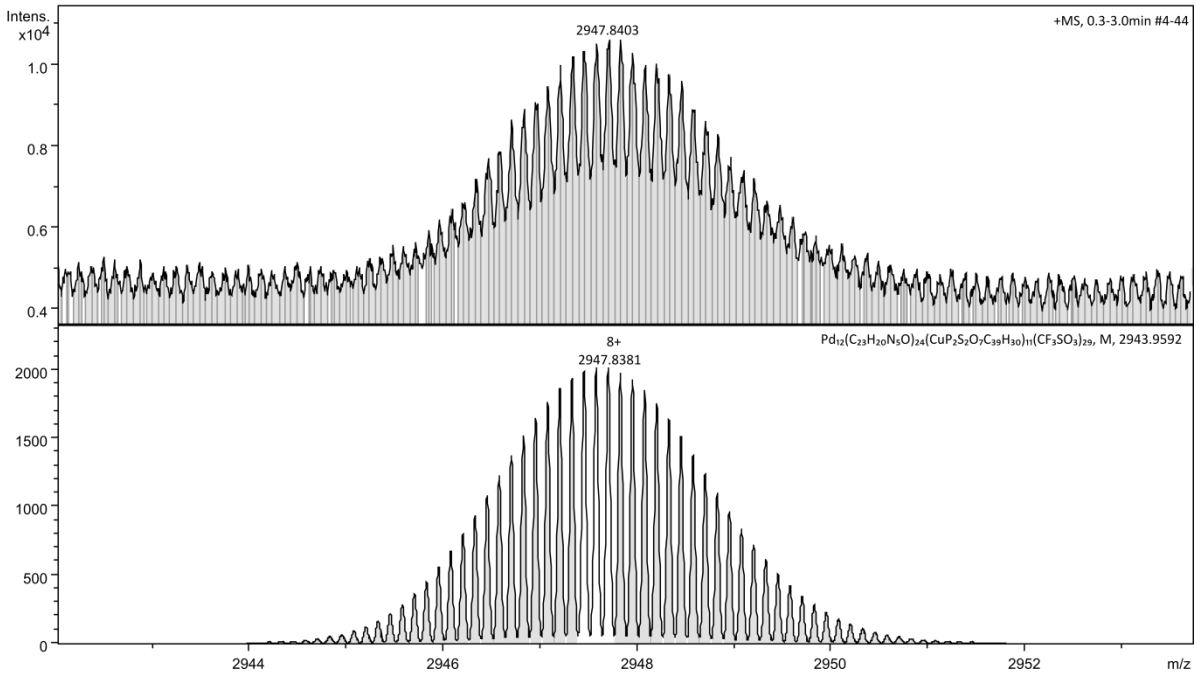

Figure S40. Expanded spectrum for the charged species $[Pd_{12}L_{24}(\mathbf{SXanpthosCu(I)})_{11}(OTf)_{29}]^{8+}$ observed (above) in the UHR CSI-TOF mass spectrum and simulated isotopic distribution (below)

3. Catalytic experiments

All catalytic experiments were carried out under aerobic conditions, in pre-dried and degassed CD_3CN, at room temperature. Stock solutions of sphere, substrate + 1,3,5-trimethoxybenzene as internal standard, base and catalyst were first prepared. The appropriate volumes of these solutions were taken and mixed directly in an NMR tube to get the desired concentration of each component (total volume 600 mL). The reaction process was monitored by ^1H NMR spectroscopy. Each entry was repeated at least 2 times, giving reproducible results.

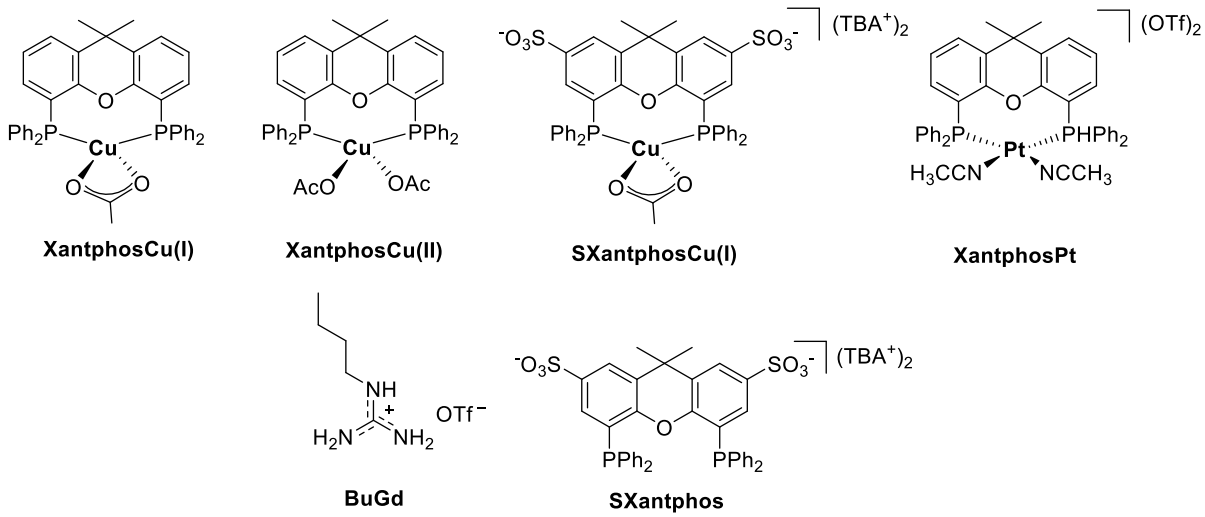

Figure S41. Catalysts and additives used in the catalytic studies and control experiments

Stock solutions prepared:

[**1**] = 150 mM (containing internal standard 1,3,5-trimethoxybenzene as 50 mM)

[XantphosCu] = 5 mM

[Cu(OAc)] = 5 mM

[XantphosCu(II)] = 5 mM

$[Cu(OAc)_2]$ = 5 mM

[Sphere] = 10/24 mM

[SXantphosCu] = 50mM

$[Et_3N]$ = 50 mM

$[Pt(MeCN)_4(OTf)_2]$ = 50 mM

[XanthposPt] = 5 mM

[SXantphos] = 50 mM

[BuGd] = 30 mM

For entry 1 in Table S2 the stock solution of sphere was synthesized with a higher concentration ([Sphere] = 20/24 mM) in order to avoid to change the total volume of catalytic mixture.

3.1 Nano-concentrator effect

Table S3. Cycloisomerization of 4-pentynoic acid with different number of SXantphosCu(I) complexes in the sphere[a]

Entry	Cu/Sphere	Local [Cu] (M)[b]	Yield (%)[c]	TOF_{ini} (h^{-1})[d]
1[e]	1	0.05	8	0.033
2[f]	2	0.09	31	0.374
3[g]	4	0.18	59	0.866
4[h]	6	0.27	69	1.29
5[i]	8	0.36	70	1.42
6[j]	12	0.54	80	1.50

[a]Reaction conditions: [**1**] = 10 mM, [SXantphosCu(I)] = 0.5 mM, [Et_3N] = 1.5 mM, CD_3CN, RT, 24 h. [b] Estimated local concentration of Cu complex within the sphere. [c]Yield determined by ^1H NMR spectroscopy using 1,3,5-trimethoxybenzene as internal standard. [d]TOF_{ini} calculated at *ca.* 15% conversion for all samples. [e][Sphere] = 0.5 mM, [f][Sphere] = 0.25 mM, [g][Sphere] = 0.125 mM, [h][Sphere] = 0.083 mM, [i][Sphere] = 0.063 mM, [j][Sphere] = 0.042 mM.

3.2 Control experiments

The influence of single guanidinium groups in the reaction outcome was studied by using BuGd as additive (Entries 5 and 6), proving that does not influence the activity of the Cu catalyst. Platinum is known to be able to promote the cyclcization of alkynoic acids.[4] Therefore **XantphosPt** was synthesized and tested in the cyclization of **1**, as well as $Pt(MeCN)_4(OTf)_2$ (the metal precursor used for the synthesis of the nano-concentrator, entries 15-18). Under our catalytic condition, Pt proved to be an inefficient catalyst. Pre-organization of the substrate through binding of the substrate with the guanidinium group was ruled out by performing the reaction in presence of *para*-toluene sulfonate (*p*-$TolSO_3TBA$) as a competitive guest against the substrate that gave the same conversion than without *p*-$TolSO_3TBA$ with 6 eq of Cu per sphere (entry 19 and table S2 entry 4).[2]

Table S4. Control experiments in the presence of different additives[a]

Entry	Conditions	Yield (%)[b]
1	SXantphosCu(I)	2
2	SXantphosCu(I) + Et_3N	14
3	SXantphosCu(I) + Sphere	7
4	SXantphosCu(I) + Sphere + Et_3N	59
5	SXantphosCu(I) + BuGd	3
6	SXantphosCu(I) + BuGd + Et_3N	12
7	XantphosCu(I) + Sphere	3
8	XantphosCu(I) + Sphere + Et_3N	6
9	XantphosCu(I) + Et_3N	39
14	Et_3N	0
15[c]	$Pt(MeCN)_4(OTf)_2$	0
16[c]	$Pt(MeCN)_4(OTf)_2$ + Et_3N	4
17[c]	XantphosPt	0
18[c]	XantphosPt + Et_3N	15
19[d]	SXantphosCu(I) + Sphere + *p*-$TolSO_3TBA$	69

[a]Reaction conditions: [**1**] = 10 mM, [Cu] = 0.5 mM, [Et_3N] = 1.5 mM, [BuGu] = 1 mM, [Sphere] = 0.125 mM, CD_3CN, RT, 24 h. [b]Yield determined by ^1H NMR spectroscopy using 1,3,5-trimethoxybenzene as internal standard. [c][Pt] = 0.5 mM. [d]Reaction conditions: [1] = 10 mM, [Et_3N] = 1.5 mM, [Sphere] = 0.083 mM, [SXantphosCu(I)] = 0.5 mM, [p-$TolSO_3TBA$] = 1 mM, CD_3CN, RT, 24 h.

3.3 Higher TON experiment

Table S5. Experiment with a catalyst loading of 1 mol% at 50°C[a]

Entry	Catalyst	Yield (%)[b]
1	SXantphosCu(I) + Sphere	94
2	XantphosCu(I)	37

[a]Reaction conditions: [**1**] = 50 mM, [Cu] = 0.5 mM, [Et_3N] = 2.25 mM, [Sphere] = 0.042 mM, CD_3CN, RT, 24 h. [b]Yield determined by ^1H NMR spectroscopy using 1,3,5-trimethoxybenzene as internal standard.

3.4 Kinetic analysis and detection of intermediates

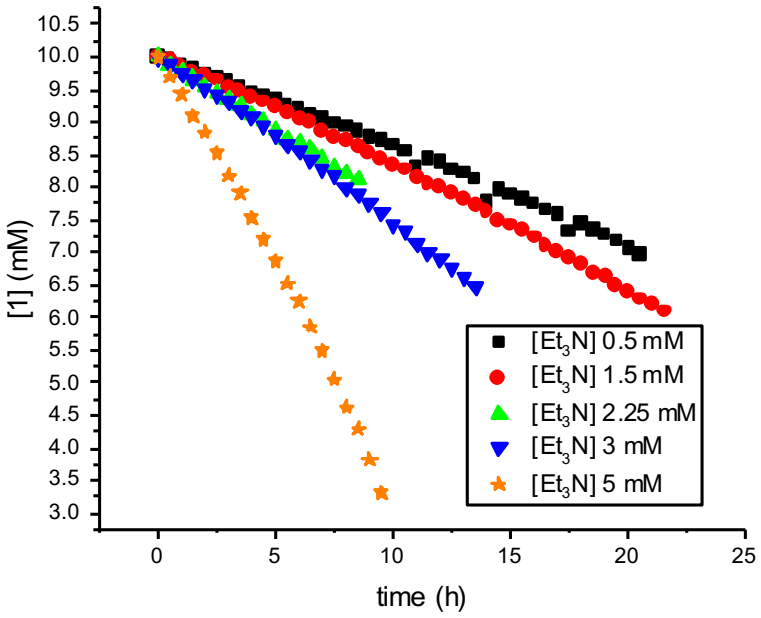

Figure S42. Top: Reaction progress for the conversion of **1** at different base concentration. Reaction conditions: [**1**] = 10 mM, [**XantphosCu(I)**] = 0.5 mM, CD_3CN, RT, 24 h. [**Et_3N**] = 0.5 mM (black), [**Et_3N**] = 1.5 mM (red), [**Et_3N**] = 2.25 mM (blue), [**Et_3N**] = 3 mM (green) and [**Et_3N**] = 5 mM (orange).

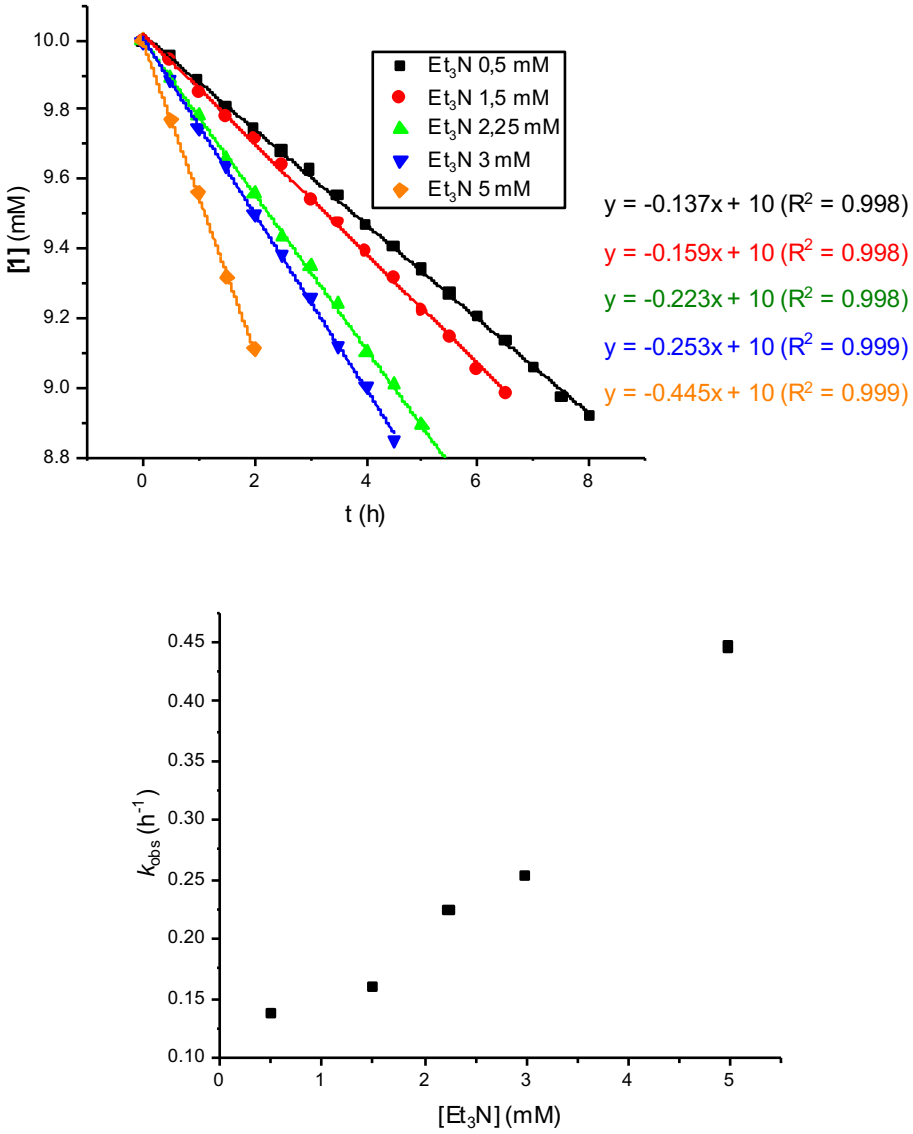

Figure S43. Top: Reaction progress for the conversion of **1** at different base concentration. Reaction conditions: [**1**] = 10 mM, [**XantphosCu(I)**] = 0.5 mM, CD_3CN, RT, 24 h. [**Et_3N**] = 0.5 mM (black), [**Et_3N**] = 1.5 mM (red), [**Et_3N**] = 2.25 mM (green), [**Et_3N**] = 3 mM (blue) and [**Et_3N**] = 5 mM (orange). From the slope of the data represented in this figure, the observed rate constant was obtained ($-k_{obs}$ = slope of the representation). Bottom: k_{obs} (obtained from the top figure) of the reaction at different base concentration, in which a non-linear increase on the rate of the reaction with respect the concentration of base can be observed.

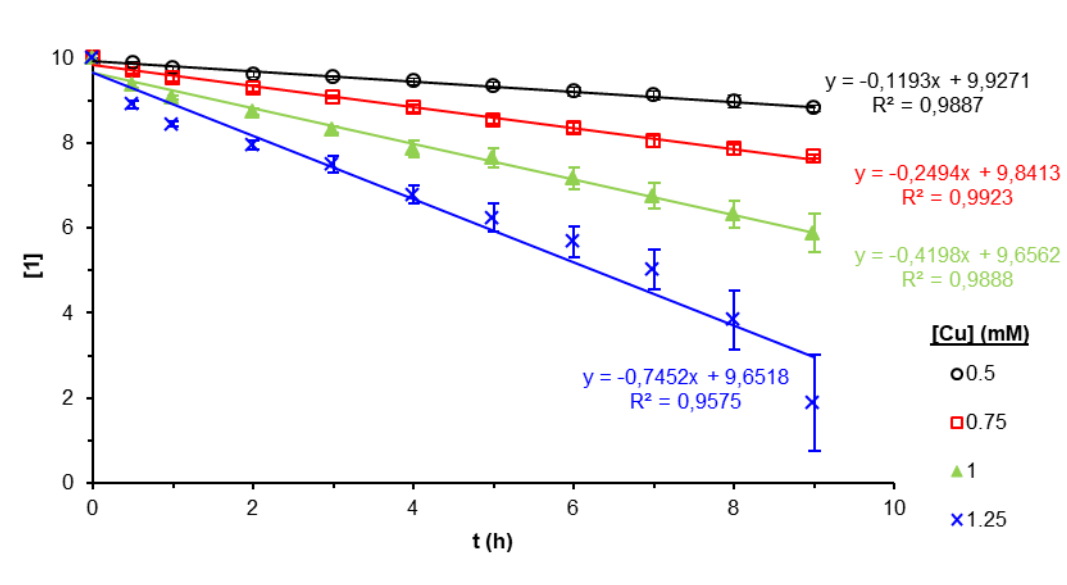

Figure S44. Reaction progress for the conversion of **1** at different catalyst concentration. Reaction conditions: [**1**] = 10 mM, [Et_3N] = 0.5 mM, CD_3CN, RT, 24 h. [**XantphosCu(I)**] = 0.5 mM (black), [**XantphosCu(I)**] = 0.75 mM (red), [**XantphosCu(I)**] = 1.0 mM (green), [**XantphosCu(I)**] = 1.25 mM (blue). From the slope of the data represented in this figure, the observed rate constant was obtained (– k_{obs} = slope of the representation). By representing the lnk_{obs} versus ln[**XantphosCu(I)**] (slope = reaction order, Figure S45) the order of the reaction with respect the concentration of **XantphosCu(I)** was determined.

.

Deuterium scrambling experiment

The Deuterated substrate was synthesized according to the reported literature procedure.[5]

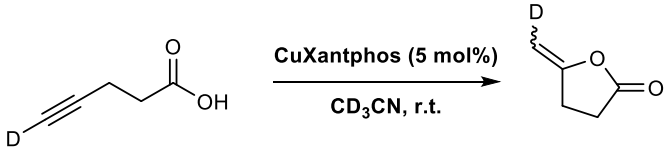

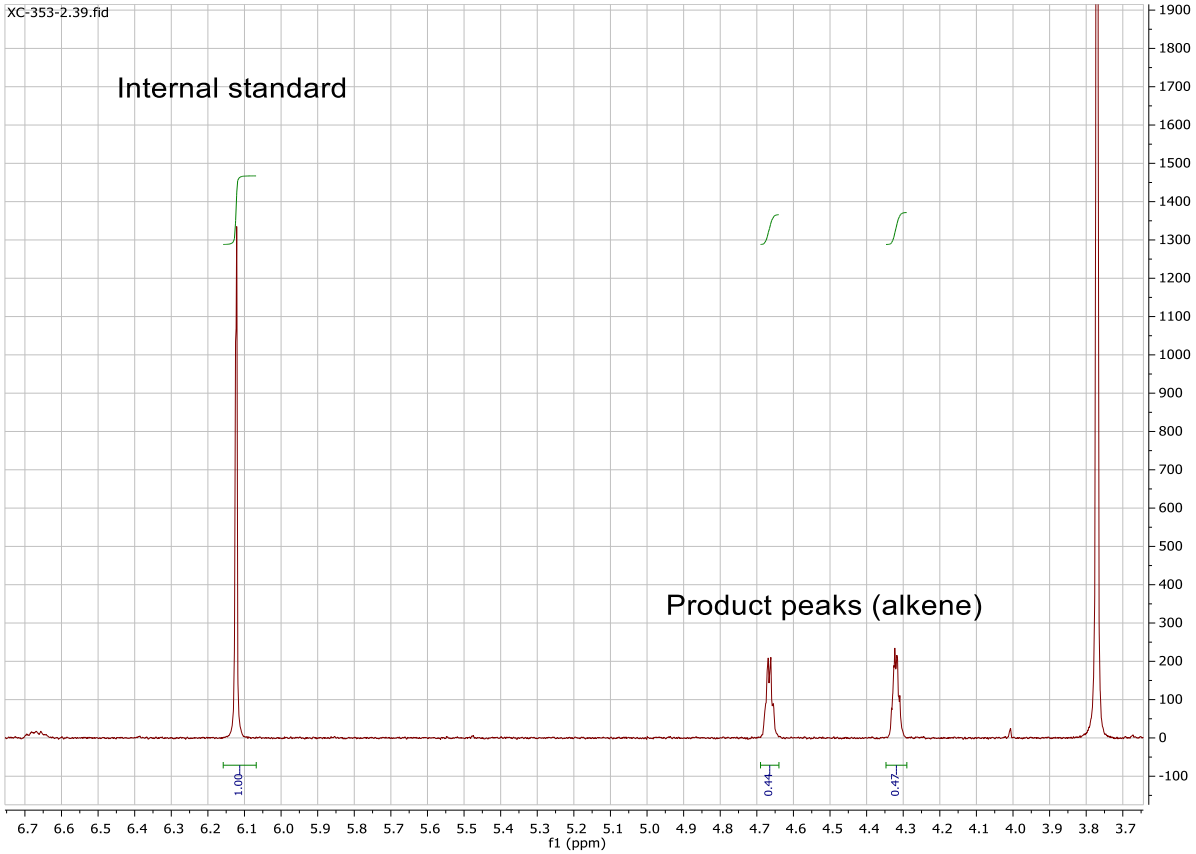

Figure S45. Deuteration experiment with deuterated substrate. Conditons [**substrate**] = 10 mM, [Et_3N] = 1.5 mM, [**XantphosCu(I)**] = 0.5 mM, CD_3CN, RT, 24 h.

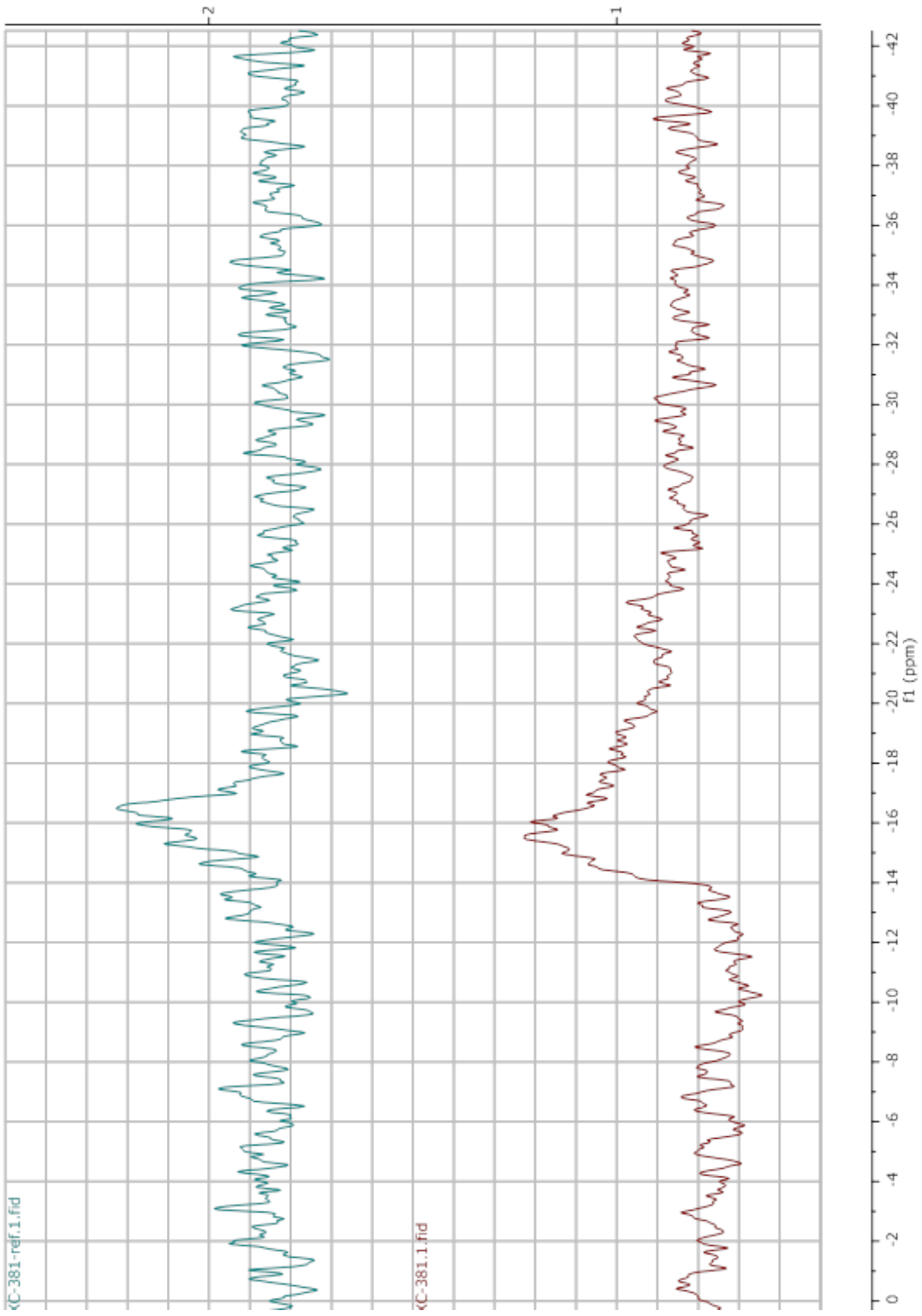

Figure S46. ^{31}P NMR of pre-catalyst (green, top) and during catalysis (red, bottom). Conditions [**substrate**] = 10 mM, [Et_3N] = 1.5 mM, [**XantphosCu(I)**] = 0.5 mM, CD_3CN, RT, 24 h

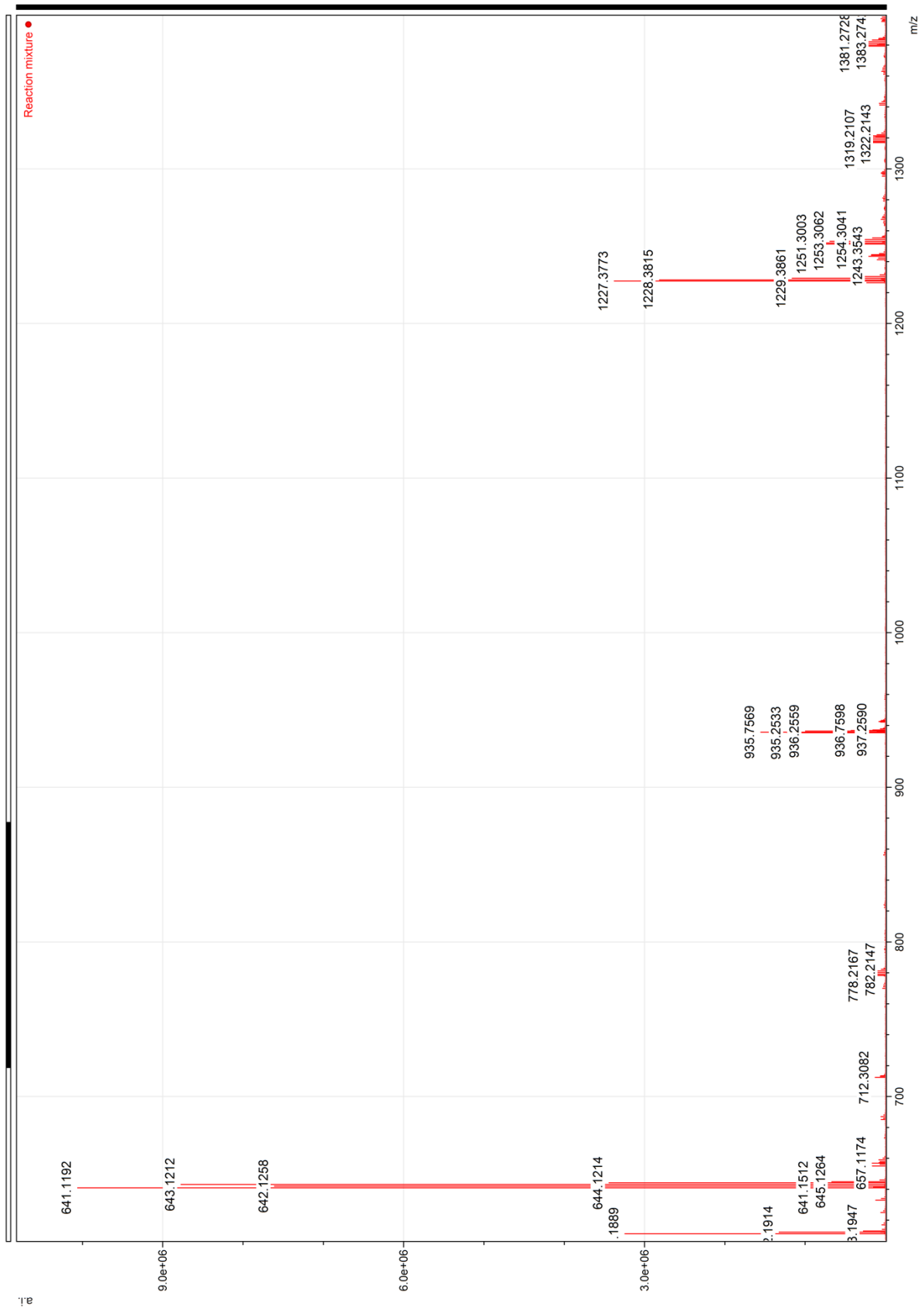

Figure S47. Mass analysis of the reaction mixture, conditons [**1**] = 10 mM, [Et_3N] = 1.5 mM, [**XantphosCu**] = 0.5 mM, CD_3CN, RT, 5 h

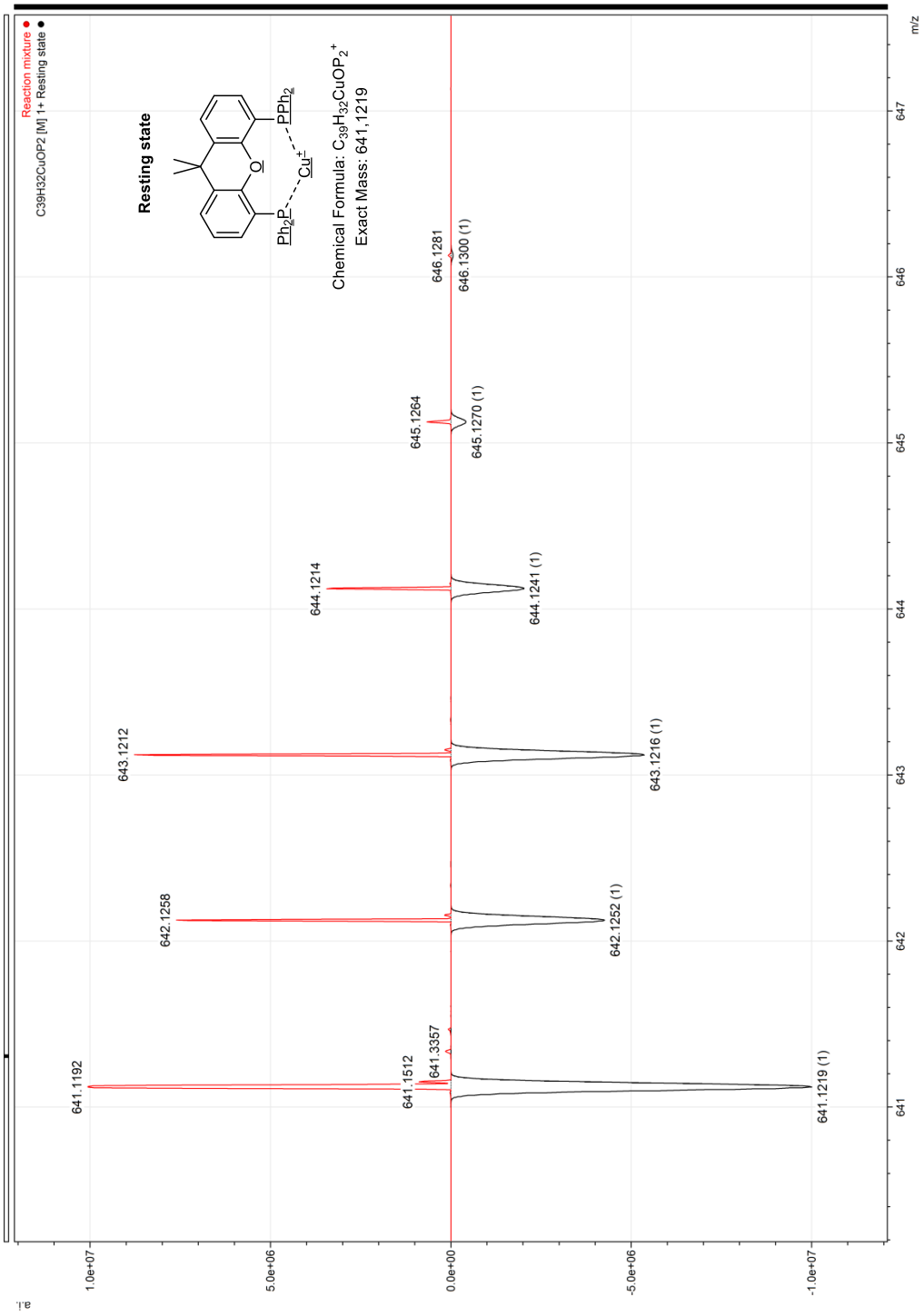

Figure S48. Mass analysis of the reaction mixture, conditons [**1**] = 10 mM, [Et_3N] = 1.5 mM, [**XantphosCu**] = 0.5 mM, CD_3CN, RT, 4 h, peak corresponding to the resting state **XantphosCu(I)**$^+$, in red experimental spectra and in black simulated spectra.

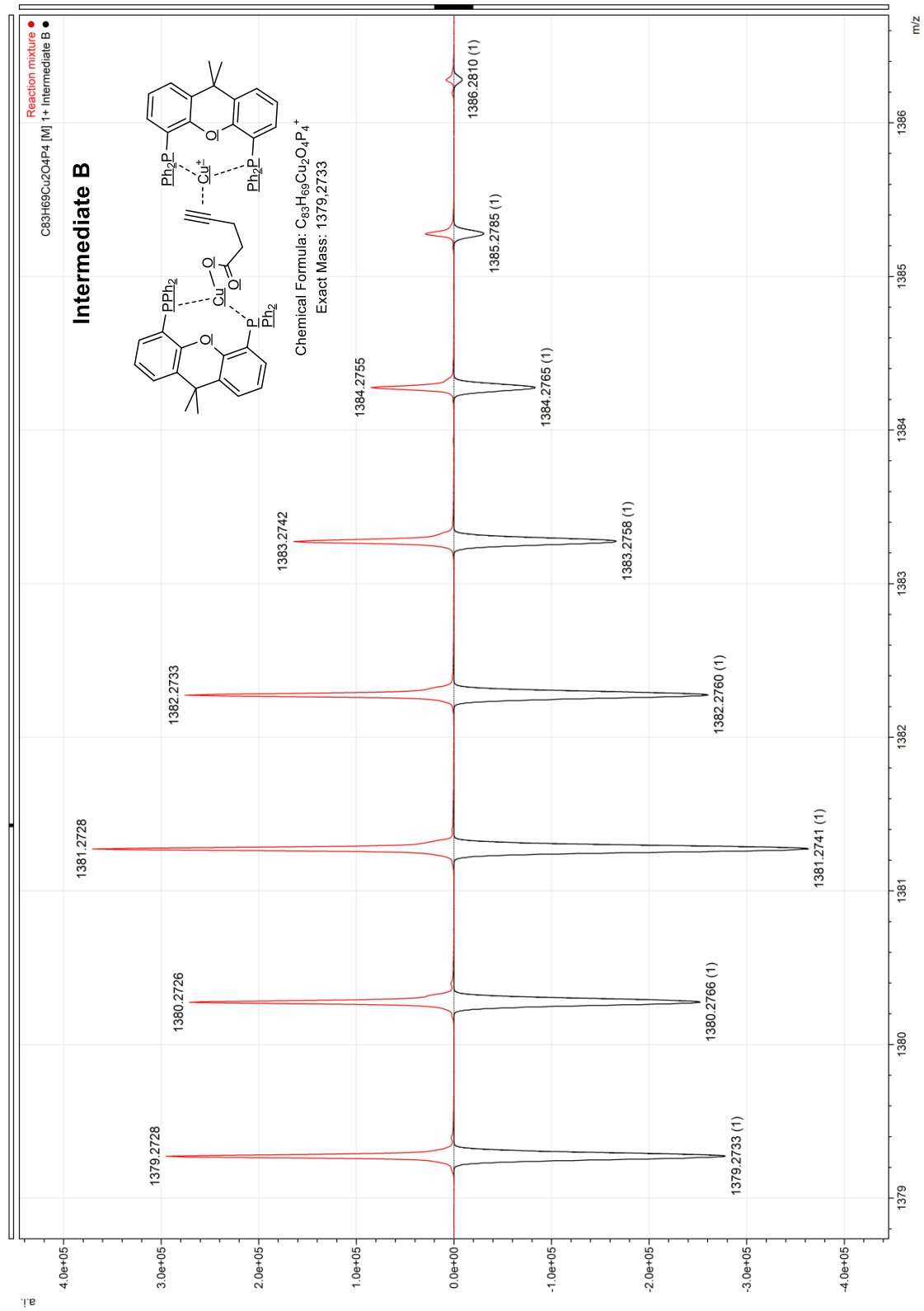

Figure S49. Mass analysis of the reaction mixture, conditons [**1**] = 10 mM, [Et_3N] = 1.5 mM, [**XantphosCu**] = 0.5 mM, CD_3CN, RT, 4 h, peak corresponding to the **Intermediate B**, in red experimental spectra and in black simulated spectra.

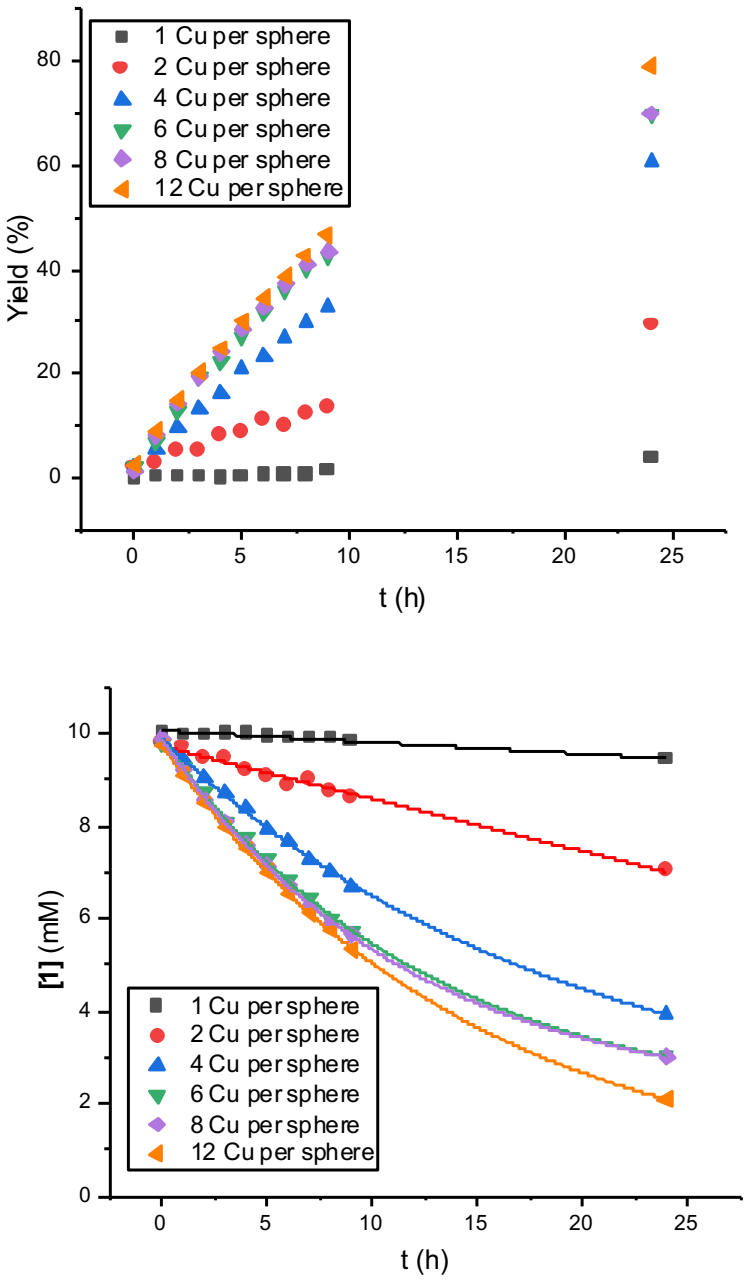

Figure S50. Top: Reaction progress for the formation of **2** at different **SXantphosCu(I)**/Sphere ratios. Bottom: [**1**] versus time at **SXantphosCu(I)**/Sphere ratios, the line are only guide for the eyes. For reaction conditions see Table 3 in the main text.

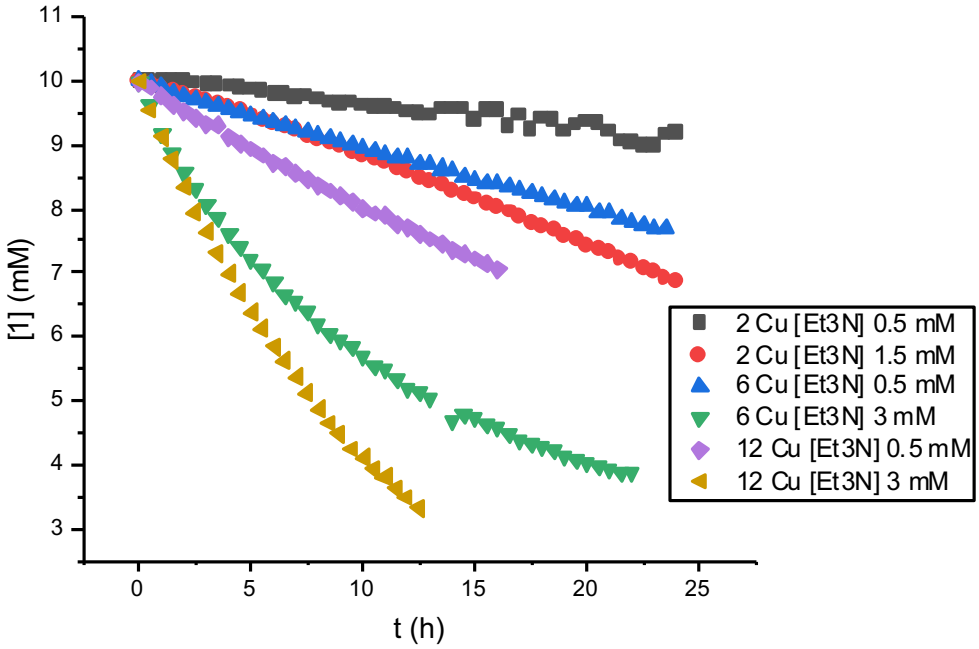

Figure S51. [**1**] vs time at different **SXantphosCu(I)**/Sphere ratios and different base concentrations. Reaction conditions: [**Cu**] = 0.5 mM, [1] = 10 mM, CD_3CN, RT, 24 h, **SXantphosCu(I)**/Sphere = 2 : [Sphere] = 0.25 mM, **SXantphosCu(I)**/Sphere = 6: [Sphere] = 0.083 mM, **SXantphosCu(I)**/Sphere = 12: [Sphere] = 0.042 mM.

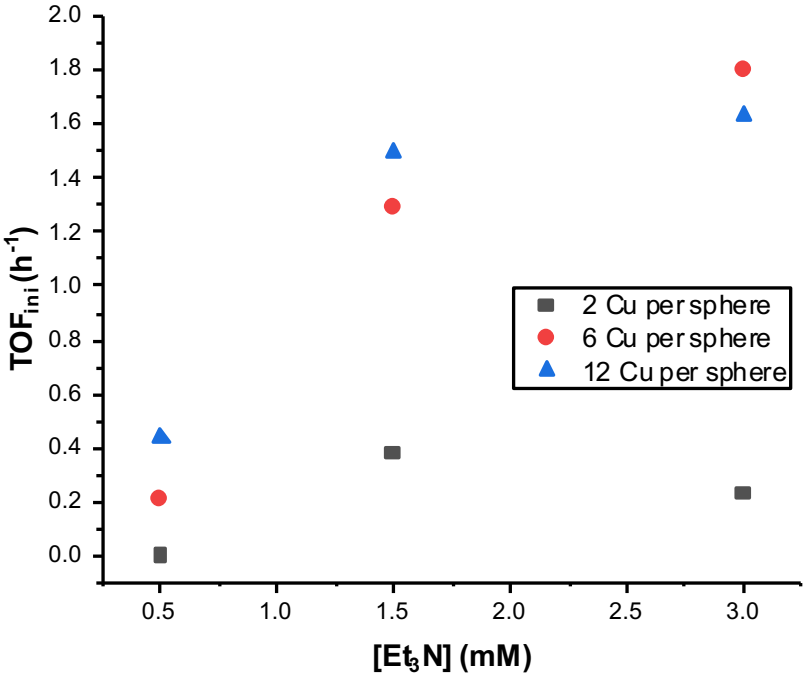

Figure S52. Evolution of TOF_{ini} with respect to the base concentration with different amount of copper per sphere. For reaction conditions S53.

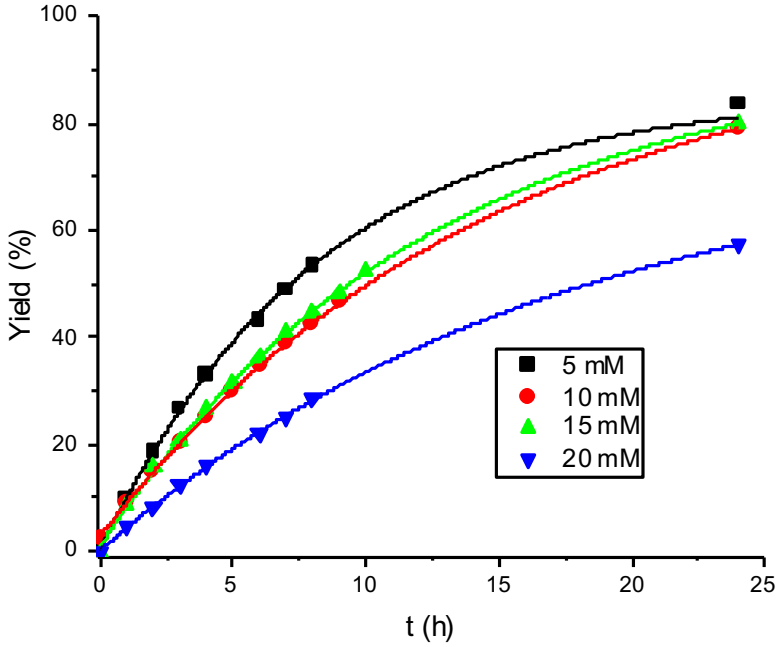

Figure S53. Reaction progress for the formation of **2** in the presence of sphere with 12 eq of **SXantphosCu(I)** per sphere. Reaction conditions: [**1**] from 5 to 20 mM, Et_3N (15 mol%), [Sphere] = 0.042 mM, [**SXantphosCu(I)**] = 0.5 mM, CD_3CN, RT, 24 h.

4. Spectra

4.1 ^{1}H, ^{31}P and ^{13}C NMR spectra of **XantphosCu(I)**

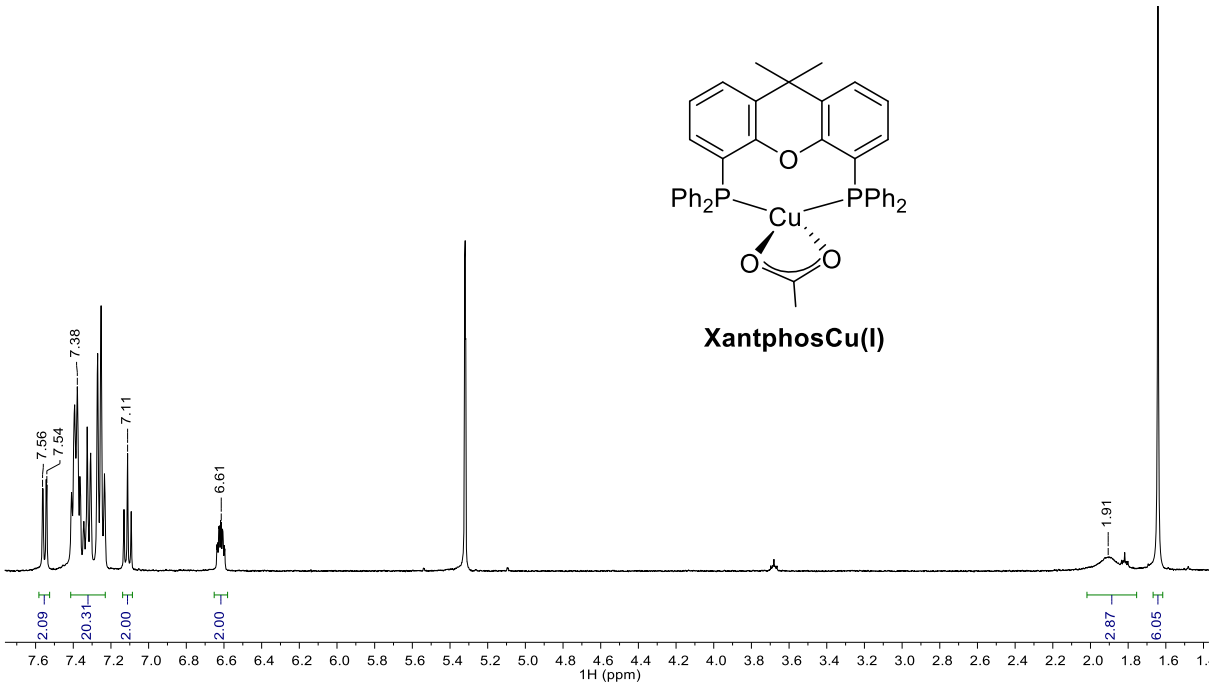

Figure S54. ^{1}H NMR spectrum of **XantphosCu(I)** in CD_2Cl_2

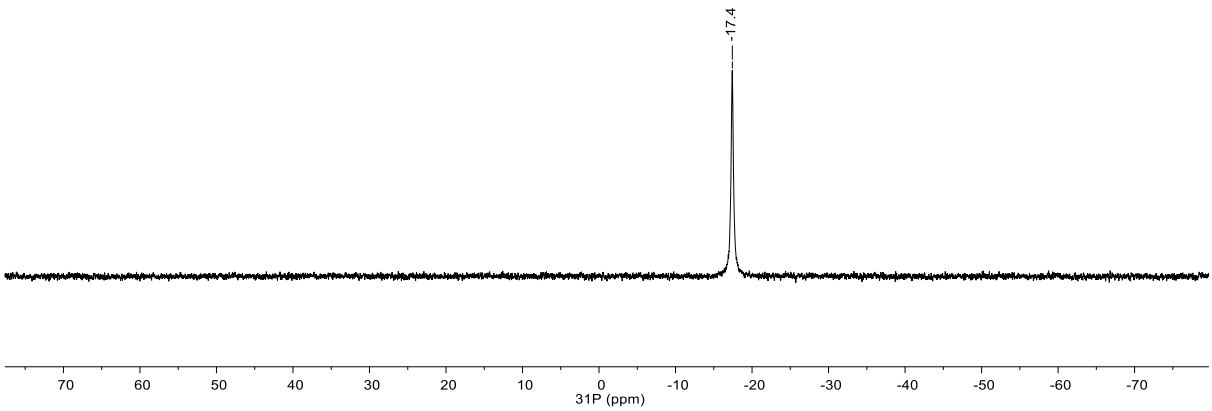

Figure S55. ^{31}P NMR spectrum of **XantphosCu(I)** in CD_2Cl_2

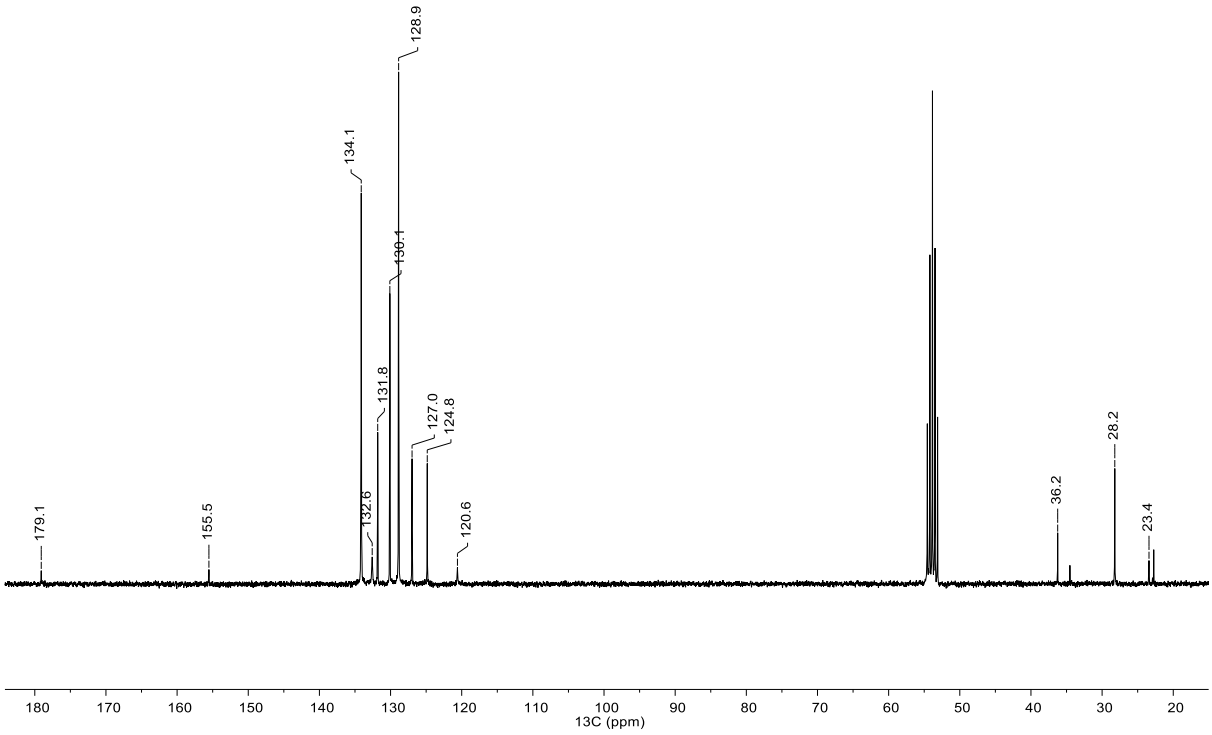

Figure S56. ^{13}C NMR spectrum of **XantphosCu(I)** in CD_2Cl_2

4.2 ^{1}H, ^{31}P and ^{13}C NMR spectra of **SXantphos**

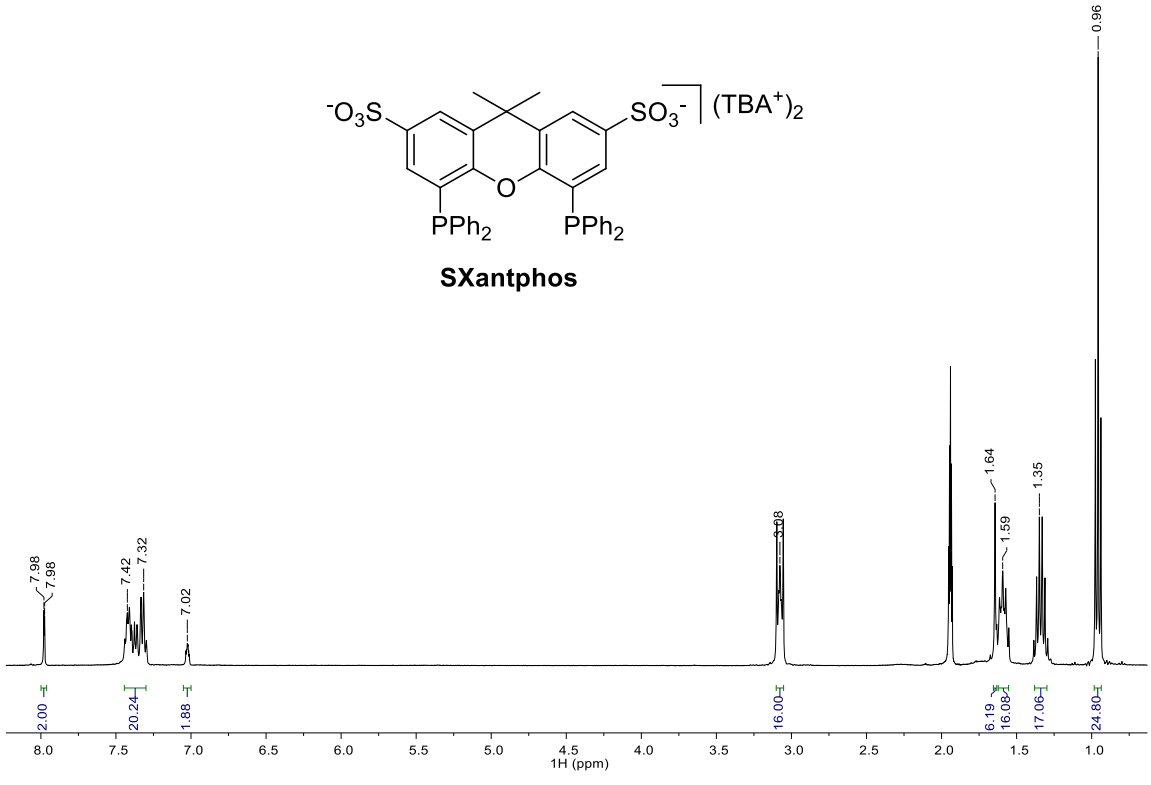

Figure S57. ^{1}H NMR spectrum of **SXantphos** in CD_3CN

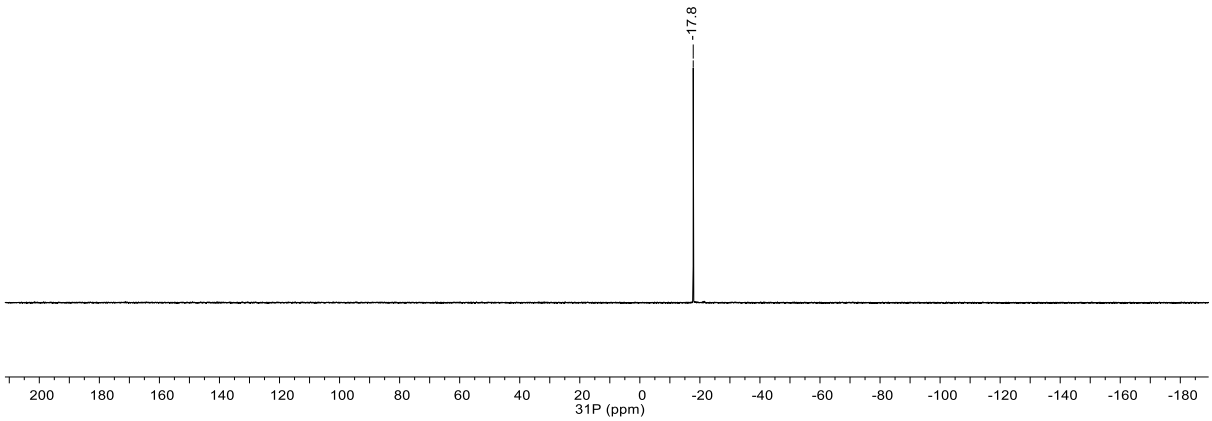

Figure S58. ^{31}P NMR spectrum of **SXantphos** in CD_3CN

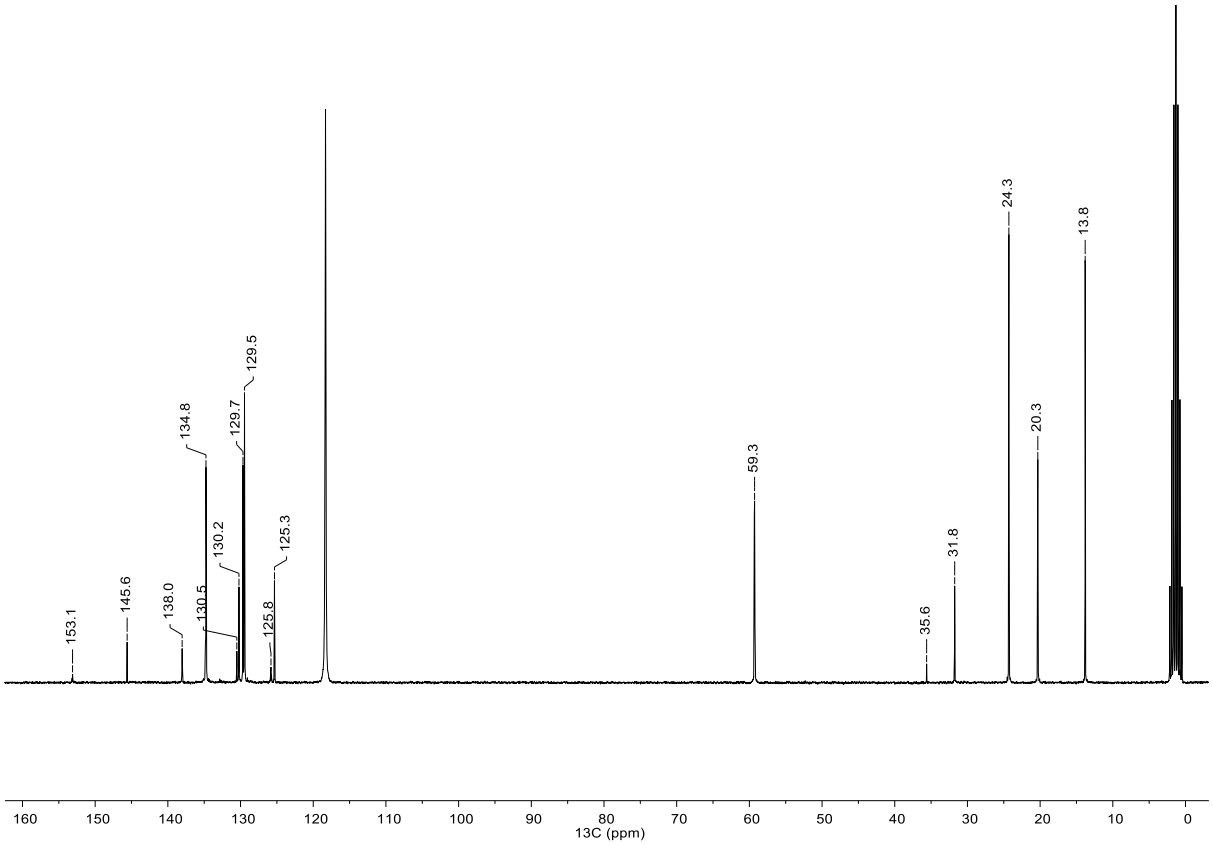

Figure S59. ^{13}C NMR spectrum of **SXantphos** in CD_3CN

4.3 ^{1}H, ^{31}P and ^{13}C NMR spectra of **SXantphosCu(I)**

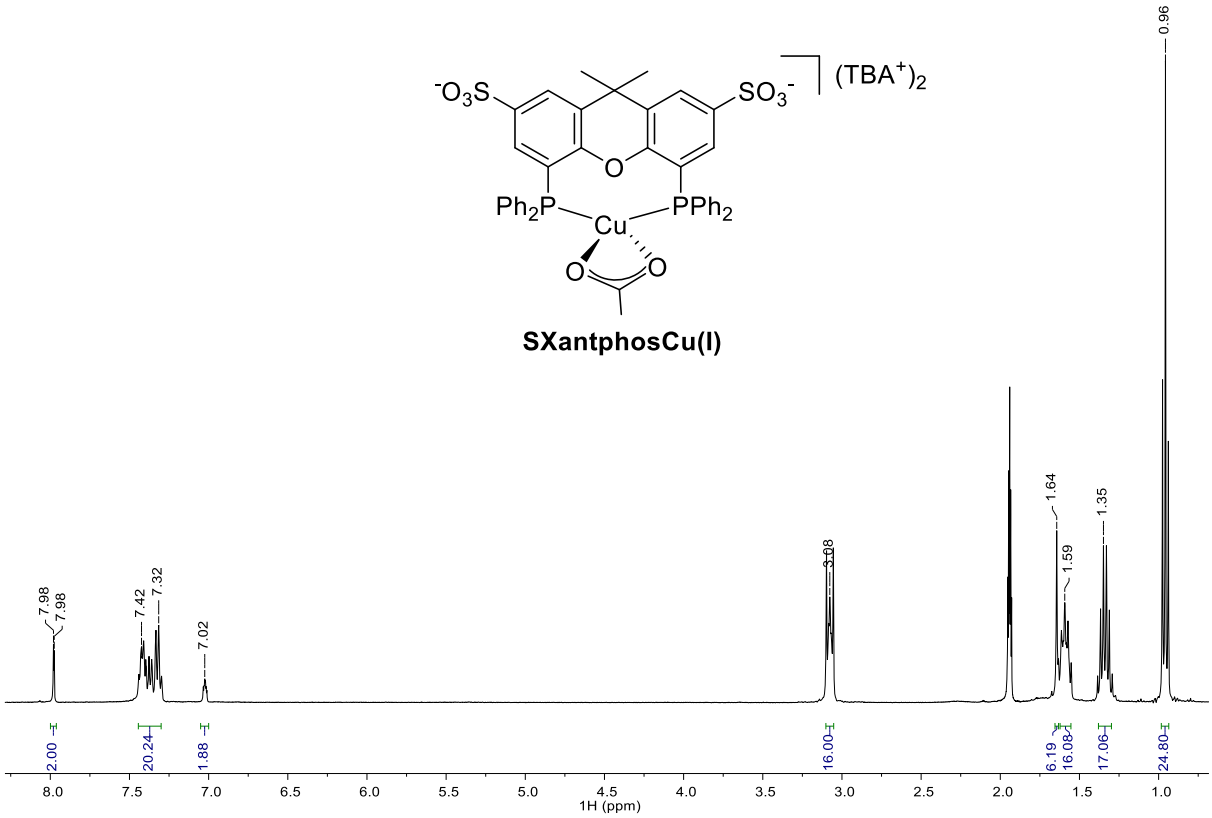

Figure S60. ^{1}H NMR spectrum of **SXantphosCu(I)** in CD_3CN

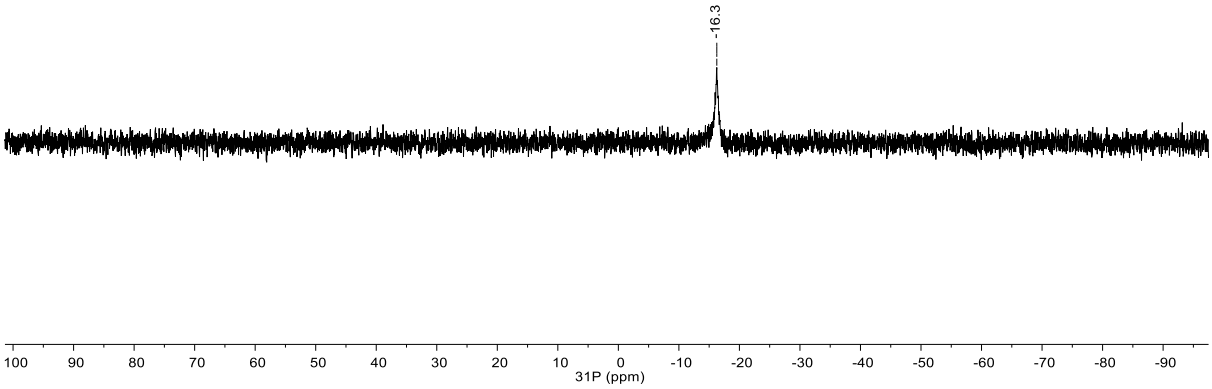

Figure S61. ^{31}P NMR spectrum of **SXantphosCu(I)** in CD_3CN

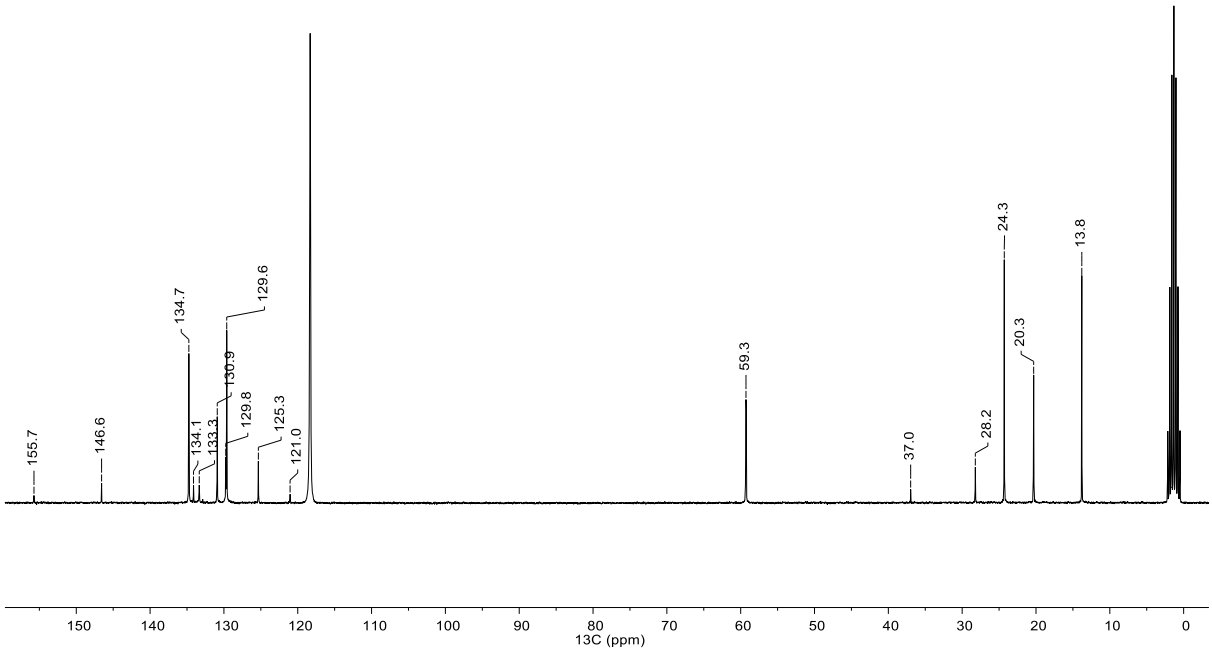

Figure S62. ^{13}C NMR spectrum of **SXantphosCu(I)** in CD_3CN

4.4 ^{1}H, ^{31}P and ^{13}C NMR spectra of **XantphosPt**

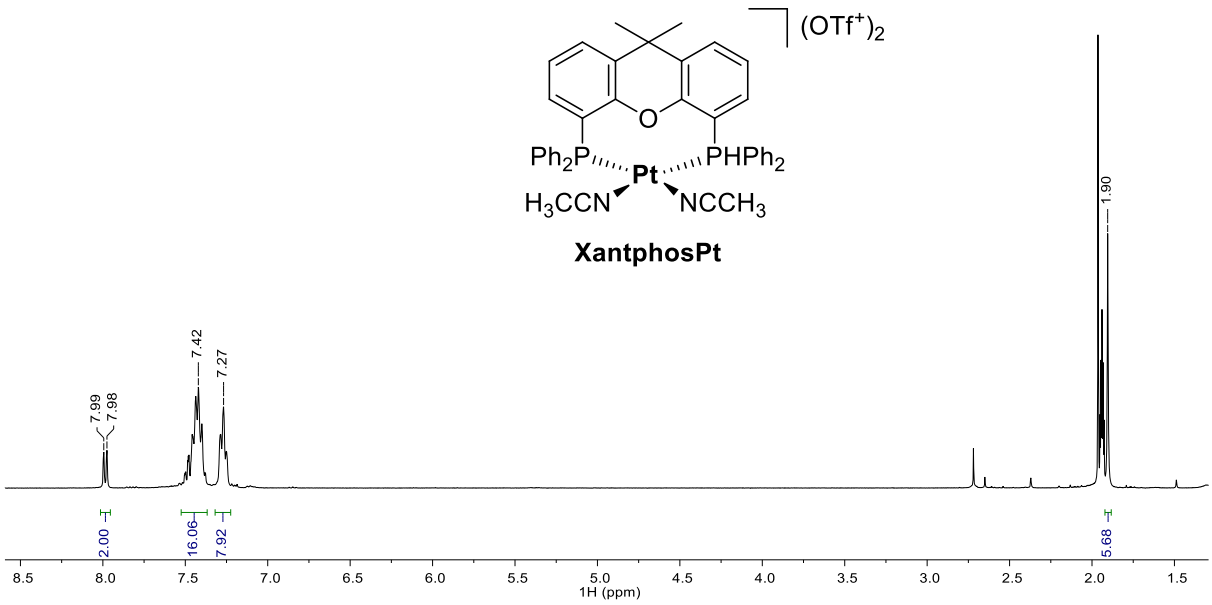

Figure S63. ^{1}H NMR spectrum of **XantphosPt** in CD_3CN

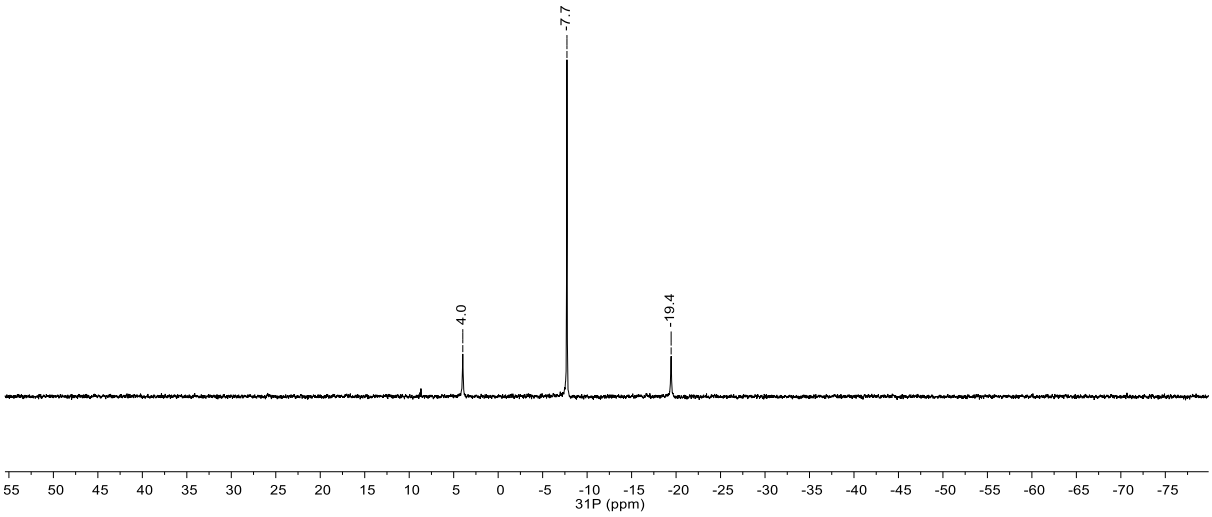

Figure S64. ^{31}P NMR spectrum of **XantphosPt** in CD_3CN

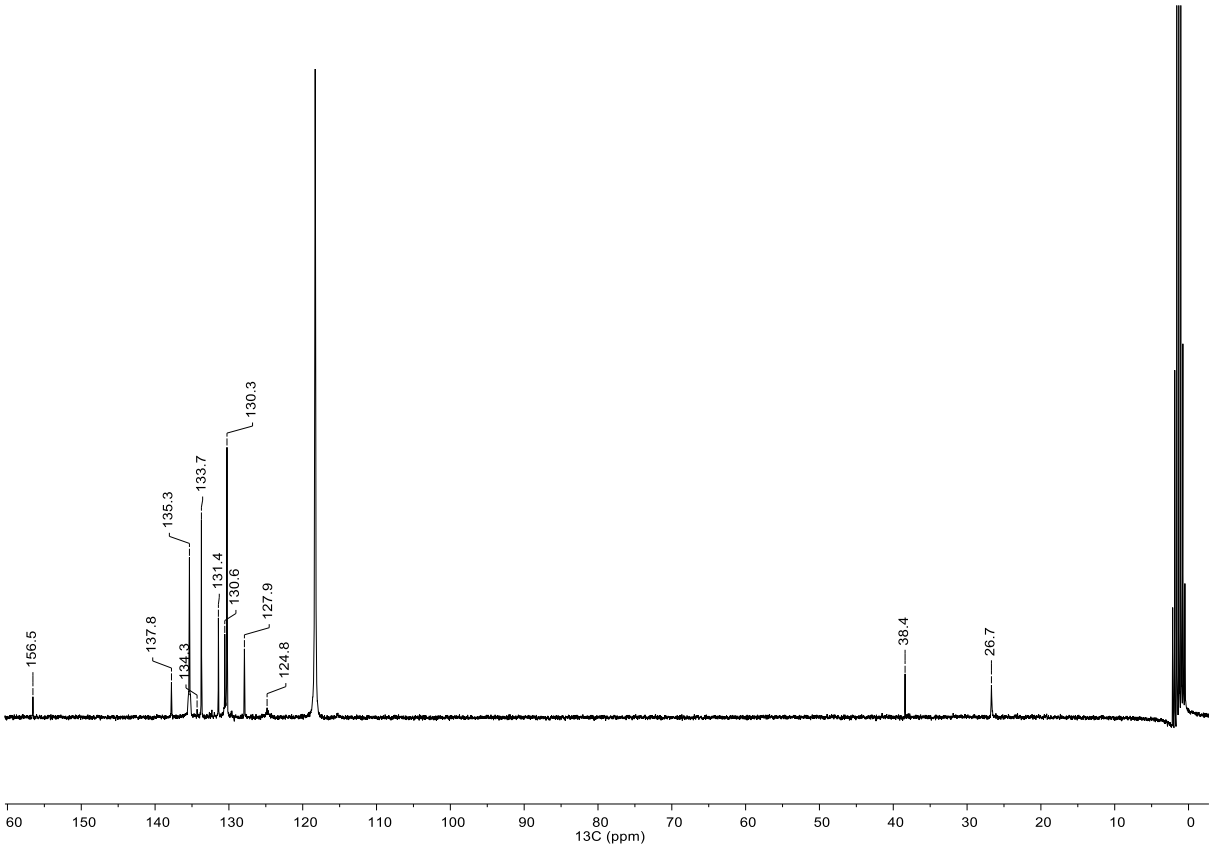

Figure S65. ^{13}C NMR spectrum of **XantphosPt** in CD_3CN

5. References

(1) Mul, W. P.; Ramkisoensing, K.; Kamer, P. C. J.; Reek, J. N. H.; Van Der Linden, A. J.; Marson, A.; Van Leeuwen, P. W. N. M. *Adv. Synth. Catal.* **2002**, *344* (3–4), 293.

(2) Wang, Q.-Q.; Gonell, S.; Leenders, S. H. A. M.; Dürr, M.; Ivanović-Burmazović, I.; Reek, J. N. H. *Nat. Chem.* **2016**, *8* (3), 225.

(3) Goj, L. A.; Blue, E. D.; Delp, S. A.; Gunnoe, T. B.; Thomas R. Cundari; Petersen, J. L. *Organometallics* **2006**, *25*, 4097.

(4) Alemán, J.; del Solar, V.; Navarro-Ranninger, C. *Chem. Commun.* **2010**, *46* (3), 454.

(5) Arcadi, A.; Marinell, F.; Burini, A.; Pietroni, B. R.; Cacchi, S.; Delmastro, M. *J. Org. Chem.* **1992**, *57* (3), 976.